The Self-Assembly of Nucleic Acid Bases on Metal and Mineral Surfaces

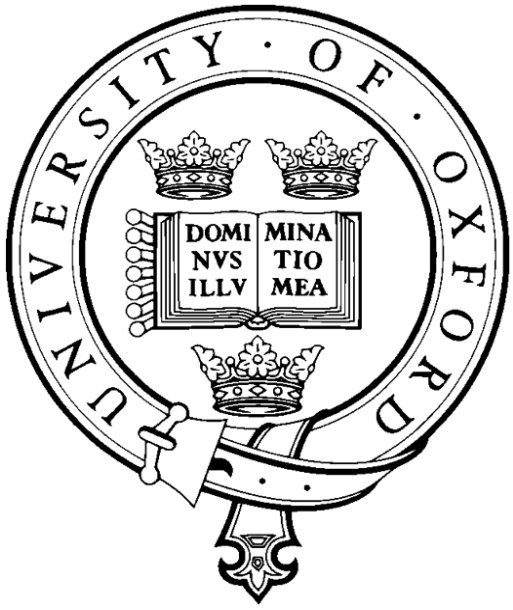

Olga Y. Shvarova

Trinity College

University of Oxford

A thesis submitted for the degree of
Doctor of Philosophy

Trinity Term 2011

To Daddy

Preface

The work described in this thesis was carried out by the author from October 2007 to October 2011, under the supervision of Prof. M. R. Castell (Department of Materials), and Prof. D. G. Fraser (Department of Earth Sciences), in the Department of Materials at the University of Oxford. It has not been previously submitted for any degree of this or other university. Work of other researchers, which has been drawn upon is acknowledged appropriately in the text. No parts of this work have been published or are in press.

Acknowledgements

This thesis would not exist if not for the generous support of many people within the University and outside it. As a D.Phil student at the Department of Materials I was very fortunate to have Martin Castell as my principle supervisor, to work with and learn from him was a pleasure and a privilege. Martin has not only introduced me to the intriguing field of nanotechnology and surface science but taught me to think like a physicist, which was no mean feat, considering my background in Geology and Environmental Sciences. I am very grateful for all the time Martin has spent discussing, guiding and thinking about my project and for all the encouragement and the free rein I was given in pursuing my goals, both scientific and personal. No less fortunate I was in meeting Don Fraser, my co-supervisor, who was the first person to endorse this project and helped me to take it from an interest to a proposal to a thesis. I am very grateful to Don for the inspiration, the constant support and the rare but fascinating discussions we had, which sometimes concerned the art of painting and poetry writing rather then scientific research at hand.

It was a great pleasure to work within the Surface Nanoscience group, which over the years included amazing postdoctoral researches and D.Phil students. My special thanks to David Deak, David Newell, Matt Marshall, and Chen Wu who taught me how to use both STMs which belong to our group without getting frustrated or dispirited, were always happy to explain difficult points and were friends all the way through. I would like to thank Jules Gardener, who was a post-doc in our group when I was starting the molecular deposition work and was an extremely supportive and knowledgeable figure. Jules is missed greatly here after her move to Harvard. And many thanks to Adam Shaw, Bruce Russell, Helen Marsh, Jingyu Sun, and Shams ur Rahman who created the amazing atmosphere within the

group which was both friendly and inspirational.

I would like to extend the special thanks to Kyriakos Porfyrakis and particularly to Sverre Myhra for all the help with the AFM, and to John Murphy, Ben Britton and Ben Mansfield for the necessary assistance with the EBSD. I am very grateful to our JEOL engineer, Chris Spenser, for all the support, advice, answering the late night panicked phone calls, and the miraculous fixing of many problems we came across with the STM, a difficult and capricious instrument at best of times. It was a great pleasure to have George Smith as my Graduate Advisor. I would like to extend my gratitude to the Department of Materials, particularly to Adrian Taylor, Marion Beckett, Alison Crossley, Peter Flaxman, Paul Abbott, Paula Topping, Barry Fellows, Ian Sutton and Lyn Richmond for making my life easier with real technical and administrative support.

I am very grateful to the EPSRC for granting the doctoral training award, which covered all my expenses for 3.5 years. I am extremely grateful to Trinity College, for accepting my application and making me a part of a community that has defined my experience in Oxford; for providing the accommodation within the main grounds almost for the full duration on my study, the opportunity to enjoy the music and the talks by distinguished speakers in a variety of fields, letting me organize weekly wine tastings in the Danson room in my second year, offering the pastoral and the financial support when needed. A great number of close friends I met in its Common Rooms I hope I will stay in touch with for many years to come. I would like to mention here Matthias Fruth, Henry Shevlin, Corwin Wright, Felix Hoffman, and Ben Cartlidge, who were always ready to help or advise, Sarah de Haas, Ben Bertoldi, Elisa Forestan Barnes, Madjdy Fawzy Al Qaramani, Hanaan Marwah, Dunja Aksentijevic, Marie Schroeder, Sinead Keegan, Mette Bundvad, and MJ Leith, who all provided much needed

emotional support with remarkable consistency.

I would like to extend my thanks to those outside the University, who have helped me to complete my project. First and foremost I would like to express my gratitude to my oldest friend I have known for 19 years, Anastasia Kartuzova (née Andreeva), who has been instrumental in sustaining (and recovering) my happiness. I would like to thank Dmitri Lakshtanov for much needed advice on pyrite polishing techniques and general scientific commentary. I would like to acknowledge Ekaterina Lakshtanova, Yuri Dederer, Alex von Dimmer, Gustav Alexander Berner and Olwyn Walker for friendship which enabled me to carry on with my research.

And finally, I would like to thank my family. Daddy, to whom this work is dedicated, who would always offer a solution to a problem, does not matter how far removed from his own field, who instilled the appreciation for the scientific method in me from the early childhood, and when the time came read the entire thesis. Mummy, who put up with me over the years and, though in doubt about everything else, has never doubted my ability to achieve my goals.

Abstract

The ability of RNA bases to self-assemble into larger structures is an important research area relevant to the origins of life. In the RNA helix the bases are arranged on a sugar-phosphate carcass but it has been suggested that the initial ordering could form on a flat surface. This thesis is an attempt to establish experimentally whether the complementary RNA bases, adenine and uracil, have the ability to self-assemble into large ordered structures when adsorbed on metal and mineral surfaces. The Au (111) surface was chosen as a preferred substrate as it is flat, relatively free of defects, chemically inert and reconstructs in a characteristic pattern of corrugation lines, which provide a reference for crystallographic directions. Six of the molecular phases shown were observed for the first time with molecular resolution and the possible two-dimensional arrangements of adenine and uracil molecules for these phases are proposed. The pure adenine and pure uracil structures have chiral unit cells and in the case of pure uracil alternating monochiral domains within the polychiral islands are created. Well-ordered intricate uracil-adenine bimolecular networks were also observed. The self-assembly of both uracil and adenine appears to be weakly influenced by the surface crystallography. The (100) surface of the mineral pyrite (FeS_2) was chosen as the alternative substrate as it is the most common face that occurs naturally in pyrite crystals. The experiments show the formation of small adenine and uracil crystals at the terrace edges. Neither uracil nor adenine were observed to form a monolayer on the surface of the terraces. The results of the experiments described in this thesis are very interesting in terms of establishing the possible mechanisms for creating regular chiral molecular networks and provide a useful insight into the role of surfaces in the processes of self-assembly of RNA bases.

CONTENTS

Chapter 1

Introduction

> "A hole had just appeared in the Galaxy … it seriously traumatised a small random group of atoms drifting through the empty sterility of space and made them cling together in the most extraordinary patterns. Those patterns quickly learned to copy themselves (this was part of what was so extraordinary about the patterns) and went on to cause the massive trouble on every planet they drifted on to. That was how life began in the Universe."
>
> Douglas Adams
>
> "The Hitchhiker's Guide To The Galaxy"

This thesis is an attempt to establish whether the complementary RNA bases, adenine and uracil, have the ability to self-assemble into large ordered structures when adsorbed on metal and mineral surfaces and to find experimental evidence to test parts of the iron-sulphur world theory. This theory is one of the proposed scenarios of the origin of life and suggests that the surface of the most common sulphide mineral on Earth, pyrite, could provide the necessary energy for the self-assembly of the small abiological molecules into the first biomolecules, which would remain on the surface and interact with each other, forming larger, more complex biomolecules, and eventually, living systems.

1.1. Background

The origin of life is one of the biggest unsolved problems in natural science today. It is always difficult to define what it meant by word “life”. To avoid possible misunderstandings I suggest that a chemical system can be called “life” if it fulfills two criteria – it has to be able to self-replicate and to transfer its molecular information fairly faithfully but can make occasional accidental errors. RNA molecule answers to these minimal requirements, so, if we accept this definition of life, we need to look into the RNA formation to answer the question “How could life originate?” Many researchers from different fields, from astrophysics to biology, have tried to find an answer to this question and slowly some stages in the evolutionary origin of life became established, though we still are far away from a full and clear picture of the process. We assume that before the biological evolution on Earth, chemical evolution took place in the dense clouds in interstellar space, during which simple organic or, more accurately, prebiotic molecules were created[1]. Subsequent prebiotic reactions and molecular selection followed until the first self-replicating RNA and RNA-coded proteins appeared in the early Earth environment, which eventually led to the beginning of biological evolution via the last universal common ancestor. The last universal common ancestor (LUCA) is the first living organism of a hypothetical nature from which all current living organisms including Eukaryotes, Bacteria, etc, have arguably descended[2]. This hypothesis is known as the “RNA world theory” and though it is not the only scenario offered by modern science, it is the one that I have chosen as a basis for this thesis.

If we agree that the sequence of events outlined above is plausible and we start searching for more details, we can see that the very first step, the link between the cosmic and the chemical evolution has no coherent proof. The inability of scientists to provide a conclusive

answer to how a cocktail of organic molecules could produce a self-replicating helical macromolecule, which can act simultaneously as an informatic and catalytic system points out the missing information at the very beginning of any origin of life hypothesis. Once RNA molecules appear in the picture, it becomes possible to speculate on how the more complex and more efficient systems evolved, though the origin of the encoded proteins presents another serious challenge[3]. Thus, when speaking about the origins of life as the chemical evolution of self-replicating molecules, it is very important to establish plausible pathways for the synthesis of complex organic molecules, like RNA, from basic organic components acting as building blocks. Since my research interest lies predominantly in the self-assembly of organic molecules, out of all blank spots in the origins of life hypothesis, my attention was drawn to the problem of the accumulation of simple organic molecules and their subsequent self-organisation in larger structures.

The life as we know it today is centered around protein and RNA-catalized reactions. Since none of these reactions have high enough kinetics in the absence of catalysts, it has been suggested that catalysis was essential for the early stages of the prebiotic synthesis[4]. The most commonly accepted hypothesis is that water was the medium that carried prebiotic molecules, mineral surfaces acted as catalysts, and that self-assembly reactions took place on these surfaces. Adsorption on the surfaces might have provided a high local concentration of prebiotic molecules necessary for the self-assembly process, and high energy defect sites of the mineral surface may have been the place where the synthesis started[3].

The surfaces of a particular sulphide mineral, pyrite (FeS_2) were suggested as one of the likely energy sources for catalysis[5]. Interest in the role of pyrite surfaces in the origins of life

arose from the discovery of life forms in active hydrothermal systems in oceans[3]. These life forms, mostly bacterial, are reported to utilise chemical rather then photosynthetic metabolism and are associated with the sulphide minerals that are constantly forming in vast quantities in such systems. This fact has encouraged research on the possible role of pyrite, which is abundant in the Earth's crust, in the origins of life and in particular in the potential of pyrite surfaces to catalyse reactions that may lead to the formation of complex organic molecules that are essential for life on Earth. Active research is being carried out into the possible role of clay and other aluminosilicate minerals in the origins of life, but the interactions of nucleobases with sulphide surfaces have received very little attention so far. While there is still little known about the mechanisms and the exact pathways of the self-assembly of nucleobases on pyrite, the scanning tunneling microscope (STM) seemed to be the perfect tool for studying the self-assembly of the RNA bases on surfaces *in situ* and the availability of this wonderful technique steered my research in this direction.

The experimental part of this thesis was carried out in ultra high vacuum (UHV) on the Au (111) and pyrite (100) surfaces using an STM. The (100) surface of pyrite was chosen as a mineral substrate as it is the most common face that occurs naturally in pyrite crystals and is chemically active, i.e. in theory is capable of forming ionic bonds with the RNA bases, which are strong enough to ensure a sufficiently long residence time for the adsorbed material but weak enough to allow lateral diffusion on the surface[6]. However, to judge accurately the impact of surface-molecular interactions on the process of self-assembly we must also consider a process of self-assembly of nucleobases on a catalytically inert surface, and I chose the Au (111) surface to act as a control substrate. The Au (111) surface is very flat, relatively free of defects, chemically inert and reconstructs in the characteristic pattern of corrugation lines, which provide a useful reference for the

crystallographic directions. On Au (111) I should be able to observe the process of self-assembly, which is determined by the spatial arrangements of the molecules and by the intermolecular bonds while the surface has a weak or negligible effect on the molecular ordering and compare it to the self-assembly process determined to a larger degree by the active surface of pyrite.

A greater understanding of the role of the molecular-surface interactions in the process of the self-assembly of the RNA bases may assist in filling in the gaps in knowledge of the formation of the first RNA precursors. More broadly, it may also contribute to the knowledge of molecular networks stabilised by hydrogen bonds, surface chiral selectivity, surface-induced catalytic effects, and chiral packing mechanisms.

1.2. Plan of thesis

This thesis is based on the experimental study of the self-assembly on the two complementary RNA bases, adenine and uracil, on the Au (111) and pyrite (100) surfaces using a UHV STM. The plan of the thesis is as follows:

Chapter 2 – gives a brief introduction to the surface characterisation techniques used for my research purposes.

Chapter 3 – introduces the nucleic bases (fundamental building blocks for complex helical organic molecules like RNA and DNA), their properties and molecular structure, and the current state of knowledge about the self-assembly of the RNA bases on the metal and mineral surfaces. It includes the published STM images of the resulting molecular networks

and the proposed molecular models.

Chapter 4 – is a review of the current state of knowledge about the “DNA world” hypothesis, it provides an explanation how the self-assembly of the RNA bases on sulphide surfaces could be relevant to the problem of the origin of life and the current alternative theories of the origin of chirality.

Chapter 5 – provides a detailed description of sample preparation techniques used, the problems that arose from some sample treatments, and the resulting bare surfaces that were used for the self-assembly experiments. The crystallography, surface structure and surface chemistry of pyrite are also described in here.

Chapter 6 – is concerned primarily with the separate self-assembly of uracil and adenine on the Au (111) surface. New experimental results reported in this thesis are shown here and in the following chapters. The observed monomolecular structures, the effects of low-temperature annealing on the molecular networks and the formation of chiral domains are described here.

Chapter 7 – is concerned with the co-adsorption of adenine and uracil on the Au (111) surface. The resulting regular bimolecular networks are shown and analysed and the effects of low temperature annealing and the relative coverage on the surface are discussed.

Chapter 8 – is devoted to the self-assembly of the adenine and uracil, applied to the sample separately and simultaneously, on the pyrite (100) surface. No 2-dimensional networks can be observed. Both nucleic bases form small crystals located at the edges of the terrace

steps. Low-temperature annealing has no visible effect on the distribution of the crystals.

Chapter 9 – serves as a conclusion to this thesis and briefly summarises the research results and suggestions for the further research and applications.

Chapter 2

Experimental techniques

In this chapter I will provide a brief description of the main and supplementary experimental techniques relevant to this thesis.

2.1. The equipment

I have chosen to use scanning tunneling microscopy as the main surface characterisation technique in my research project. The scanning tunneling microscope (STM) is an excellent tool for studying surface structures and surface processes. It usually operates under UHV (ultra high vacuum) conditions and can resolve the electronic and topographic structure of virtually any clean, flat, solid conducting surface, often achieving atomic resolution. The base pressure in the STM vacuum chambers is of the order of 10^{-8} Pa. I decided to perform the experiments in UHV conditions as it allows one to keep the surface clean of contamination (adsorbed atmospheric gases, water molecules, dust particles, etc) and observe the deposited molecules individually.

The additional characterisation techniques I used were:

Atomic Force Microscopy (AFM)

Electron Backscatter Diffraction (EBSD)

These techniques were relevant to the sample preparation process, and a short description of both methods will be given in this chapter.

2.2. Scanning tunneling microscope (STM)

The scanning tunneling microscope (STM) developed in the 1980s[7] is still one of the most powerful and exciting tools available in surface science. It can resolve the local topography and the electronic structure at the atomic level of any kind of conductive solid material, provided it has a clean and flat surface, while making no damage to the surface itself, thus allowing it to scan repeatedly over one area as required for observing surface processes such as molecular self-assembly at various stages of development.

The STM is based on the following principle: when a conducting tip is brought very close to the surface of a conducting sample in vacuum and a bias voltage is applied, a small current will tunnel through the gap between the tip and the sample. This small current is called metal-vacuum-metal tunneling[8] and is a function of the distance between the tip and the sample, the applied voltage and the local density of states of the sample at the Fermi level* (E_F) at the position of the tip. The effective lateral resolution of the STM is $[(2\ \text{Å})(R + d)]^{1/2}$, where R is the radius of the tip curvature and d is the distance between the tip and the sample[9]. The tunneling current I is related to the applied bias voltage V and the distance between the tip and the sample, d, as:

* The Fermi level is a hypothetical level of potential energy for an electron inside a crystalline solid, and can be described as a state with 50% chance of being occupied by an electron for the given temperature of the solid.

$$I \propto V\rho_s(0, E_F)e^{-2kd},$$

where ρ_s is the local density of states at the Fermi level and k is the decay constant of a sample state near the Fermi level in the barrier region and is proportional to the square root of the V[8].

As the tip scans over the surface of the sample, the information about the surface topography and localised electronic structure is collected by measuring the tunneling current as a function of the tip position on the scan and is displayed as a 2D line scan image, where the dark spots represent the topographical depressions or low local density of states and the bright spots represent the topographical protrusions or the high electron density. The STM has two modes of operation: constant current mode, when the tunneling current between the tip and the sample surface is kept at the constant level and the height of the tip varies according to the surface topography and the local density of states, and the constant height mode, when the height of the tip is fixed and the variations in tunneling current are recorded. For electronic states at Fermi level, the surface can be seen as a potential barrier with a height equal to the work function ϕ, the current varies exponentially with the vacuum gap distance and in the constant current mode the tip may be expected to follow the surface topography to 0.1 Å[9].

The quality of the image depends on the shape, physical and chemical stability, the sharpness of the tip, and the cleanliness and flatness of the scanned area. The tip is usually made from W (tungsten) and the typical tip radius of curvature is over 100 nm, which would make atomic or even molecular resolution virtually impossible. However, there is usually an

atom that is protruding from the surface of the tip and this atom is accountable for the majority (over 90 %) of the tunneling current and for the exceptional image resolution in the STM. It is also possible to have two or more atoms which are prominent on the surface of the tip, and in such cases the image becomes distorted due to various tip effects, of which the so-called “double tip” is the most common, when the shape of the tip surface causes all topographical features to be imaged twice. Also, the tunneling current is very responsive to the tip-sample distance, making the instrument extremely sensitive to vibration, which in turn is a source of lateral interference lines, another common problem with image quality. The suppression of all factors that can cause environmental vibration including movement of the pumps and temperature control systems becomes vital for obtaining a good quality image, especially if one is to achieve molecular or atomic resolution. The spatial resolution of a few Å is routinely achieved with modern STMs and in low temperature systems (77 K or lower) tip-induced manipulation of individual atoms, molecules and molecule parts can be achieved.

The Department of Materials of the University of Oxford owns a specially built low temperature JEOL 4500S UHV STM microscope. The JEOL 4500S UHV STM is a very complex instrument, only the part of it relevant to this thesis is shown in Figure 2.1. The instrument also incorporates a third chamber (not shown) within the same system with a UHV scanning electron microscope (SEM), an X-ray photoelectron spectroscopy (XPS) and an Auger electron spectroscopy (AES) with a SPECS hemispherical analyser, ultra-violet photoelectron spectroscopy (UPS), photoluminescence (PL), cathodoluminescence (CL) and residual gas mass spectroscopy (MS) facilities.

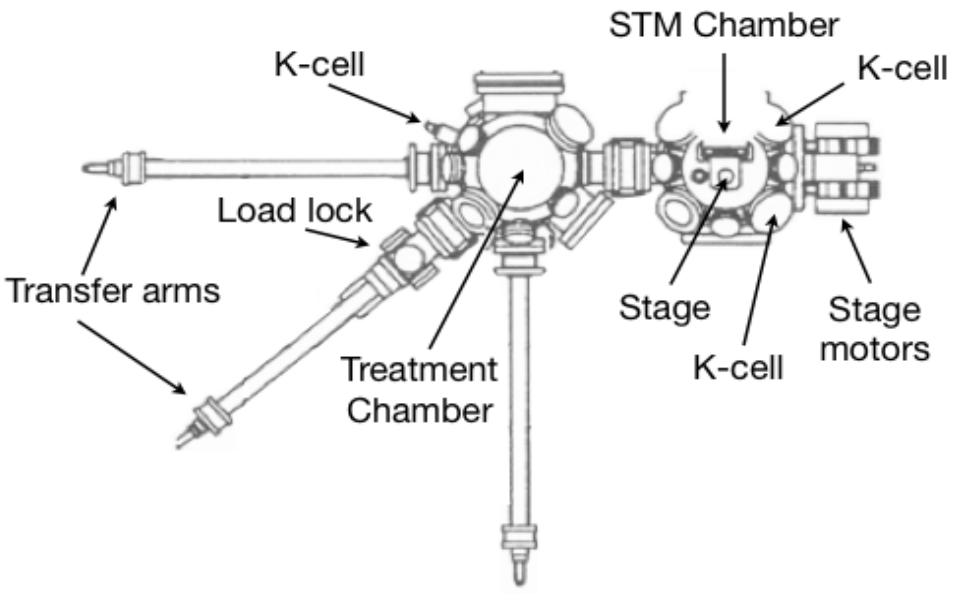

Fig. 2.1. JEOL 4500S UHV STM, the schematic view from the top with two chambers listed. A number of facilities are labeled in both chambers. The image was adapted from JCPM-4500S/TM-51021 UHV STM manual, JEOL. All experiments needed for the completion of this thesis were performed in the Treatment and STM vacuum chambers.

All degassing, sputtering and annealing procedures were performed in the STM treatment chamber, where the pressure was allowed to rise up to 8×10^{-6} Pa. Sample sputtering *in situ* was performed by using a PSP ion gun system. This gun operates at pressures of 4×10^{-4} Pa and produces an Ar^+ ion beam with energies of up to 2 keV and beam currents of 1-3 μA. Sample degassing and annealing *in situ* in STM experiments was performed by using direct DC resistive heating via a computer controlled power supply. Temperatures above 650 ºC, needed for Au (111) surface preparation, was measured by a Leeds and Northrup disappearing filament optical pyrometer, which is a direct method of measuring the temperature of hot bodies emitting energy in the visible range of the optical spectrum. For the low temperature annealing (<100 ºC) used on pyrite samples and in the sample-to-sample deposition technique there was no direct method to monitor the temperature. In his D.Phil thesis[10] D. Newell provided an experimentally obtained equation $1.4739x^3 - 34.546x^2 + 325.3x + 15.58$ representing the best fit line with an R^2 value of 0.9997 for a calibration

curve plotted for the sample temperature above 750 ºC against the power of output of the power supply between 0 and 5 W[10]. All low temperature annealing procedures were performed using this equation as the only way to estimate the sample temperature. After annealing, the samples were allowed to cool down naturally to room temperature *in situ*.

STM imaging was performed in the main (STM) chamber, where the pressure was kept at $3x10^{-8}$ Pa or lower. The tips were produced by electrochemical etching of W (tungsten) wire in a 2 M KOH (potassium hydroxide) solution using a DC current. All STM images used in this thesis were taken by me unless indicated otherwise and were obtained at ambient temperature (25 ºC) in constant current mode with a negative bias voltage applied to the sample.

Molecular vapour deposition was performed using two different methods. At first I used a Createc Knudsen cell (K-cell), which hosts a crucible filled with the molecules in powder form and is orientated towards the sample inside the treatment chamber (see Fig. 2.2). As the crucible is heated by an external filament coil to the molecule sublimation temperature the molecules evaporate through the aperture in the lid and into the chamber, when the K-cell shutter is open. The aperture diameter is fixed so that the flux of molecules is controlled by the temperature only. Some of the molecules I used for deposition have very low sublimation temperatures (within a 80-120 ºC interval), and it proved to be difficult to control the temperature of the K-cell to maintain constant flux in subsequent depositions at such low temperatures, especially when low coverage was sought.

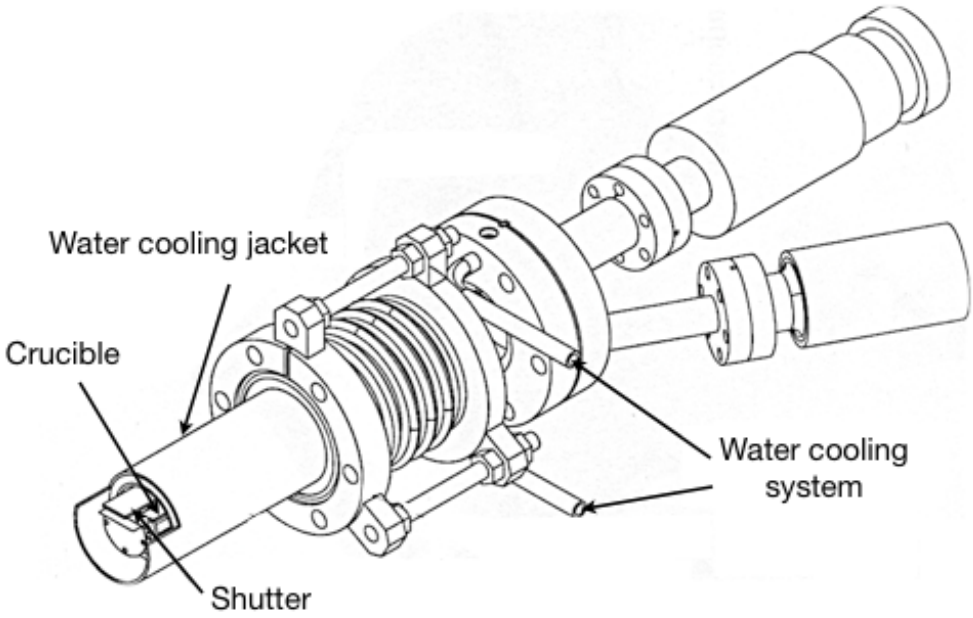

Fig. 2.2. K-cell with the main features and the cooling system shown. Adapted from SFC-H-5-SH manual, Createc Fischer & Co. GmbH.

To improve control over the flux I decided to use an alternative method of molecular deposition, where a conducting sample with the surface completely covered by the molecules was introduced into the treatment chamber and degassed to just below molecule sublimation temperature. This achieved, the sample was heated to the approximate sublimation temperature for the type of molecules on its surface (this was estimated by using the temperature approximation curve as described previously and by monitoring the changes in the base pressure in the vacuum chamber closely) and placed within 1 cm distance from a clean sample, facing it. In this case, it was much easier to control the temperature and the flux using the distance between the two samples and the power output of the power supply. I called this method a sample-to-sample deposition and used it for most experiments where a higher precision in the amount of molecules deposited at lower temperatures was required. Typical deposition, either via a K-cell or using sample-to-sample method, was carried out for a few minutes, depending on the desired coverage of molecules on the sample surface. When the deposition was complete the sample was left for an hour

at the ambient temperature before imaging or sometimes heated to slightly below the molecule sublimation temperature, to encourage the surface diffusion of the molecules without supplying the molecules with enough energy to enable them to leave the surface.

Between the experiments all samples were stored under UHV conditions in the treatment chamber.

2.3. Additional surface characterisation techniques

The surface preparation and characterisation techniques described in the following section were used to prepare the pyrite samples for STM experiments. Single crystals of naturally formed pyrite from an unknown locality were obtained from Prof. Don Fraser at the Earth Sciences Department and the samples were cut, polished and prepared for the STM experiments manually. The sample preparation including the effect of polishing procedures on the surface is described in detail in Chapter 5. Two additional methods were required to verify the correct alignment of the samples to the desired crystallographic plane and the roughness of the polished surfaces prior using the samples for the STM experiments.

2.3.1. Atomic force microscopy (AFM)

Atomic force microscopy (AFM) was used to check the surface of the prepared pyrite samples for pits, scratches and embedded material after the final polishing stage. The schematic picture of an AFM is shown in Figure 2.3.

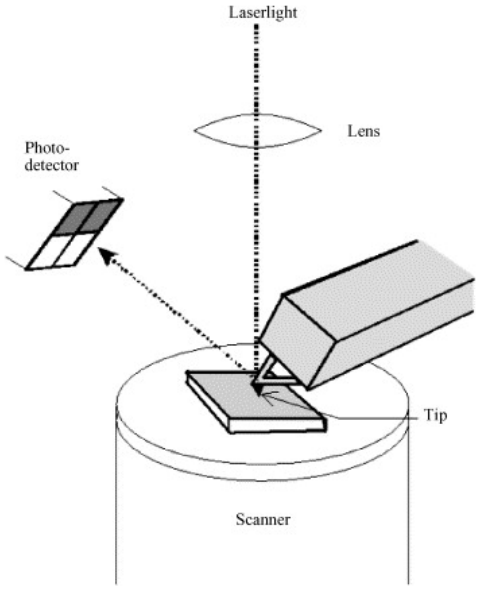

Figure 2.3. A schematic picture of an AFM, adapted from Butt, et al.[11] Laser light from a solid state diode is reflected from the back of the cantilever and collected by a position sensitive photodetector, which detects cantilever deflections <10 nm and produces an output signal, proportional to the deflection of the cantilever.

AFM is a similar technique to STM, only the tunneling tip is replaced with a mechanical one and, instead of measuring the small variations in the tunneling current, the small variation in deflection of the cantilever is measured; in this way non-conducting surfaces could be imaged in the AFM. In AFM a force-sensitive cantilever is raster scanned over the surface of the sample and the force between the cantilever and the surface causes minor flexing of the cantilever, which is detected and used to construct a topographic image. Image contrast arises due to the force between the tip and the sample being a function of both tip–sample separation and the physical and chemical properties of the tip and the sample, and is obtained from the very short range repulsion, which occurs when the electron orbitals of the tip and the sample overlap (Born repulsion)[11]. The force between tip and sample is composed of many short- and long-range contributions: electrostatic, magnetic, van der Waals, chemical and meniscus forces. It is possible to achieve an atomic resolution in the

AFM by operating in vacuum when the long-range force contributions are negligible[12].

Once the cantilever deflection is detected, the AFM can be used in two modes to take topographical images: the constant height mode (the height of the scanner is fixed and the spatial variation of the cantilever deflection is measured) and the constant force mode (the cantilever deflection is constant and so is the force applied to the sample, and the scanner motion is measured in z-direction). Constant force mode is generally preferred for most applications and constant height mode is primarily used for taking images of solid atomically flat surfaces or real-time images of changing surfaces where the scan speed needs to be high[11].

AFM can be operated in a contact mode used primarily for obtaining the topographical information or in a non-contact (tapping) mode for more detailed investigation of surface composition, i.e. its magnetic, chemical, electrostatic features, etc. The quality of an AFM image depends on the size, shape, stiffness, and resonance frequency of the cantilever and also on the sharpness of its tip. The cantilever is a key element of the AFM and is largely responsible for the instrument's performance. Commercial cantilevers are typically made of silicon or silicon nitride with an oxide layer of 1–2 nm thickness. The mechanical properties of cantilevers are characterised by the spring constant and the resonance frequency, both can be calculated from the material properties and dimensions of the cantilever[11]. Similar to STM, AFM must be operated in an environment protected from external vibrations.

The Department of Materials of the University of Oxford owns an Agilent 5400 AFM at the Begbroke site within the University of Oxford Begbroke Science Park. This instrument was used to perform a high resolution imaging of the surface of the sample after the final stage

of polishing on 100 μm^2 areas and 100 nm^2 areas in air. The topography imaging was performed in tapping mode for surface roughness analysis. Only one sample from each batch was characterized in AFM; as the samples needed to be transported in air from central Oxford site to Begbroke Science Park, the surface of pyrite was considered to become completely oxidised during the journey and these samples were not used in the STM experiments.

2.3.2. Electron backscatter diffraction (EBSD)

Electron backscatter diffraction (EBSD) was used to confirm the pyrite crystal orientation prior to cutting into samples. It is a microstructural technique mainly used to establish the crystallographic orientation of any crystalline material; the crystallographic orientation of surface features such as particles, grains or subgrains in a specimen can also be determined. EBSD is performed using modified scanning electron microscope (SEM) with an EBSD detector, which usually contains a phosphor screen, a compact lens and a low light charge-coupled (CCD) camera.

In this technique, the electron beam is kept stationary on the sample and the backscattered electrons are collected on a phosphor screen. To achieve a good contrast in an electron backscatter pattern the sample must be tilted to a large angle (70°). At small angles the majority of the electron signal is absorbed by the specimen; in order to achieve the backscattering of the signal the path length must be shortened by tilting the specimen[13]. It is suggested that the substantial number of electrons in a crystal impinge on the lattice planes from all directions; the atoms inelastically scatter the electrons with a small loss of energy and a divergent source of electrons close to the surface is formed. Some of these electrons

incident on atomic planes at the angles which satisfy the Bragg equation:

$$n\lambda = 2d \sin \theta,$$

where n is an integer, λ is the wavelength of the electrons, d is the spacing of the diffracting atomic plane, and θ is the angle of the incidence. These electrons give rise to a Bragg reflection[14] and the regions of enhanced electron intensity detected on the phosphor screen form Kikuchi lines of the electron backscatter diffraction pattern, which can be used to determine the orientation within a small fraction of a degree[15].

If the geometry of the system is known, the lines, which can be seen in the diffraction pattern, can then be related to the corresponding atomic lattice planes of the crystalline structure and indexed by the Miller indices. In most crystals three intercepting bands are enough to describe a unique solution to the crystal orientation. Direct measurements from the EBSD can be used to identify Bravais lattices and point groups, and it is a particularly good instrument for the detailed crystallographic analysis as it captures a single, directly recorded diffraction pattern[13]. The pattern obtained experimentally is usually compared with the computer simulations based on the known lattice parameters, crystal system and the lattice type of the material that is being investigated. The software provided with the instrument also uses the international crystal databases to perform indexing and determine the crystal phase orientations. The depth resolution of the diffracting volume is 10-20 nm and is limited by the electron backscattering, the lateral resolution is in order of 100 nm and is a function of the angle of the tilt of the specimen, working distance, probe current and accelerating voltage[13].

The Department of Materials of the University of Oxford owns a 1312M-FW-TE EBSD camera made by DVC company, which is set up at the Begbroke site within the University of Oxford Begbroke Science Park. This instrument was used to perform the measurements of the crystallographic orientation of a sample cut from a pyrite monocrystal parallel to the naturally formed (100) face. The specimen was tilted at 70 degrees from horizontal position towards the diffraction camera to increase the contrast in the resulting diffraction pattern. The pattern obtained was characteristic of a (100) surface of a cubic single crystal.

2.4. Summary

This chapter has introduced the concepts of the experimental techniques used for my research and provided brief descriptions of the instruments used. The methodology and the general procedures needed for the sample preparation and main experiments have been outlined. This includes verifying the crystallographic orientation of the sample, the roughness of its surface, degassing, sputtering, annealing, molecular deposition and STM imaging. The techniques described here are sufficient for obtaining and imaging the surfaces of Au (111) and pyrite (100) in clean state or with molecules deposited, and the instruments mentioned provide all the necessary tools for the experimental work on which this thesis is based.

Chapter 3

RNA-bases molecular networks on surfaces

Our understanding of molecular self-assembly has increased significantly over the last ten years. The molecular networks that have been studied by many research groups all over the world have been growing in complexity, and molecular self-assembly has become a rapidly emerging field of nanoscience. Biomolecules – proteins, DNA components, lipids, etc, have all been studied extensively within this new field. These molecules self-assemble through specific molecular interactions in natural chemical and biological processes, and, in principle, the mechanisms of their assembly, if understood, could be to used to create 2-dimensional networks with high precision on a nanometer scale. DNA and RNA bases are particularly interesting in this respect as the complementary bases of these two biomolecules use sequence self-assembly via intermolecular hydrogen bonding to encode genetic information. In this Chapter, I will review the chemical structure, chirality and biological role of the RNA bases and provide a review of the current state of knowledge regarding the self-assembly of these molecules on mineral and metal surfaces.

3.1. Chemical structure and biological role of RNA bases

The RNA structure contains four nucleobases: adenine (A), guanine (G), cytosine (C) and uracil (U).

Cytosine and uracil are single heterocyclic aromatic molecules similar to benzene, called pyramidines. Adenine and guanine are heterocyclic aromatic molecules that consist of a pyrimidine ring fused with an imidazole ring, called purines[16]. In RNA base pairing, adenine pairs with uracil via two hydrogen bonds, uracil acting as the bond acceptor. Guanine pairs with cytosine via three hydrogen bonds; the amino group acts as the hydrogen donor and the C-2 carbonyl and the N-3 amine groups act as the hydrogen-bond acceptors. Purine bases, adenine and guanine, are known to be more stable and to form significantly stronger bonds with surfaces than piramidines[17].

The chemical structures of the four bases are shown in Figure 3.1. All information in this section is given according to Gilchirst's *Heterocyclic Chemistry*[16].

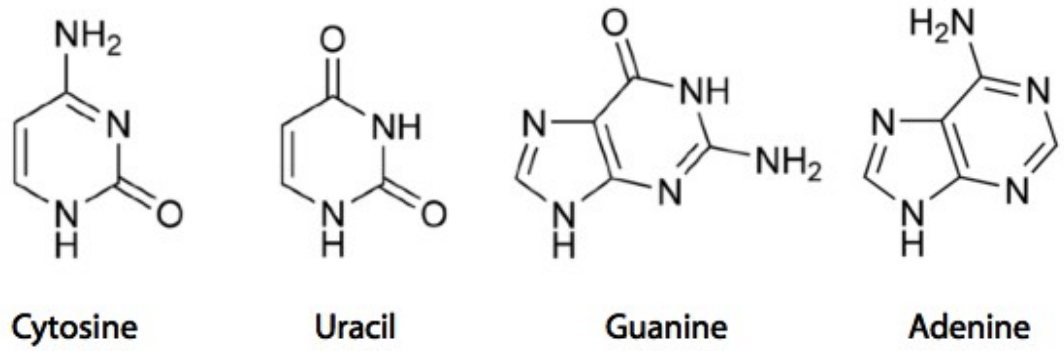

Figure 3.1. The chemical structures of RNA nucleobases.

Cytosine is a planar pyrimidine derivative with a molecular formula $C_4H_5N_3O$. It has a molar mass of 111.300 g/mol, decomposes at 320-325 ºC and is soluble in water. Its structure is composed of a heterocyclic aromatic ring, a keto group at position 2 and an amino group at position 4. In DNA and RNA, cytosine is paired with guanine but is inherently unstable, and can spontaneously change into thymine.

Uracil is a planar pyrimidine derivative with a molecular formula $C_4H_4N_2O_2$. It has a molar mass of 112.09 g/mol, decomposes at 335 ºC and is soluble in water. Its structure is composed of a heterocyclic aromatic ring and two keto groups at positions 4 and 2.

Guanine is a planar purine derivative with a molecular formula $C_5H_5N_5O$. It has a molar mass of 151.13 g/mol, decomposes at 360 ºC and is insoluble in water. Its structure is composed of a fused pyrimidine-imidazole ring system with conjugated double bonds containing a nitrogen atom at position 1, an amino group at position 2 and a keto group at position 4 of the pyrimidine ring.

Adenine is a planar purine derivative with molecular formula $C_5H_5N_5$. It has a molar mass of 135.13 g/mol, decomposes at 360-365 ºC and is insoluble in water. Its structure is composed of a fused pyrimidine-imidazole ring system with conjugated double bonds, containing two nitrogen atoms at positions 1 and 3 and an amino group at position 4 of the pyrimidine ring.

Aside from their role in protein synthesis as RNA and DNA (deoxyribonucleic acid) components, purines and pyrimidines play important roles in the synthesis of a number of other vital biomolecules, such as CTP (cytidine triphosphate), ATP (adenosine triphosphate), ADP (adenosine diphosphate), FAD (flavin adenine dinucleotide), NAD+ (nicotinamide adenine dinucleotide) and coenzyme A. They may also function directly as neurotransmitters, acting upon purinergic receptors[18]. Biochemical functions specific for each RNA nucleobase are described below.

Cytosine is an important component of CTP, it is used in cells to construct coenzymes that are utilised in the formation of phospholipids and can transfer a phosphate to convert ADP to ATP[18].

Uracil is used for the synthesis of most enzymes necessary for cell functions, for the synthesis of polysaccharides and the transportation of sugars containing aldehydes. It also acts as an allosteric regulator and a coenzyme for various reactions in animals and plants[19].

Guanine is an essential component for the synthesis of guanine deaminase (or guanine aminohydrolase), a key enzyme that takes part in metabolic processes in animals, birds and reptiles converting oxypurines to uric acid[18].

Adenine has a variety of biological roles including synthesis of ATP, molecule that provides energy for most physiological processes, and FAD, a redox coenzyme, very important in several metabolic processes. Adenine is also a compound of NAD+, a redox coenzyme that provides electron transfer in all living cells and also acts as substrate for enzymes that add or remove chemical groups from proteins[18].

3.2. Self-assembly of RNA bases on metal surfaces

It has been demonstrated recently by STM that self-assembly of nucleobases and related molecules occurs on interaction with the surfaces of metals (Cu, Au and Si). Pro-chiral molecules such as nucleobases and related organic molecules were predicted to form homochiral domains when adsorbed on a metal surface[20], and several STM observations of the adsorption of proto-chiral molecules, such as adenine, on metal and graphite surfaces

have provided evidence for the formation of 2-dimensional chiral arrays or domains consisting only of a single chiral form[5,21,22,8]. Also, importantly, even in the absence of polymerases, base pairing occurring via hydrogen bonds could play an important role in polymerisation of the RNA precursor[5].

Adsorption of all four RNA bases on an Au (111) surface[23], uracil on Ag (111) surface[7], and adenine, guanine and cytozine on a Cu (111) and (110) surfaces[24,25] have been reported showing the molecules bonding to each other via hydrogen bonds and to the surface via the nitrogen lone pair[21].

Chen and Richardson[21] demonstrated that adenine bonded to the (110) copper surface via the amino nitrogen atom and formed chain homochiral structures. They suggested that the chains originate as a formation of homochiral dimers, linked by H-bonding interactions, and the diffusion of these dimers at room temperature leads to the separation of enantiomers on the surface and formation of short monochiral chains. These chains are formed along to directions on the surface – [1,2] and [-1,2], which are not high-symmetry directions but are related by reflection across the [001] direction (see Fig. 3.2). The direction of the chain corresponds to the chirality of each domain - molecules of one chirality are aligned along the (1,2) direction and rotated clockwise from [001] direction and molecules of the opposite chirality are aligned to (-1,2) direction and rotated anticlockwise from [001] direction. Chen and Richardson propose that the correlation between chirality of the adenine molecules adsorbed on the Cu (110) surface and the direction of the chain are driven not only by the configuration of intramolecular hydrogen bonds, but by the preference of the nitrogen atoms of the amino group in the adenine molecule to adsorb directly above a copper atom on the surface. Thus, the arrangement of copper atoms along the (1,2) direction constitute a chiral

template, which suits the interaction only with adenine chains of the correct chiral configuration[21].

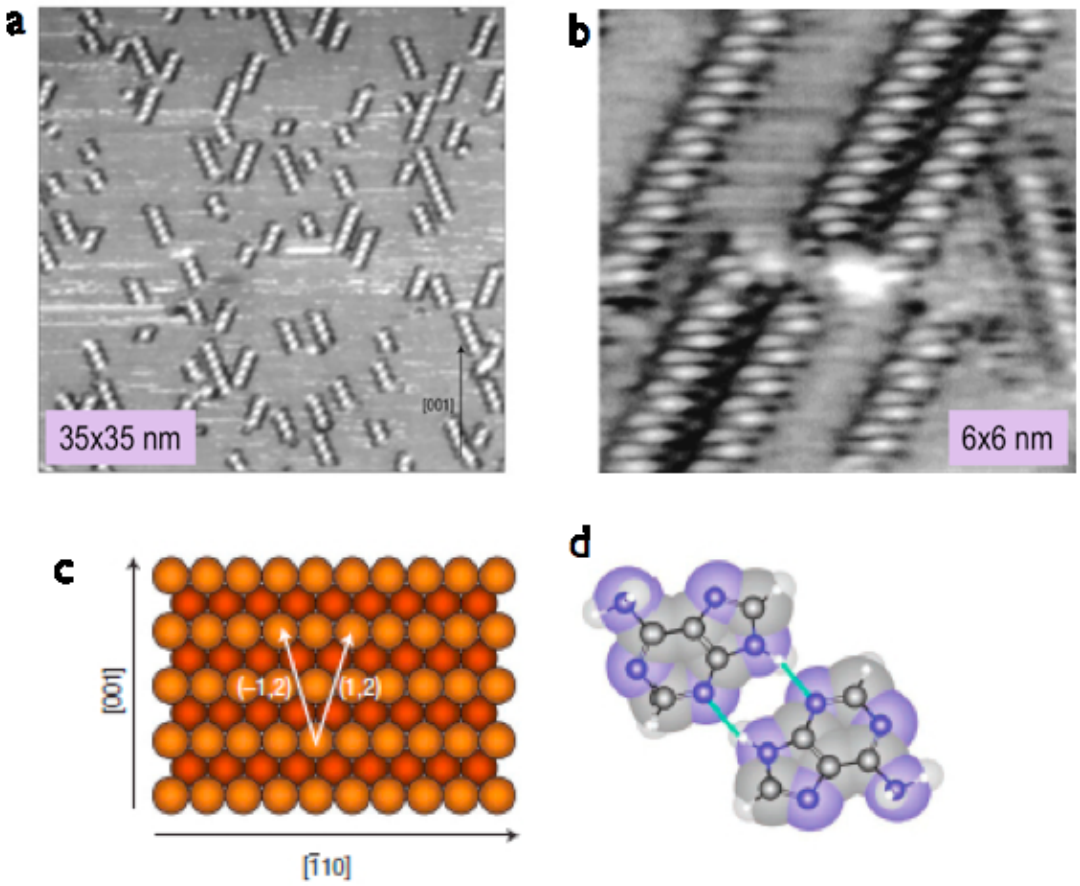

Figure 3.2. STM image of the Cu (110) surface with sub-monolayer coverage of adenine by Chen and Richardson in ultra-high vacuum[21]. (a) Medium size STM image of adenine arrays on Cu (110) surface; (b) Molecular resolution STM image of adenine on Cu (110) surface; (c) Model of (110) surface defining (-1,2) and (1,2) directions and showing the coordinate system directed along [1-10] and [001] directions; (c) homochiral dimer of two adenine molecules.

It was suggested by Tanaka et al.[26] that the relative inertness of the Cu (111) surface allows organic molecules to diffuse over the surface to assemble themselves spontaneously. Furukawa et al.[25] have investigated the self-assembly of three RNA bases (adenine, guanine, and cytosine) on the Cu (111) surface. The results demonstrated that adenine

forms parallel 1-dimensional chains and 2-dimensional hexagonal structures. Cytosine forms highly ordered parallel 1-dimensional chains and guanine forms 1-dimensional irregular structures[25].

Tao et al.[23] have investigated the self-assembly of same three RNA bases on the Au (111) surface. Adenine and guanine were reported to form "wormlike" polymeric aggregates; adenine aggregates were stretched along the Au [110] direction, guanine aggregates were disordered with respect to the underlying surface. Cytosine formed a highly ordered tilted lattice orientated at 30º with respect to the [111] direction[23].

The experiments on the self-assembly of the RNA bases on the Au (111) surface were continued by Kelly et al[27-31] more recently. The co-existence of two distinctly different homo- and heterochiral domains of adenine at the ambient temperature were observed for the first time at the liquid/solid interface and then in vacuum, and the findings supported by the *ab initio* density functional theory calculations. Adenine was found to form distorted honeycomb type domains on the Au (111) surface and the orientation of these domains is different within homochiral and heterochiral phases (see Fig 3.3).

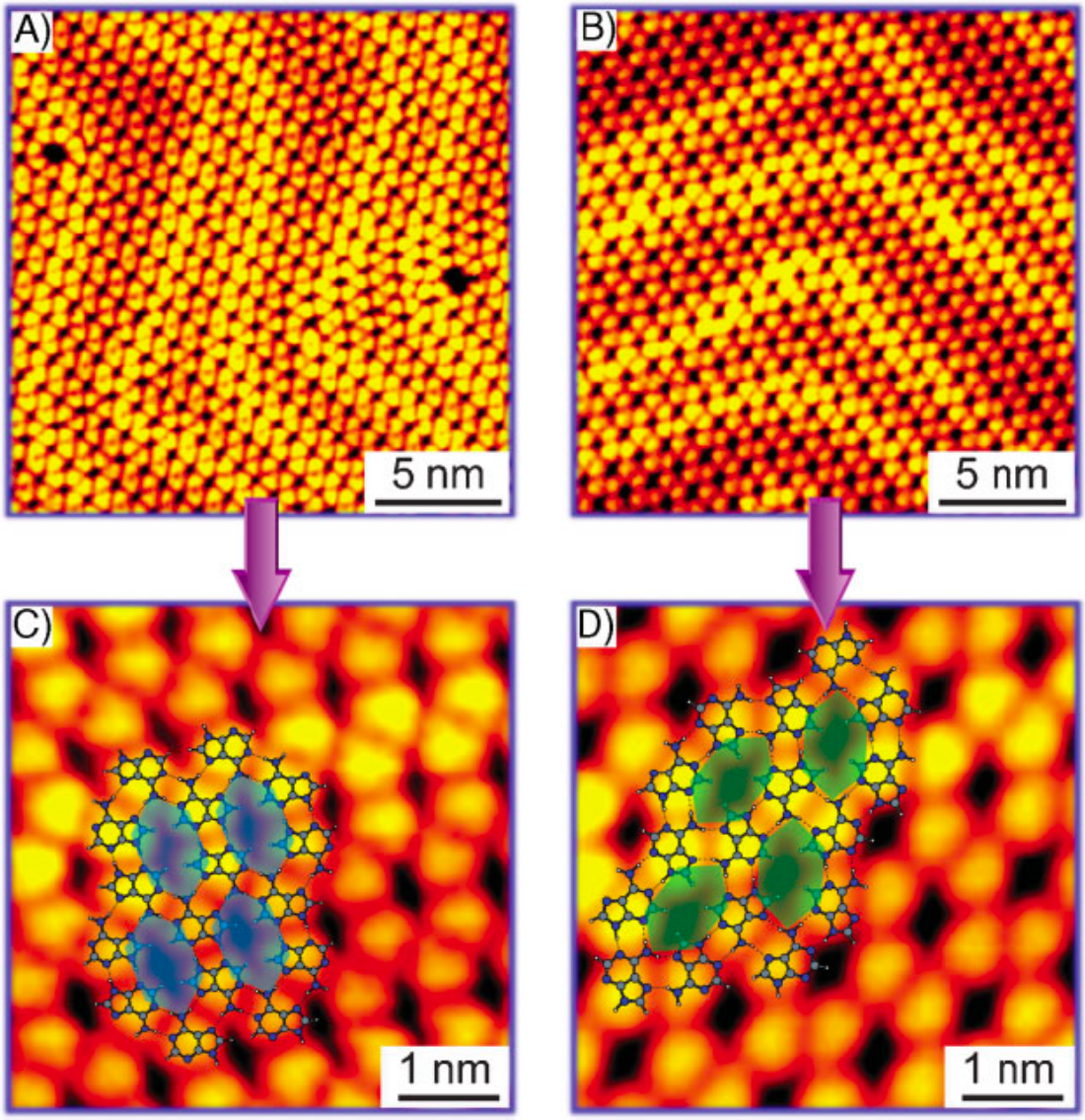

Fig. 3.3. STM images and theoretical models for the adenine monolayers on Au (111) surface by Kelly et al[31]. Images A and B show large areas of two different domains (homo- and heterochiral respectively), and images C and D show the close-up images with model overlays.

Adenine superstructures were also observed on Ag-terminated Si (111) surface. Adenine formed hexagonal networks, similar to the ones observed on Au (111) surface, constructed from homochiral dimers and stabilised by hydrogen bonds[32].

The structures formed by cytosine on the Au (111) surface were investigated by Wandlowski[33] on solid/liquid interface and, later, in vacuum by Kelly et al[34,35]. Cytosine was

found to form densely packed disordered 2-dimensional domains at high coverages and complicated transitional clusters consisting of linear zigzag arrangements and 5- and 6-ringed structures at lower coverages. At high coverages the 5- and 6-ringed structures are still present together with the elements of the hexagonal packing (see Fig. 3.4)

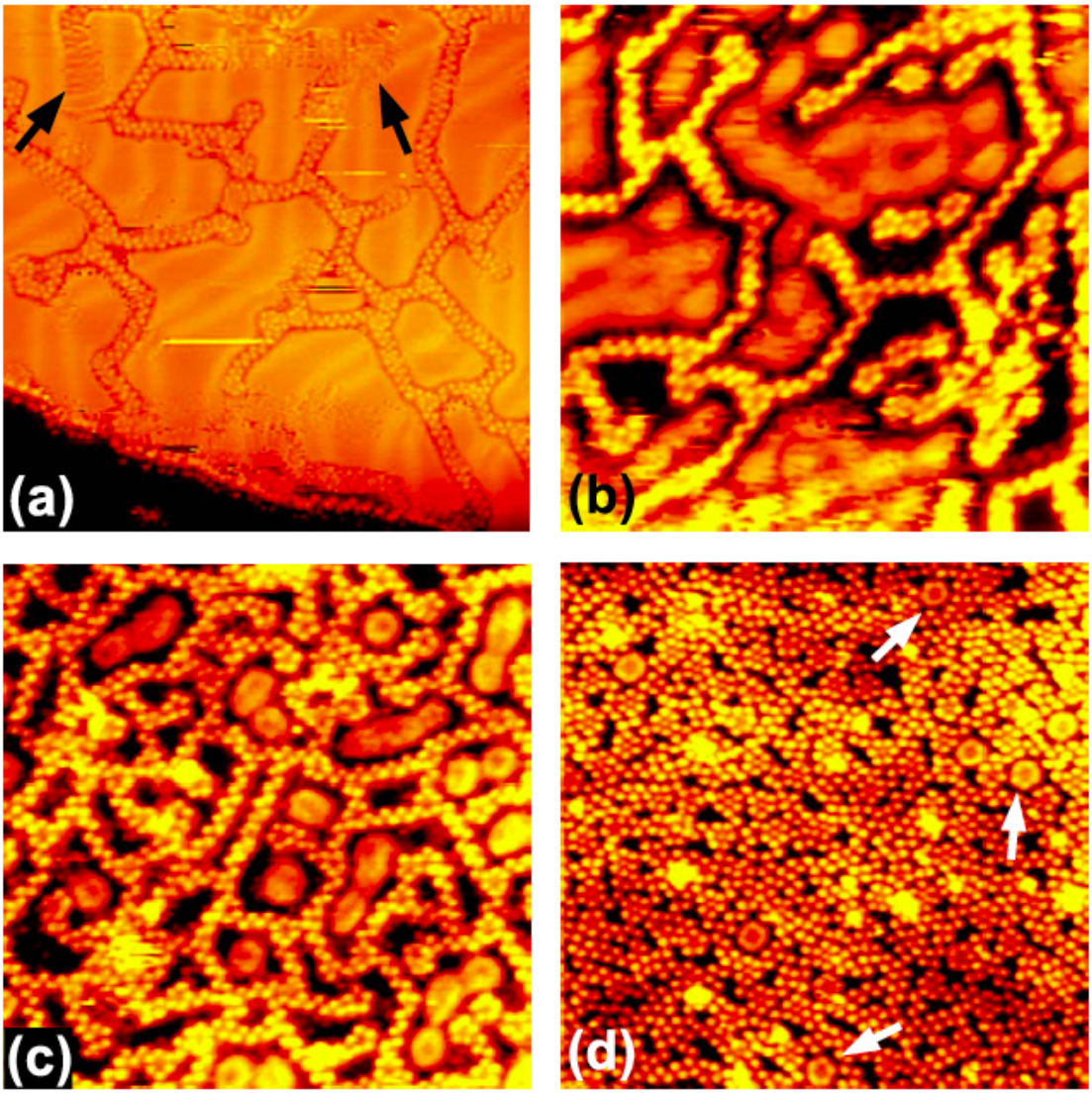

Figure 3.4. The cytosine structures by Kelly et al[34]. Image (a) shows the zigzig arrangements, image (b) shows the 5-fold rings, image (c) shows the 6-fold rings, and image (d) shows the high coverage structure, which is still disordered, and contains all the elements shown in the previous images (with 6-membered rings indicated by arrows), and the elements of the hexagonal packing.

The adsorption of guanine molecules on the Au (111) surface shows that the molecules

form well-ordered enantiometrically pure monochiral domains with a small “quartet” unit cell as shown in Figure 3.5. The prochiral guanine molecules self-assemble on the Au (111) surface in a way, that leads to the formation of heterochiral phase consisting of two monochiral networks/islands, which coexist on the surface at the ambient temperature.

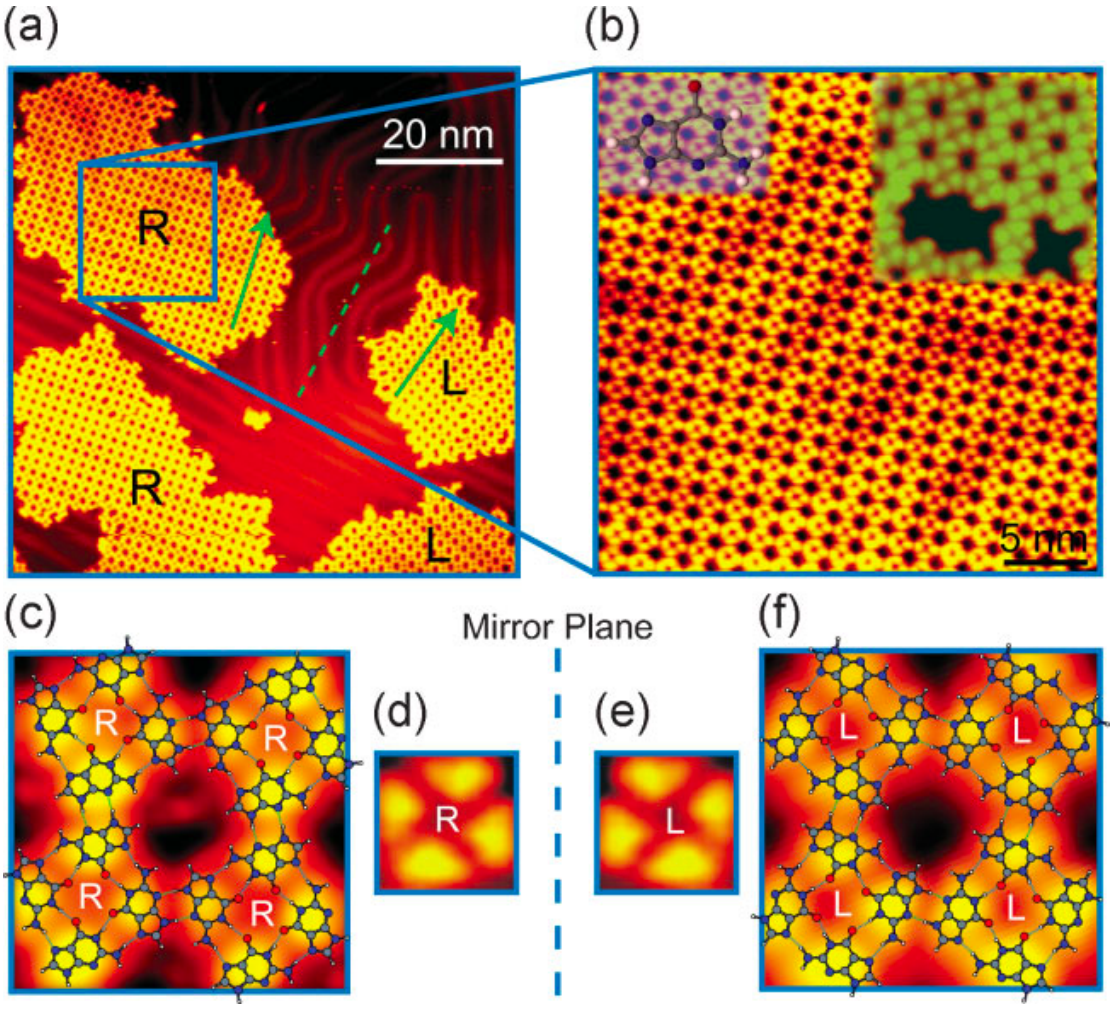

Figure 3.5. The guanine structures by Xu et al[36]. Image (a) shows the mirror phases of monochiral right (R) and left (L) quartet arrangements; image (b) shows an R guanine network, the R molecular orientation of guanine and a close up STM image of the R guanine network in the incert; image (c) shows the R guanine network superimposed with a theoretical molecular model showing hydrogen bonds; image (d) shows the unit cell of the R guanine network; image (e) shows the unit cell of the L guanine network; and image (f) shows a close up of the L guanine network superimposed with a theoretical molecular model.

After the subsequent annealing of the sample at 127 ºC, a new heterochiral phase was

created by the pure monochiral domains intermixing. In this new phase the pure monochiral "quartets" still exist but they are surrounded by the quartlets of opposite chirality as shown in Fig 3.6.

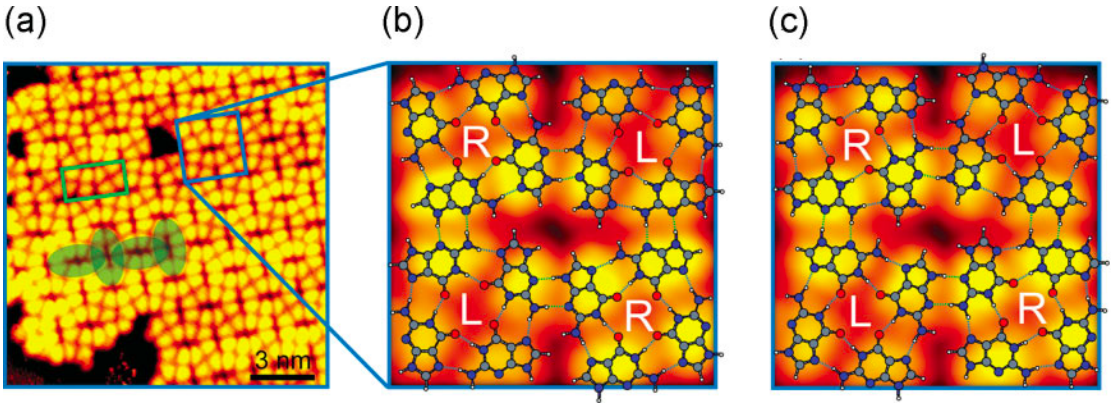

Figure 3.6. The guanine structures by Xu et al[36]. Image (a) shows the intermixed heterochiral phase of right (R) and left (L) quartet arrangements; images (b) and (c) show two alternative theoretical molecular models with hydrogen bonds, superimposed onto the same close-up STM image.

The heterochiral phase of guanine molecules of right and left orientation consists of "quartets" of alternating chirality, and this phase becomes energetically more favourable at higher temperatures[36]. The theoretical calculations yielded two atomistically different structures where guanine molecules are connected to each other in a different manner, which are indistinguishable in the STM images (compare Fig. 3.6 (b) and (c).

The co-adsorption of the two complementary RNA bases cytosine and guanine, as well as the paring on the two non-complementary bases adenine and cytosine, were observed on the Au (111) surface[37].

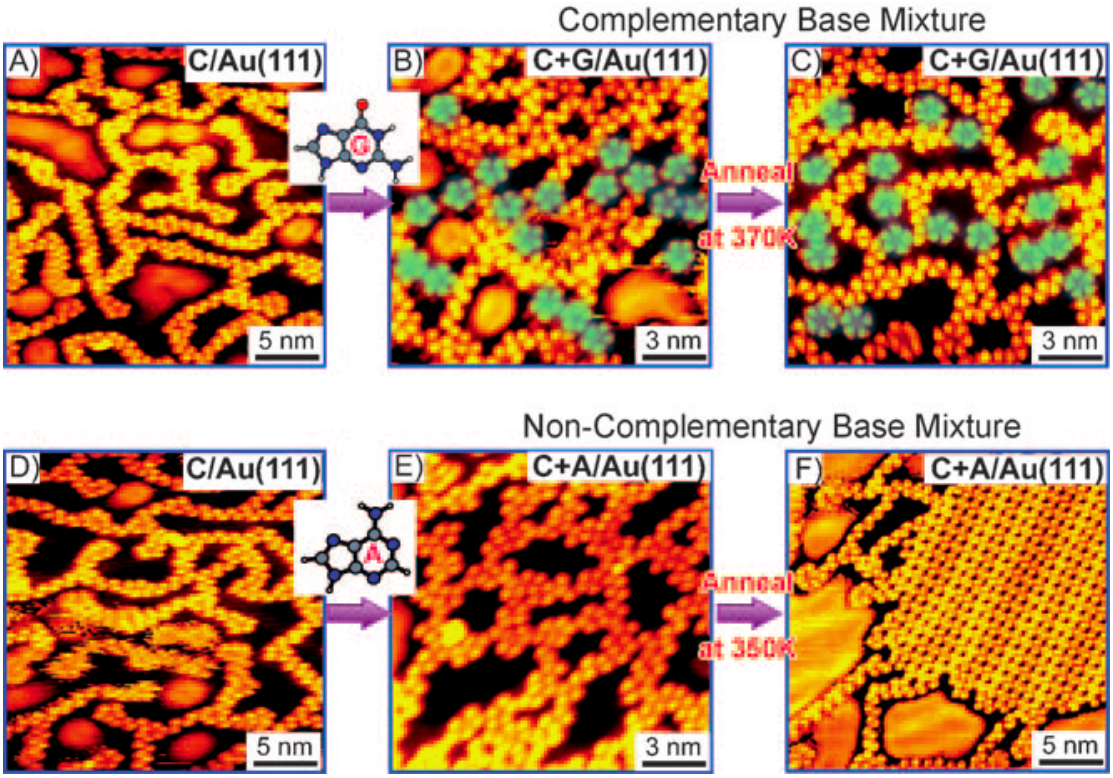

Fig. 3.7. STM images of complementary (guanine and cytosine) and non-complementary (cytosine and adenine) bases deposited on the Au (111) surface at room temperature by Otero et al[37]. Images (a) and (d) show the typical cytosine network, image (b) shows the evolution of the network as guanine molecules were added (sharp increase in 5-membered ring structure, shaded green); image (e) shows the evolution of the network as adenine molecules were added (disordered structure). After heating the complementary guanine-cytosine structure remained disordered and bi-molecular, the non-complementary adenine-cytosine structure segregates into two separate phases – typical cytosine 1-dimensional structure and adenine 2-dimensional regular network.

Interestingly, this study demonstrated that though both pairs form a mixed phase at room temperature, they behave differently when heated to 100 ºC with a complementary pair bi-molecular phase showing higher resistance to temperature.

It has been suggested that the Watson-Crick bond configuration, found in the DNA molecule, which has the highest stability (with stabilization energy of – 1.21 eV[30]) is the only configuration to survive the heating above 80 ºC[37]. This is an important experimental result as it could mean that the DNA (or RNA) backbone may not be a prerequisite for the

Watson-Crick pairing in DNA (or Hoogsteen pairing in RNA), and the surface-molecular interactions could be sufficient to start the processes of recognition and replication of the complementary base pairs.

Uracil self-assembly on the Ag (111) and the Cu (111) surfaces was recently studied by Papageorgiou et al[22]; who found that while Ag (111) is inert and does not act as a directional template, the Cu (111) surface acts both as a template and a catalyst. On the Ag (111) surface uracil molecules form stable 2-dimensional close-packed structures as shown in Figure 3.8. These structures are stabilized by hydrogen bonds, and composed of uracil molecules lying flat on the surface. The interaction between the surface and the uracil molecules is formed via the overlapping of the π orbital of the molecule with the delocalized charge of the metal surface, is very weak, and the long range ordering of molecules is poor. In contrast, on the Cu (111) surface uracil molecules form two co-existing complex structures at room temperature shown in Figures 3.9 and 3.10, which are accompanied by gradual deprotonation of uracil, as shown by the XPS study, and demonstrate significant coverage and annealing temperature dependence. According to the authors, the surface-mediated deprotonation at the N3 site and the subsequent electron localisation in the uracil molecule adsorbed on the Cu (111) can be interpreted as coordinative anchoring with a significant charge redistribution within the molecule[22]. At lower coverages ("tiare" phase) the intrinsically monochiral domains are formed by uracil molecules lying flat on the surface. At higher coverages (zigzag phase) uracil molecules were found to tilt at an average 65° angle to the surface in order to accommodate a higher packing density and bind to Cu atoms along the (1,-1,0) direction[22]. After annealing to 127 ºC tri-lobed structures, oriented along (-2,1,1) direction, are formed in a similar adsorption geometry to the zigzag phase (see Fig. 3.11). Papageorgiou et al propose that the electron charge of the uracil molecule is also

relocalised in this phase, and the uracil molecule is doubly deprotonated, tilted at an average angle of 60° and is chemically bonded to the Cu (111) surface via the O atoms.

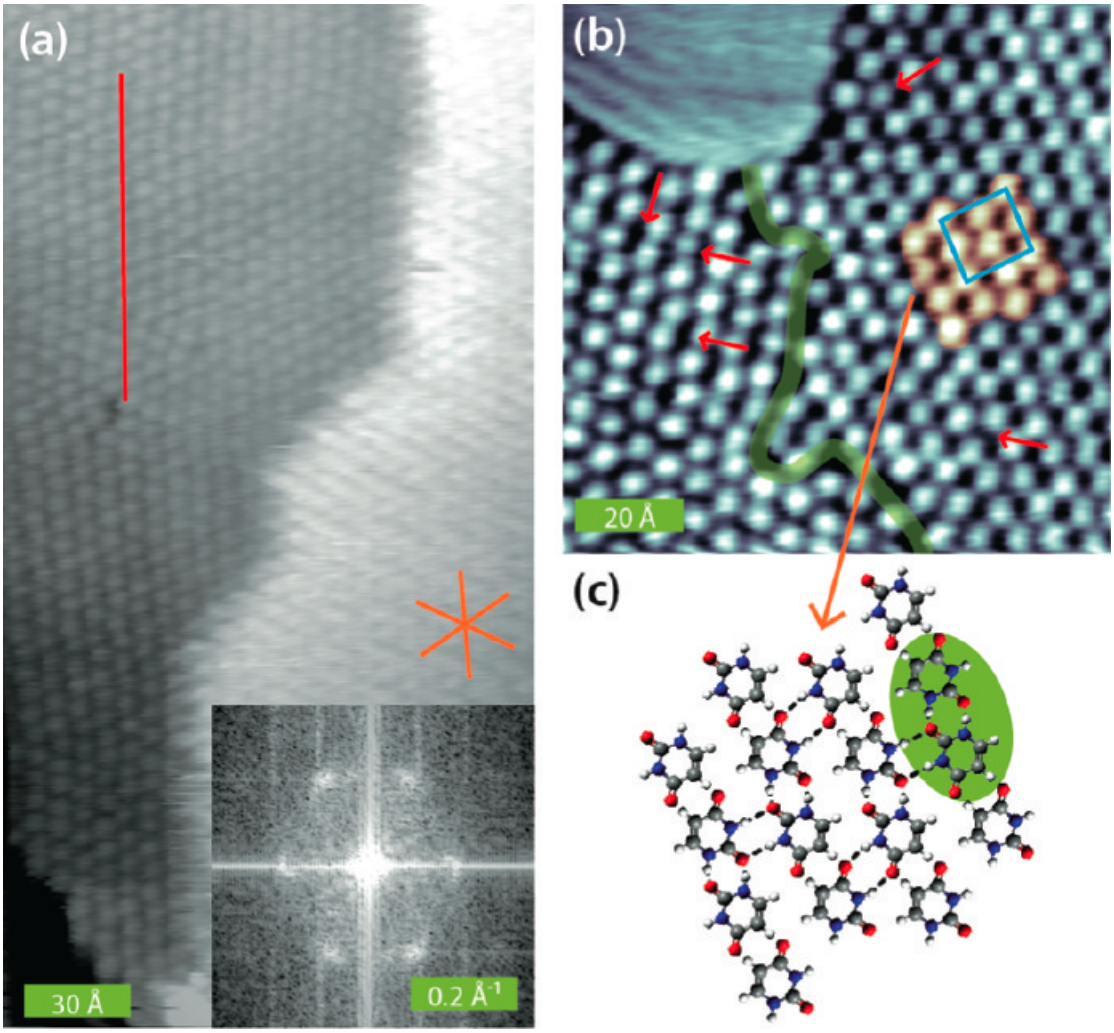

Fig. 3.8. STM images of the self-assembly of uracil on Ag (111). Image (a) shows the network overview, image (b) shows the close-up STM image with molecular resolution, and image (c) shows the tentative molecular model based on most stable uracil dimers (highlighted in green). Red marks and arrows indicate deviations from the molecular model, green line marks the domain boundary, and the Ag (111) symmetry axes are shown in orange in image (a).

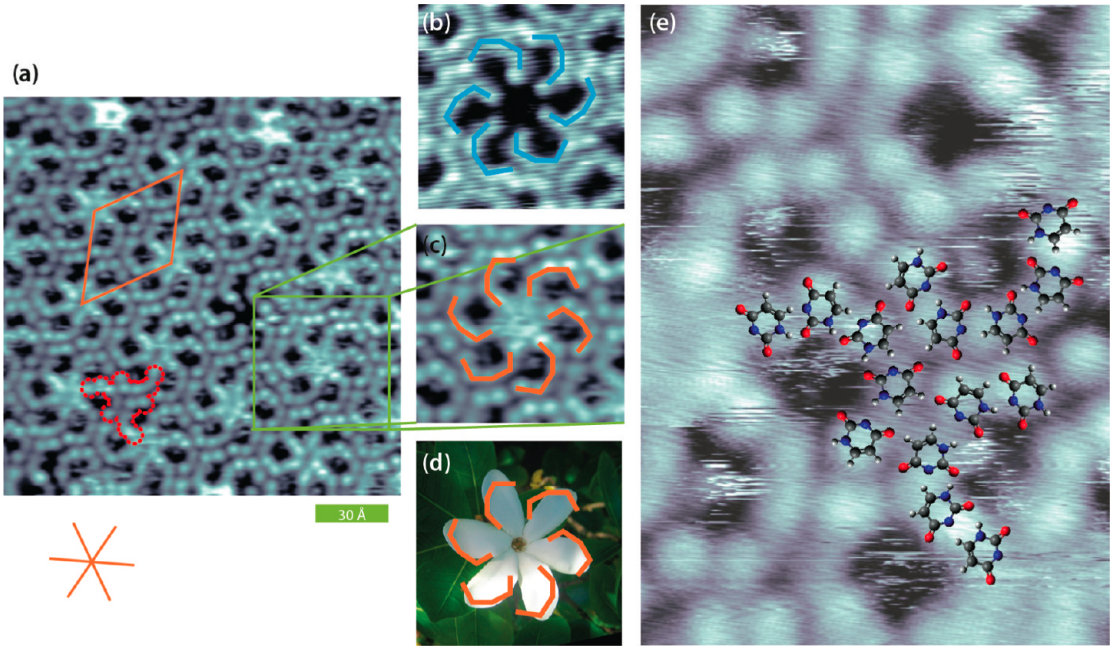

Fig. 3.9. STM images of 0.5 ML of uracil on Cu (111) at ambient temperature by Papageorgiou et al[22]. Image (a) shows the "tiare" network overview, image (b) shows the left-handed petalled domain with molecular resolution, image (c) shows the right-handed petalled domain, and image (d) is a photograph of a right-handed petalled flower for comparison. Image (e) shows the tentative molecular model based on most stable uracil dimers (highlighted in green). The unit cell and the Ag (111) symmetry axes are indicated in orange.

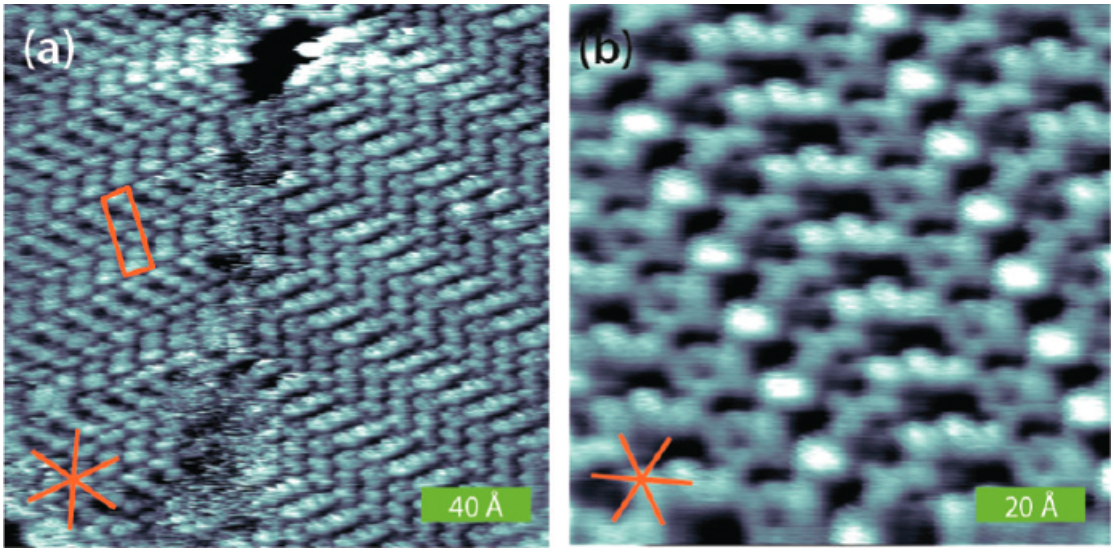

Fig. 3.10. STM images of a zigzag of uracil on Cu (111) formed at ambient temperature at hight coverages (0.8-1 ML) by Papageorgiou et al[22]. Image (a) shows the network overview, image (b) shows the detailed STM scan with molecular resolution. The unit cell and the Ag (111) symmetry axes are indicated in orange.

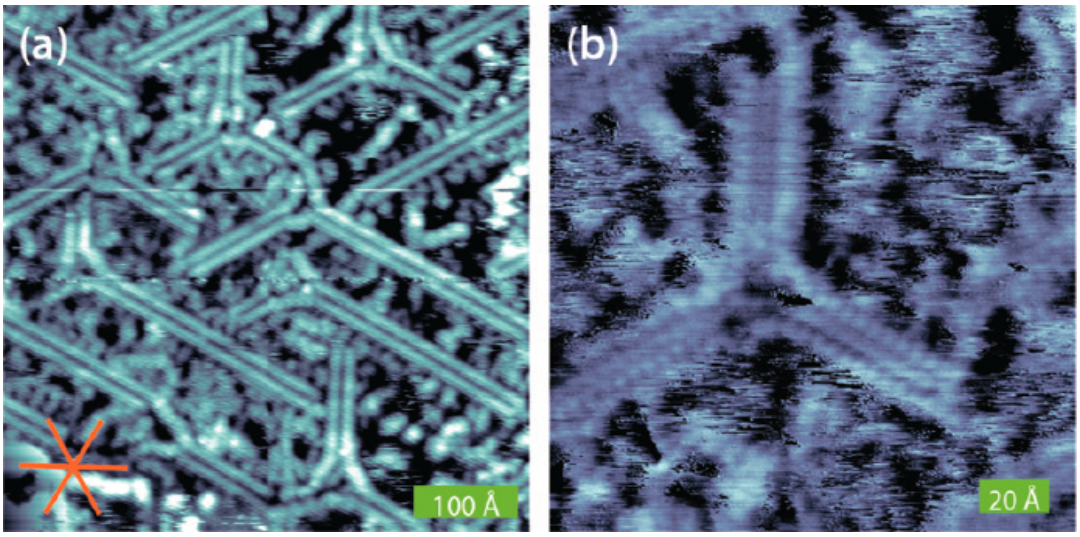

Fig. 3.11. STM images of a tri-lobed structure of uracil on Cu (111) formed at after annealing at 120 ºC height coverages (0.8-1 ML) by Papageorgiou et al[22]. Image (a) shows the network overview, image (b) shows the detailed image of the structure oriented along <-2,1,1> direction. The unit cell and the Ag (111) symmetry axes are indicated in orange.

3.3. Self-assembly of RNA bases on mineral surfaces

High-resolution molecular imaging and manipulation of nucleobases, other amino acids and DNA oligomers has been successfully carried out on perovskite ($SrTiO_3$), molybdenite (MoS_2) and graphite in ultra-high vacuum conditions by STM[38]. The experiments carried out on a graphite surface and theoretical calculations have demonstrated that even chemically inert surfaces influence the electronic structure of organic molecules[39].

Adenine is believed to chemisorb on pyrite surfaces via its lone nitrogen pair; this process was predicted theoretically and has been experimentally proved by sigma-potential measurements, photoemission and soft X-ray photo absoption spectroscopy[40]. However, I do not know yet of any successful STM investigations of self-assembly of adenine or other

nucleobases on the surfaces of pyrite.

Fraser et al.[41] have published results on self-assembly of adenine on nanostructured (001) surfaces of Nb-doped perovskite. This STM investigation demonstrated poor ordering at low density of adenine. However, highly ordered adenine monolayers were observed at higher densities distributed on the surface with agreement to underlying nanostructures.

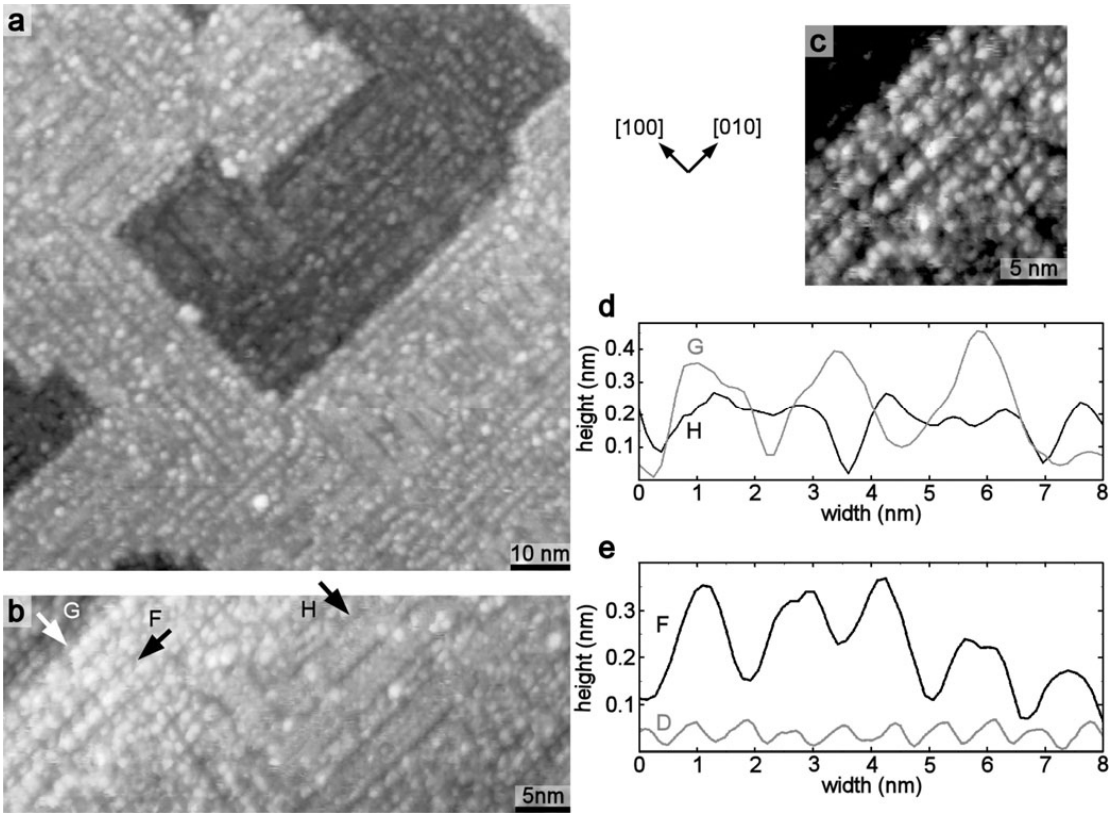

Figure 3.12. STM images of adenine on the nanostructured (001) Nb-doped perovskite by Fraser et al[41]. (a) Typical STM image of a monolayer of adenine assembled on diline and triline domains; (b) An STM image illustrating structural features of the adenine ordering on the surface nanostructures; (c) A close-up high-contrast STM image showing the surface ordering of adenine with molecular resolution; (d) and (e) The grey and black profiles are relative heights and are drawn from where the arrows G and H (d) point in image (b), and from where the arrow F (e) points in image (b).

STM observations of the self-assembly of adenine on graphite have demonstrated adenine organisation in lateral bi-layered island-type superstructures in which the upper layer has a

slightly larger unit cell and is slightly rotated with respect to the lower layer[38]. Freund et al.[39] and Edelwirth et al[42] have published STM images of adenine monolayers on graphite and suggested that the monolayers and the bilayers similar to those described above are close-packed structures of adenine dimers, containing two dimers in a unit cell with a symmetry group p2gg.

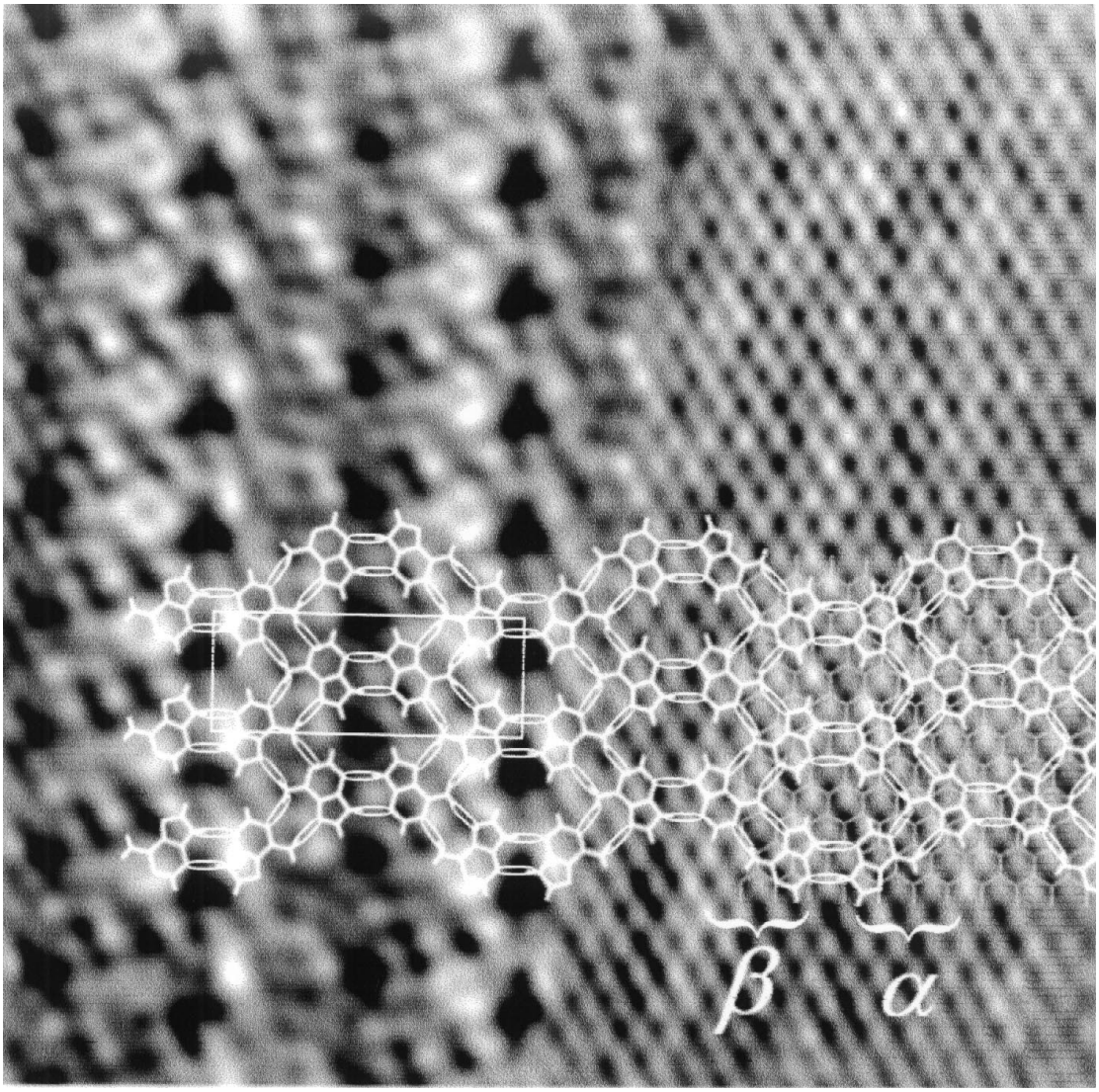

Figure 3.13. A lowpass filtered STM image of a monolayer of adenine on a graphite (0001) surface. By decreasing the tunneling resistance in the middle of the image while scanning it was possible to visualize directly the underlying graphite lattice. The estimated molecule positions, the hydrogen bonds and the unit cell are indicated. Because of the different positions (a and b) of the molecules relative to the substrate atoms the image displays a moire´ pattern[42].

More recently Xu et al[43] observed the co-adsorption of two complementary RNA bases, guanine and cytosine, organised into well-ordered rows formed from Watson-Crick pairs in 1-octanol solvent (see Fig. 3.14). The intermolecular interactions were confirmed by self-consistent charge density-functional based tight-binding (SCC-DFTB) calculations. The bi-molecular structure observed is significantly different from pure cytosine and pure guanine molecular arrangements published by the same authors[43] and shown in Figures 3.15 and 3.16 respectively. Pure cytosine molecules arrange in rows similar to those observed in domains I and II in the co-adsorption experiment (see Fig. 3.14), pure guanine molecules arrange in a quasi-square networks. Domain III shown in Figure 3.14 is recognized is a mixed cytosine-guanine phase and the lowest energy configuration identified for this phase is a Watson-Crick pair with a binding energy of 0.9 eV, which makes it the most preferential dimmer to form in the areas where both molecules are present on the surface.

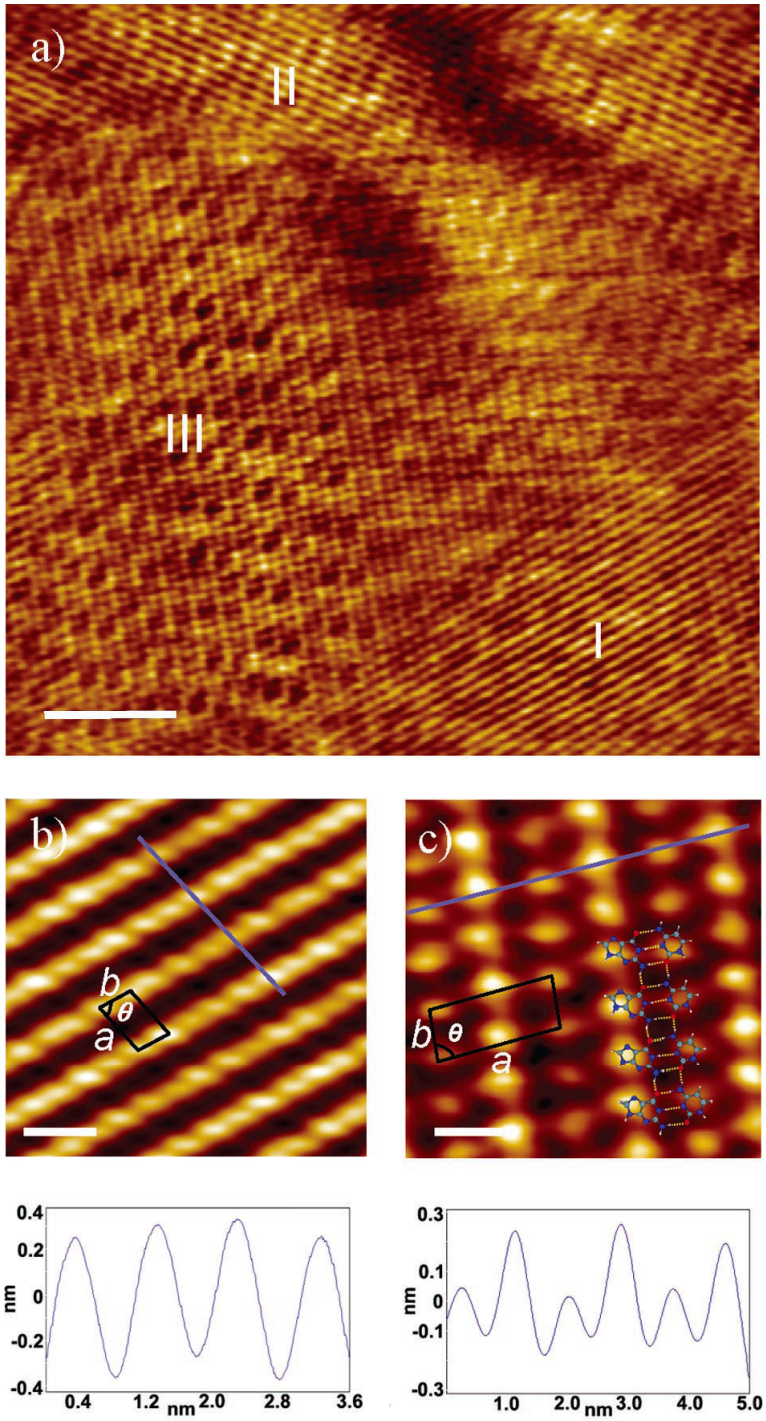

Figure 3.14. Co-adsorption of guanine and cytosine at the 1-octanol/HOPG interface by Xu et al[43]. (a) An STM image, showing three different domains, marked I, II and III (scale bar 10 nm). (b) Close-up STM image of the domain I (scale bar 1 nm, a unit cell indicated on the image). (c) Close-up STM image of the domain III (scale bar 1 nm, a unit cell and a molecular model indicated on the image). Height profiles along the blue lines in (b) and (c) are shown at the bottom of the figure.

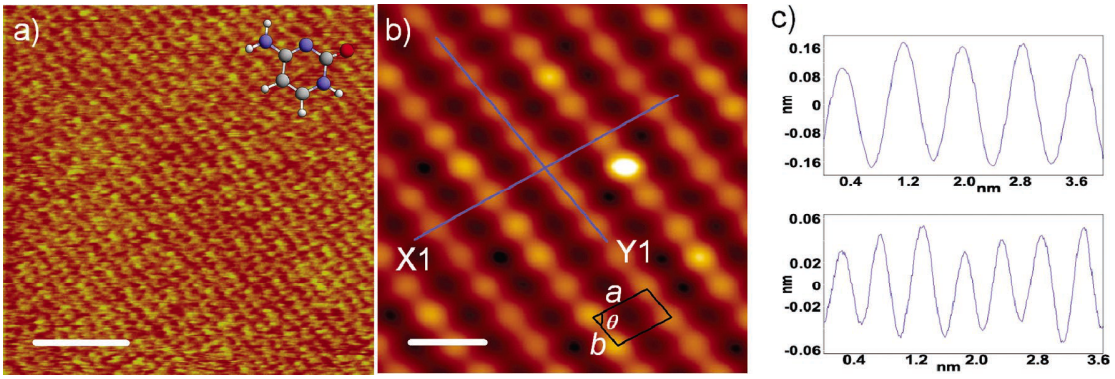

Figure 3.15. A cytosine monolayer at the 1-octanol/HOPG interface. (a) Typical STM image (scale bar 5 nm); (b) Correlation-averaged close-up STM image (scale bar 1 nm, a unit cell is indicated); (c) Height profiles along the indicated lines X1 (top) and Y1 (bottom) are shown on the right of the figure.

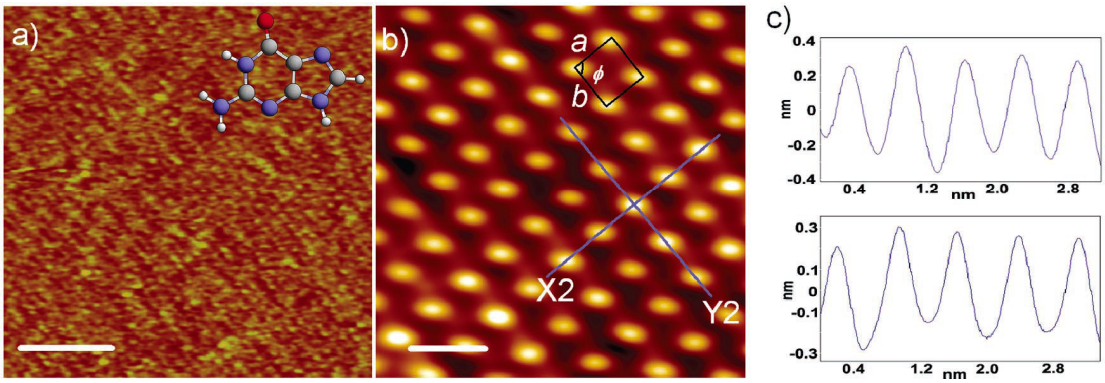

Figure 3.16. A guanine monolayer at the 1-octanol/HOPG interface. (a) Typical STM image (scale bar 5 nm); (b) Correlation-averaged close-up STM image (scale bar 1 nm, a unit cell is indicated); (c) Height profiles along the indicated lines X2 (top) and Y2 (bottom) are shown on the right of the figure.

Self-assembly of adenine, guanine and uracil was also studied on molybdenite (MoS_2) surface[44,45]. The STM images of the 2-dimensional structures of adenine molecule on MoS_2 showed the enantiomorphic chiral structures as shown in Figure 3.17.

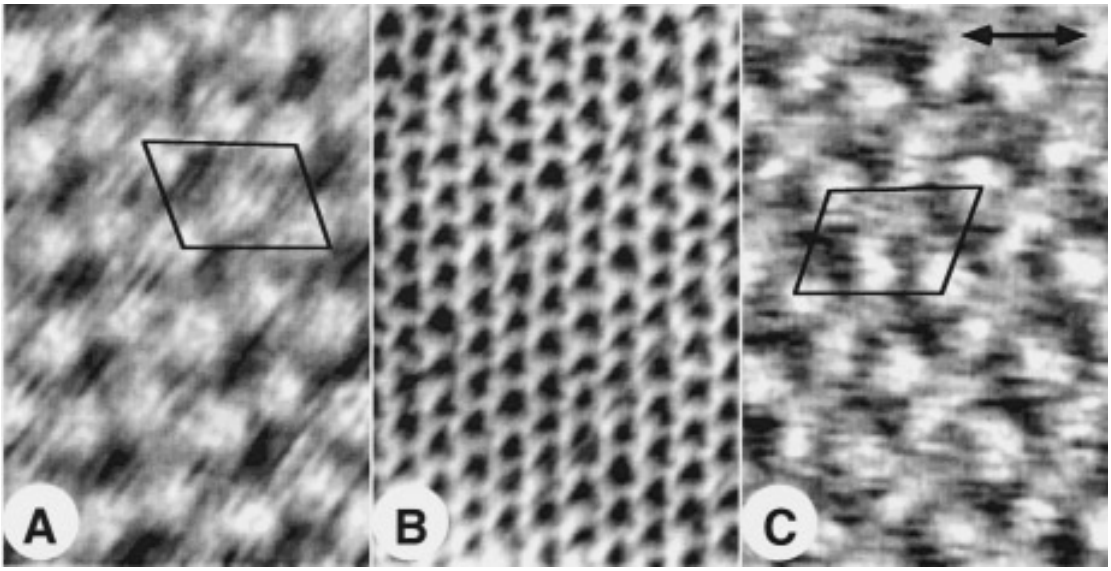

Figure 3.17. An adenine monolayer on the MoS_2 surface. (a) An STM image of an ordered array of adenine molecules. (b) The STM image of the underlying molybdenite substrate showing the uppermost sulfur atoms, the distance between atoms is 3.16 Å. (c) The second STM image of adenine molecules on the MoS_2 surface that is a mirror reflection of image (a). All STM images shown here were low-pass filtered, the scale bar represents 1 nm.

The STM images of the self-assembly of uracil on the MoS_2 showed a herring-bone pattern, which possibly originated from the initial hydrogen bonded dimmer formation as predicted by theoretical calculations of planar arranged uracil molecules on the MoS_2 lattice (see Fig. 3.18). These proposed molecular configurations required some skewing to accommodate the observed substrate-dependant networks but the extent of skewing was minor and allowed by the flexibility of the hydrogen bonds[45]. The structures resemble closely the crystal structures of 3-dimensional uracil crystals.

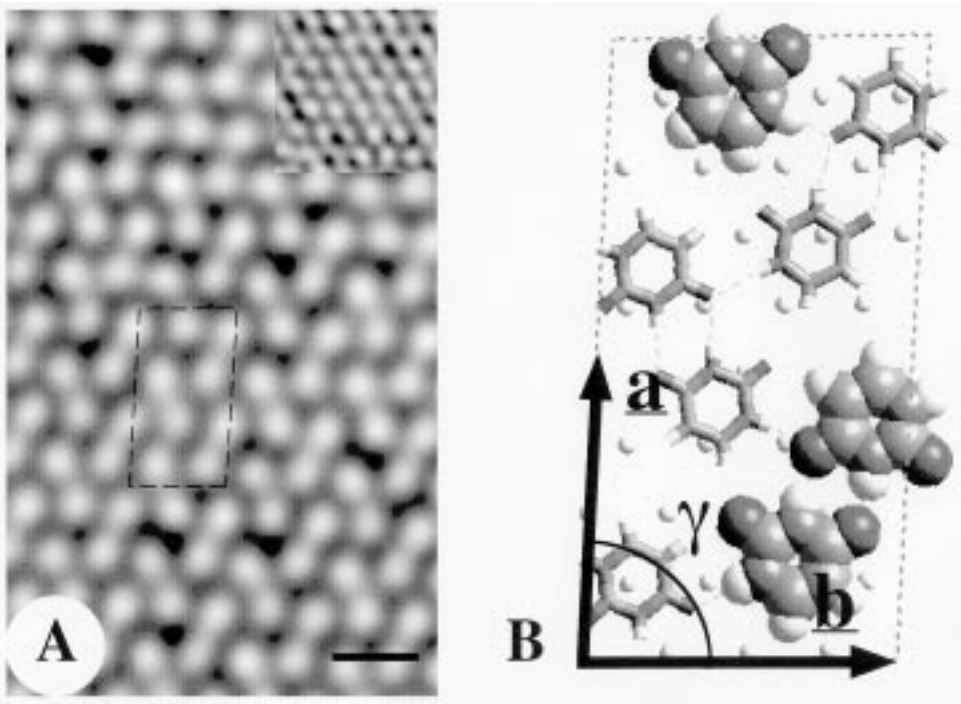

Figure 3.18. Uracil self-assembly on the MoS_2. (a) A lowpass filtered STM image of uracil monolayer on MoS_2, the underlying MoS_2 structure is shown in the inset. The black scale bar represents 1 nm. (b) An energy minimized model of the structure and molecular arrangement of uracil molecules on the underlying MoS_2. The lattice vectors a and b describe the primitive unit cell and are 1.27 and 1.23 nm respectively, the dashed lines represent hydrogen bonds.

The self-assembly of the mixture of the two RNA non-complementary bases, uracil and guanine, on MoS_2 was also investigated by STM on the liquid-solid interface. The results showed that two bases coexist on the surface as two separate phases and form regular close-packed arrangements. Occasionally, the semi-stable disordered regions were observed, presumably, of the bi-molecular aperiodic structure. Sowerby et al[45] suggested that these regions probably consist of uracil with a small guanine impurity, however, it was not possible to distinguish between the two bases based on the STM images alone (see Fig. 3.19).

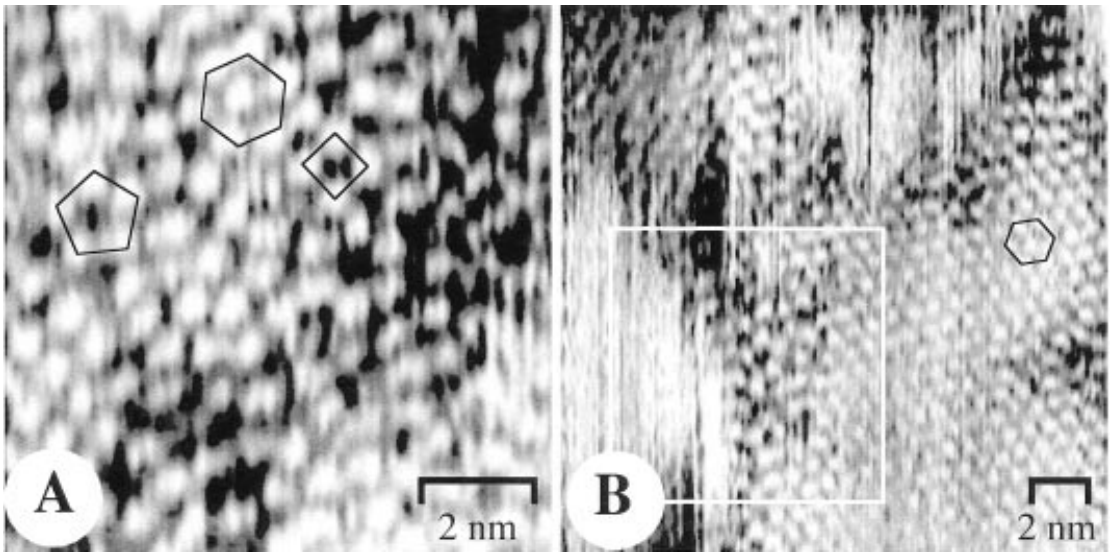

Fig. 3.19. STM images of a mixture of uracil and guanine on MoS_2 by Sowerby et al[45]. (a) A semi-stable disordered region of the possible bi-molecule structure showing 4-folded, 5-folded and 6-folded symmetry molecule arrangements. (b) A STM image of the same area showing the stable ordered uracil monolayer, the changes have occurred after a few scans.

3.4. Summary

This chapter has introduced the RNA bases as molecules and their role in the biochemistry of the living systems, and the current state of knowledge regarding the self-assembly of the RNA bases on mineral and metal surfaces. The adsorption of pure RNA bases and their complementary and non-complementary mixtures on some metal and some mineral surfaces has been studied by the direct observation in the UHV and liquid STMs and the findings described above. The consensus is that the resulting self-assembled structures are stabilized by hydrogen bonds and some of the proposed models were supported by theoretical calculations. Some of the structures described in this chapter are chiral, though the mechanism of the chiral selectivity is not yet clear, and it was suggested that one of the bi-molecular structures utilizes the Watson-Crick bonding arrangement as found in DNA molecule. The Hoogsten configuration of the hydrogen bonds in such structures as found in

RNA molecule has not yet been reported.

Understanding of the process of the self-assembly of ordered structures formed by the RNA bases on the inorganic substrate and stabilized by the hydrogen bonds not only by the theoretical modeling but also by the direct observation in the STM is very important. Such processes might have played a role in the early formation of the RNA precursor, and this perspective adds considerable interest to the experiments. I would like to note that there is no complete study of the self-assembly of RNA bases on any surface mentioned in this chapter. The self-assembly of the three RNA bases, adenine, guanine and cytosine on the Au (111) surface have been described in some detail recently but the self-assembly of uracil and complementary uracil-adenine pair has not yet been published. The effects of the degree of molecular coverage and the low-temperature annealing on the self-assembled networks have been barely touched upon. In this thesis I have made an attempt to provide a large comprehensive study of the self-assembly of pure uracil and uracil-adenine pair of the surfaces of Au (111) and pyrite (100) at the range of coverages, adenine-uracil ratios and annealing temperatures to make a contribution to the current knowledge of the self-assembly of the RNA bases on surfaces.

Chapter 4

"RNA world", "iron-sulphur world", and the origin of chirality

It is always difficult to define what it meant by word "life" and what, therefore, can be considered a "living system". To avoid possible misunderstandings I suggest that a chemical system can be called "living" if it fulfills two criteria – it has to be able to self-replicate and to transfer its molecular information to its successors fairly faithfully but can make occasional accidental errors. RNA molecule answers to these minimal requirements, so, if we accept this definition of life, we need to look into the RNA formation to answer the question "How could life originate?", and we could think of the Earth 3.8 billion years ago as an "RNA" world.

The problem of the origin of life on Earth has been discussed for a long time and there is no shortage of different scenarios. There are three main trends in attempts to explain the origin of large prebiotic molecules, such as RNA, each backed by some experimental data: synthesis in a the prebiotic soup, input in meteorites and synthesis on mineral surfaces (clay minerals or metal sulphides)[6]. There is no particular preference for either theory in the scientific world and I do not know of any work that would put one of these scenarios beyond doubt.

4.1. Origin of life: the hypotheses

The prebiotic soup hypothesis originated from the now widely accepted Urey-Miller experiments[46], which were the first attempt to recreate the prebiotic synthesis of amino acids in laboratory conditions. In these experiments the mixture of methane, ammonia and hydrogen was subjected to an electric discharge and the products placed in an aqueous solution. The experiments showed that a substantial percentage of carbon was incorporated into a small group of organic molecules, some of which were naturally occurring amino acids, aldehydes, hydrogen cyanide and ammonia, which produce glycine via the Strecker reaction[46]. Following the same route more amino acids were synthesized – adenine from cyanide and ammonia[47], and cyanoacetylene (source of pyrimidine bases uracil and cytosine) from hydrogen, cyanide and ammonia[48] among others, which indicated the plausible formation of a prebiotic soup of biomonomers on early Earth. The main critique of this hypothesis is that the atmosphere of the early Earth could never have been reducing enough to allow the reactions of the Urey-Miller experiments to take place[49]. Also, though this hypothesis provides a possible answer to the synthesis of the small amino acids, that compose modern RNA, it does not offer a scenario for the formation of the RNA precursor as the large macromolecules are destroyed by hydrolysis in aqueous solutions.

The input in meteorites hypothesis originated from the discovery of the substantial amount of organic carbon in meteorites and comets[50]. It is well established now that before the biochemical evolution on Earth, chemical evolution took place in the dense clouds in the interstellar space and simple prebiotic molecules (including nucleobases) were created there. The synthesis is thought to be initiated by collision of high energy cosmic ray particles with hydrogen and helium by photochemical processes, and, to prove this hypothesis,

comets and carbonaceous meteorites show substantial amounts of organic material, including some amino acids and nucleobases[1]. The main critique of the impact hypothesis is the question whether the prebiotic material would have survived the heating upon entry into the atmosphere and the subsequent collision with the Earth's surface. And again, this hypothesis does not provide a scenario for the formation of an RNA precursor.

Neither of the two theories described above offer an answer to the synthesis of the large prebiotic macromolecules such as RNA, however, it is possible that both of them could have collaborated in delivering material for the third hypothesis, by providing the building blocks for the formation of the RNA precursor on a mineral surface. I suggest that the fragments of extraterrestrial organic material reached the surface of the early Earth and had stocked the prebiotic soup, thus allowing the biochemical evolution to begin. If the water was the medium that carried prebiotic molecules in of the early stages of the prebiotic synthesis, mineral surfaces could have acted as catalysts, and the self-assembly of macromolecules could have taken place on these surfaces. Adsorption might have provided a high local concentration of prebiotic molecules necessary for the self-assembly process to commence and high-energy defect sites of the mineral surfaces may have been the place where the synthesis started. Subsequent chemical reactions and molecular selection would follow until the first self-replicating RNA and RNA-coded proteins appeared, which eventually led to the beginning of the biological evolution via the last universal common ancestor (LCA), and to the life as we know it today. The existence of the LCA was deduced from the uniformity of biochemistry in modern living organisms and the detailed analysis of protein sequences suggests that LCA had a complexity similar to a modern bacterium and lived 3.2-3.8 billion years ago[51].

This third hypothesis, the self-assembly of the large prebiotic molecules on mineral surfaces, is the process that in my opinion could have led to the creation of the "RNA" world. The physical isolation of the prebiotic molecules from the environment and their accumulation and subsequent self-organisation via series of self-contained redox reactions could be the necessary requirement for the evolutionary transition from abiotic molecules to the first living systems. The minerals that were considered as possible catalysts and templates in this hypothesis are iron sulphides, such as pyrite[5], and clay minerals, such as montmorillonite[52]. One of the most important aspects of this hypothesis is the availability of minerals, involved in such mineral-promoted reactions, as for a surface catalytic reaction an abundance of the mineral is required, for example, for the large number of the available active surface sites. On early Earth, besides weathering processes, the clay minerals would be formed in sufficient quantities on the ocean floors during the alteration of oceanic crust and in submarine hydrothermal systems in low temperature zones[4]. The clay minerals could have had a role in the synthesis of the prebiotic molecules as a template for reaction precursors and a source of ammonium, necessary for the synthesis and the successful experiments of the self-assembly of the long oligonuleotides from the shorter ones[53]. Pyrite and other metal sulphides are formed in substantial quantities in hydrothermal systems at ocean ridge spreading centres[54,55]. In such systems, three minerals control the redox conditions on the surface of the rocks: pyrite (FeS_2), pyrrhotite (FeS) and magnetite (Fe_3O_4)[55-57]. This process is believed to have commenced immediately after the formation of Earth's crust[3] and has not changed fundamentally since. Metal sulphides, are also formed in epitherial and magmatic systems, and are widely spread on Earth. Surface defects are common in sulfides and are important as surface reaction sites[58]; these minerals have been shown to promote catalyzing reactions in which simple organic molecules were converted

into more complex ones[53]. A surface of a particular sulphide mineral, pyrite was named as a likely candidate for such processes[59], and it was decided to concentrate on the surfaces of pyrite in this thesis to test experimentally its suitability as a potential mineral surface to act as a template and a catalyst for the formation of an RNA precursor.

The catalytic abilities of pyrite determined its selection for this study. The first organisms are believed to have been autotrophs and to have converted small non-biological molecules with biogenic elements (C, N, O, S, H and P) into biomolecules. Such reactions require additional energy for overcoming the so-called "activation barrier"[58] and therefore they need a catalyst. Biocatalysts that are known today include protein enzymes containing sulphur and transition metal clusters as active sites[60]. The discovery of such clusters and their apparent importance in microbial biosyntheses and processes of metabolism in bacteria has led to two quite similar hypotheses, in which the possibility that sulphide minerals could catalyse the formation of prebiotic molecules was first suggested.

4.2. Self-assembly in the "RNA world" hypothesis

Though there is no agreement about the source of prebiotic molecules on the early Earth, there are, as discussed above, several hypotheses[3]. Little, however, is known about the evolutions of the self-replicating systems, let alone the formation of living cells.

The biochemical evolution debate was inspired by the famous work of Cairns-Smith[61] and has been carried on for the last thirty years, but to date no agreement has been reached as to whether the early chemistry was totally unrelated to modern biochemistry and has disappeared without a trace, or whether abiotic components were incorporated into the

biochemical processes at a very early stage and the biochemistry did not change in principle. De Duve offers a plausible hypothesis that a catalysed chemical process was at the start of life and it was replaced by a biogenic process performed by enzymes at a later stage when the RNA was already formed[62].

RNA, a macromolecule with both information storage and catalyzing functions, is believed by some to be the first living system on Earth. The constituents of RNA are the nucleobases (adenine, guanine, cytosine and uracil), phosphate groups and the sugar ribose. It is thought likely that during the initial process of RNA construction, more sugars, purines, pyrimidines and other heterocyclic molecules were involved, and extant RNA might be a result of a slow process of molecular selection based on the stability of resulting oligonucleotides or their ability to act as templates and thus be reproduced, or both[63].

Schwartz and Wachtershauser have independently introduced a notion of an RNA precursor – a "nuleoacid-like polymer" or "tribonucleic acid" that included nucleobases and was attached to a surface bonding backbone[3]. One such polymer, PNA (peptic nucleic acid), has been created by Witting et al.[64] The backbone of PNA is based on a repeating peptide unit and nucleobases are attached to the backbone via nitrogen atoms. This molecule has been demonstrated to undergo self-assembly processes and, though it does not carry information, this fact reinforces the suggestion that an RNA precursor might have been able to replicate sequences of nucleobases, which is a requirement for evolution[3]. There is, however, a problem with naming the PNA an RNA-precursor as the PNA monomers cyclise when activated; this would make oligomer formation practically impossible under prebiotic comditions[54].

The self-contained world, where RNA molecules fulfilled the roles of genetic material and enzyme-like catalysts, probably did exist. But, for such a world to exist there should be a pathway for synthesis of the first genetic monomers. Though, it has been possible to find sequences that catalyse a wide variety of reactions from pools of random DNAs[65], it is very difficult to imagine that the RNA self-organised itself spontaneously into a self-contained replicating system. If the RNA world has evolved gradually through self-organisation, there must have been a simpler, possibly shorter RNA-precursor at the beginning of it, and a source of activated nucleobases initially to assemble this first macromolecule from. A mineral surface with the ability to adsorb and to catalyse nucleobases could fulfil this role. The surface of pyrite looks like a plausible candidate as the reaction between iron (II) sulphide and hydrogen sulphide, that yields pyrite and hydrogen, could provide enough free energy necessary to activate the adsorbed nucleobases[6]. The assumption that the entire metabolic cycle could take place on the surface of pyrite, acting simultaneously as the source of building material and the "sink" for the products of the reaction (which are thus exempt from the destruction by hydrolysis) is the essential part of the hypothesis I am going to introduce next, which became known as "iron-sulphur world" theory.

4.3. "Iron-sulphur world" theory

Wächtershäuser proposed an iron-sulphur world theory in 1988[5]. He suggested that the formation of pyrite could provide the necessary energy for the first conversion of a small abiological molecule into a biomolecule according to the reaction:

$CO_2(aq) + FeS + H_2S \rightarrow HCOOH + FeS_2 + H_2O$[5].

The small organic molecules that may have originated on the surface, presumably interacted with each other forming larger biomolecules. The important assumption in Wächtershäuser's theory is that the larger organic molecules such as adenine that may have adsorbed on the surface of metal sulphides stayed there and interacted with each other, creating more complex macromolecules and enzymes. Adsorbed nucleobases are protected from aqueous phase-induced decomposition[17] and may have been well positioned to participate in mineral-mediated processes that led to modern living systems. The theory of the iron-sulphur world omits the initial carbon fixation cycle and links the catalytic properties of the surface of sulphide minerals directly to the origin of life.

Wächtershäuser has suggested that the simplest of all possible metabolic processes is an alpha-cycle - "an autocatalytic cycle, whereby a food acceptor takes up food and produces a product that is catalytic for this very process"[6]. He argued that any early stage of life will be based on the archaic pattern of metabolism that consists of an alpha-cycle, a pathway of initiation or an acetyl-CoA (coenzyme A) pathway that feeds a food acceptor into the alpha cycle and biosynthetic pathway, from which all known biosynthetic processes start[66].

Several enzymes in the pathway of initiation cycle contain Fe/S clusters as active components[3]. Wächtershäuser suggested that these clusters must have come from a common inorganic (mineral) precursor and assumed that the oxidation of pyrite "is the functional precursor of all extant biochemical agents and that it is the primordial energy source of life that drives the primordial mechanisms"[5].

The pathway of initiation or the acetyl-CoA pathway is based on the mechanism of carbon fixation and Wächtershäuser has concluded that the primordial metabolism was that of an

autotroph feeding on CO_2, CO and COS[59]. The acetyl-CoA pathway is basically a multistep reaction with the enzymatic reduction of CO_2 to a methyl-pterin that is subsequently converted to acetyl-CoA by a Ni/Fe/S enzyme with coenzyme A and CO[66]. It has been assumed that in the primordial pathway CH_3-SH was the functional precursor of methyl-pterin. It has also been proposed that in conditions similar to those in hydrothermal systems, CH_3-SH is converted to CH_3-CO-SH according to the reactions:

$CO_2 + FeS/H_2S + H_2 \rightarrow CH_3\text{-}SH + FeS_2 + O_2$

$CH_3\text{-}SH + CO \rightarrow CH_3\text{-}CO\text{-}SH \rightarrow CH_3\text{-}CO\text{-}OH$.

These reactions produce a thioacid (CH_3-COSH) that is required for subsequent carbon fixation as in:

$CH_3\text{-}COSH + CO_2 + FeS \rightarrow CH_3\text{-}CO\text{-}COOH + FeS$[66].

Wächtershäuser suggested that if thioacids or other chemically similar components were formed on an iron-sulphur surface they would subsequently react with each other without leaving the surface[3]. Positively charged surfaces of pyrite provide the energy for these reactions and thus promote further reactions of the process Wächtershäuser calls “surface metabolism”[6].

This theory, though very interesting, has not yet been proved experimentally. However some of the crucial steps of the iron-sulphur world theory have been tested both theoretically and experimentally. Blöchl and his colleagues found in the early 90s that iron sulphide minerals, including pyrite, catalyse organic reduction reactions[67]. Huber and

Wächtershäuser discovered and described FeS and NiS catalysed reactions imitating carbon-inserting reactions in modern microbial enzymes vital in inorganic carbon fixation processes[68]. Bebié and Schoonen[69] reported that anionic phosphate and phosphorylated organic molecules adsorbed selectively on the surface of pyrite and suggested that metal sulphides could have assisted the removal of phosphate from aqueous solutions on the prebiotic Earth, thus promoting the concentration of organic molecules in the solid phase. Pyrite has been shown to play an important role in the evolution of photosynthesis[70] and in metabolic activity of some members of the sulphur- and iron-metabolizing bacterial genus *Thiobacillus*, commonly found in hydrothermal systems[71]. Cody et al.[72,73] showed that NiS and other common Ni containing minerals (including Ni-bearing chalcopyrite) have the ability to promote surface-catalysed conversion of small organic molecules into carboxylic acids. These reactions demonstrated a good correlation between the surface area and the reaction yield[72].

An optimistic scenario would relate the "RNA" world to the "iron-sulphur" world in the following way. First, activated mononucleobases oligomerize on the surface of pyrite via the surface-catalysed reactions, proposed by Wächtershäuser[68]. Next, the copying of longer templates, using the already existing short oligomers as substrates, leads to accumulation of a variety of double-stranded RNA-like molecules. Then, one of these double-stranded helical molecules dissociates; the activated polymerase strand copies its compliment to produce a second polymerase, which copies the first to produce another compliment and so forth. The RNA precursor and, eventually, the RNA could have originated from a collection of the activated nucleobases on the catalytic surface of pyrite[59]. The main critique for this scenario is the complexity of the RNA molecule, which structure permits both base pairing and stacking; while binding of the bases to the surface may provide the necessary

constraints to offer some other interaction between the chains of bases to stabilise the helix without the stacking, this remains to be demonstrated experimentally. Some authors have suggested that due to this difficulty the first polymer to carry genetic information, the RNA precursor, may have been synthesised in an already established bio-chemical environment. However, there is no agreement whether metabolism could develop independently and before the genetic material, and there is no reason to believe that synthesis of nucleotides and peptides could have occurred spontaneously without RNA involvement[54].

4.4. The origin of chirality

It is well known that life is not symmetric on the molecular level, and the phenomenon that describes its asymmetry is known as "biomolecular chirality". Molecules are called chiral if they cannot be superimposed onto their mirror image and do not possess a plane of symmetry, and these non-identical mirror images are called L- and D-isomers or enantiomers. If the two enantiometers are formed in equal quantities, the mixture of them is called racemic; if there is only one enantiomer in a structure, the mixture is called enantimerically pure or monochiral. With very few exceptions, life uses monochiral monomers, for example L-isomers of the amino acids and D-isomers of sugar enantiomers are predominant in biological pathways and in molecular architecture of the life's genetic material – RNA and DNA molecules. Interestingly, after the death of a living organism, the homochiral proteinaceous L-amino acids immediately start to racemize at a slow but steady rate. Enantiomers have identical physico-chemical properties, identical vapour pressures, melting points, solubilities, diffusion constants, ionic mobilities, reactive indices and reaction rates, activation energies, entropies, Gibbs energies, bond lengths, bond strengths and angles, absorption spectra in UV and IR, NMR spectra. The only characteristic of L- and D-

isomers that differs is their optical activity[74].

The observed preference of homochirality in living organisms is not accidental. The formation of homochiral protein macromolecules was found to be not self-replicable in the racemic medium; the models of biogenesis require the supply of enantiomers far from thermodynamic equilibrium[75]. The formation of polymers from enantiomerically pure monomers determined the effect of “enantiomeric cross inhibition”, when the D-enantiomer incorporated into a chain of L-enantiomer acts as chain terminator and *vice versa*[76]. The origin of chirality is still highly debatable. There are a few probable factors, that can cause the formation of an environment with a certain enantimeric excess, where enantiomerically pure molecular structures could be formed – the transfer of the asymmetry to the racemic prebiotic molecules from chiral fields in the interstellar space, from the atomic nuclei of these molecules, where the asymmetry exists in a form of the weak nuclear force, or from the surfaces of chiral minerals[74].

Recently, the observation of the chemical synthesis under simulated interstellar conditions showed the formation of chiral amino acids with a small enantiomer imbalance after subjecting the samples to interstellar asymmetric radiation[77]. Chiral organic molecules have also been discovered in carbonaceous chondrites and comets, and a small enantiomer imbalance towards L-isomers was found after the chemical analysis of the extraterrestrial organic matter[78]. Theoretically, the homochirality could have been caused by multiple or dichroic asymmetric scattering in star formation regions and by “chiral” photons in a form of circularly polarized light[79]. Any specifically oriented field – magnetic, radiation or combination of both, could induce chiral imbalance to a racemic mixture of molecules.

Another source of chirality could be the weak nuclear force, or the weak nuclear interaction, which is carried by charged $W^{\pm}$ and neutral Z^{o} bosons and is asymmetric. It is known to influence the shapes of electron paths, making them helical, thus giving atoms chirality[80]. The weak interaction only stretches to the exterior of the atomic nuclei and is 10^{13} times smaller than the binding force of the nuclei. The weak force effects β-decay, causing the emitted electrons to spin-polarise, which could induce chirality to prochiral molecules by direct asymmetric radiolysis[81]. It is possible that the asymmetry of the fundamental physical force is responsible for the asymmetry of life, however, the experimental results to date are inconclusive.

Finally, chiral or enantiomorph crystals could have played an important role in the origin of biochemical asymmetry if their surfaces were used as templates by the prebiotic synthesis. The chiral information that is spread from the crystallization nucleus to the whole crystal during its growth could subsequently transfer to the organic matter on its surface. There are 65 space group types of crystallographic structures that produce chiral crystals, which exist in two enantiomorphous forms of equal energy[82]. Chiral quartz is very well-known, the other common minerals with chiral surfaces are sodium chlorite, pyrite and montmorillonite[74]. Wächtershäuser suggested that the chirality of pyrite crystal could have been translated to the organic molecules, formed on its surface[83]. However, no chiral molecule has been produced so far under such conditions and no enantiomeric imbalance was induced by the surfaces of pyrite crystal. This suggestion remains a hypothesis only, which I attempted to test in the research work described in this thesis.

4.5. Summary

The origin of life on Earth is a subject that has been repeatedly discussed for thousands of years. It is also a subject that does not provide easy answers and despite the rapid advance of scientific methods, especially in the fields of biology and physics, many links from the suggested chains of events are still missing.

One of the scenarios that hypothetically provides some missing links is the synthesis of biomolecules on the surfaces of sulphide minerals. It is supposed that water was the medium that carried the essential organic matter and mineral surfaces acted both as catalysts for the reactions and as templates.

According to this scenario the first living system might have originated as a polymer, attached to the catalytic surface, and then used it as a source of energy for replication. Adsorption from solution onto the surface of pyrite provided necessary concentrations of organic monomers to start the spontaneous process of self-assembly and protected the resulting polymers from water-induced decomposition. The surface of pyrite being chiral, the specificity of binding interactions between the monomer and the surface could be responsible for the chiral selectivity of the prebiotic molecules. Active sites on mineral surfaces such as surface defects or step edges might have been the initial spots where the polymerisation processes started. The chemistry of the RNA world could have taken place on these surfaces to give raise to the first RNA-coded replicating systems with FeS centers playing the catalytic role.

Hydrothermal systems could have been the sites where conditions were favorable for the initial processes of adsorption of monomers onto newly-formed mineral surfaces to start. The studies of ribosomal RNA of thermophilic bacteria, which are abundant in hydrothermal systems, showed that these organisms are closer to a common ancestor of all life than any other known organism[84]. It is possible that the life originating at the ocean floor would be more likely to survive the violent environmental changes in the early Archaen and eventually could spread out from the hydrothermal systems into a wider range of lower-temperature waters.

Chapter 5

Metal and mineral surfaces used as substrates

In this chapter I provide the description of the metal – Au (111) – and mineral – pyrite (100) – surfaces I used as substrates in the experimental part of this thesis. I give the detailed description of the Au (111) surface with its typical surface reconstruction and describe the sample preparation methods. The low index surfaces of pyrite, including the (100) surface are described in some detail here and the model of the pyrite (100) surface with a unit cell indicated and the iron and sulfur atoms identified is shown in Figure 5.8. In addition, in this chapter I describe the preparation of the surface of pyrite samples and discuss the processes that took place on the surface of pyrite during the polishing procedure, which made this task more difficult than originally anticipated.

The STM images of the bare surfaces of both Au (111) and pyrite (100) together with supplementary AFM and EBSD images for pyrite (100) surfaces are also included in this chapter. All STM images shown in this chapter were taken by me and unless indicated otherwise, were at ambient conditions. The samples imaged are the same samples that were used later for the molecular self-assembly experiments, described in Chapters 6, 7 and 8.

5.1. Au (111) surface preparation

The bare Au (111) surface was imaged in preparation for the molecular deposition experiments in which two complementary RNA bases, adenine and uracil, were to be deposited on the Au (111) surface so that their interactions with the surface could be observed *in situ*. The Au (111) surface is catalytically inert and the processes of the self-assembly of adenine and uracil on it can be used as a reference for the processes of the self-assembly of these molecules on more chemically active surfaces, as I expected the surface of pyrite to be.

In the STM experiments I used commercially produced thin films of Au (111) grown on mica (Agilent). The Au-mica sheet was cut so the Au layer was only connected to the sample holder on one side. To enable us to heat the samples resistively they were mounted on top of polished SrTiO3 before being inserted into the sample holder. The typical resistance of the mounted samples was 4-5 Ω.

The samples were outgassed in the load lock of the STM for at least 4 hours and then transferred into the UHV conditions. When in the STM treatment chamber, the samples were degassed at 600 ºC until the pressure in the chamber could be kept at mid 10^{-8} Pa. and then reconstructed. The reconstructed surface of Au (111) was obtained by sputtering with Ar atoms for 15 minutes and subsequent annealing at 600-700 ºC for 1.5 hours. After the annealing the samples were allowed to cool down naturally for 1 hour either in the treatment chamber or in the STM chamber. The pressure in both chambers was in the low numbers of 10^{-8} Pa at this stage. The images were taken in the STM chamber at constant

current mode at ambient temperature (20 ºC) for most images and at constant height mode at low temperature (-190 ºC) for the atomic resolution images. To achieve the low temperature in the STM chamber, it was cooled down with liquid nitrogen and allowed to chill for at least 2 hours with the tip brought close to the sample for the temperature gradient between the sample and the tip to flatten. Bias voltage was applied to the sample.

5.2. Au (111) surface: STM

The Au (111) surface forms large flat terraces, typically 80 nm wide and larger, as shown in Figure 5.1 and typically reconstructs into a complicated pattern of corrugation lines caused by a contraction of the surface layer. The formation of corrugation lines in the surface layer is well known for elements having a large surface mismatch such as Au[85]. For a (111) surface with a local surface lattice parameter r_s^0 (the distance between surface atoms for which the surface site energy is minimal), there are $(r^0/r_s^0)^2 \times N_b$ atoms in the surface plane, where r^0 is the bulk equilibrium distance between atoms, and N_b is the number of atoms in a bulk (111) plane. For Au r_s^0 = 2.807 Å and surface occupied by one atom in (100) plane is $(\sqrt{3}/2)r_2^0$. This corresponds to an increase of 4.5% in the number of surface atoms in Au (111) plane with respect to the bulk ones along the <110> direction, while the atoms along the <11-2> direction stay in registry with the bilk, and has been observed experimentally[85]. A consequence of the stress relief along only one <110> direction is to increase the stress along the other two <110> directions. Then, because of this threefold orientational degeneracy, the stripe domain reconstruction is unstable for large areas. The best compromise is then the formation of three types of stripe domain reconstructions, each of them associated with one of the three equivalent <110> directions[85], which induces the observed stripe domain reconstruction 22 x $\sqrt{3}$ with rotational symmetry as shown in

Figures 5.2, 5.3, and 5.4.

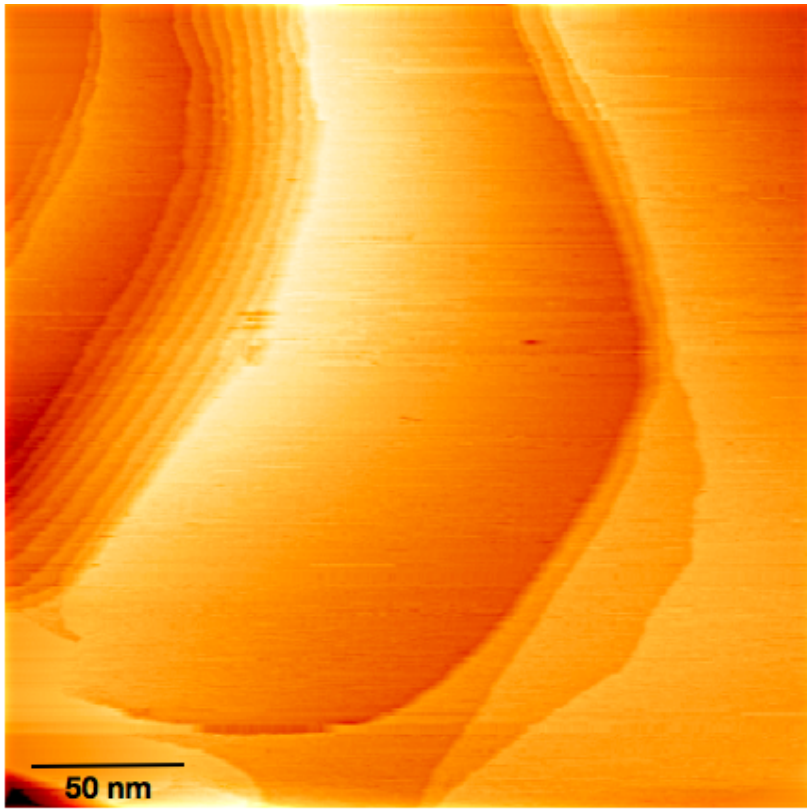

Figure 5.1. A large-scale STM image of the reconstructed Au (111) surface showing the close-packed flat terraces, and the step edges. The scale is too large to show the surface reconstruction, which is covered by the following images in this chapter. The image was taken at -1.25 V bias voltage and 0.1 nA current in constant current mode and at ambient temperature.

The electron diffraction pattern of the Au (111) reconstructed surface is interpreted as a two-fold symmetry underlined by a higher three-fold symmetry of an fcc (111) surface, which results in the existence of three rotational domains[86]. These rotational domains and the 120° symmetry are clearly visible in Figures 5.2, 5.3, and 5.4. Typically in an STM image of an Au (111) surface the corrugation lines are arranged in U-shaped domains (see Figure 5.2), parallel domains (see Figure 5.3), and rotational domains (see Figure 5.3 and 5.4). These domains represent the periodically arranged regions of the bulk atoms (fcc

arrangement), the regions with stacking faults (hcp arrangement) and the transition regions separating fcc and hcp domains (corrugation lines). Terrace steps and surface defects do not inhibit the reconstructions and corrugation lines carry on across the terraces and over the step edges.

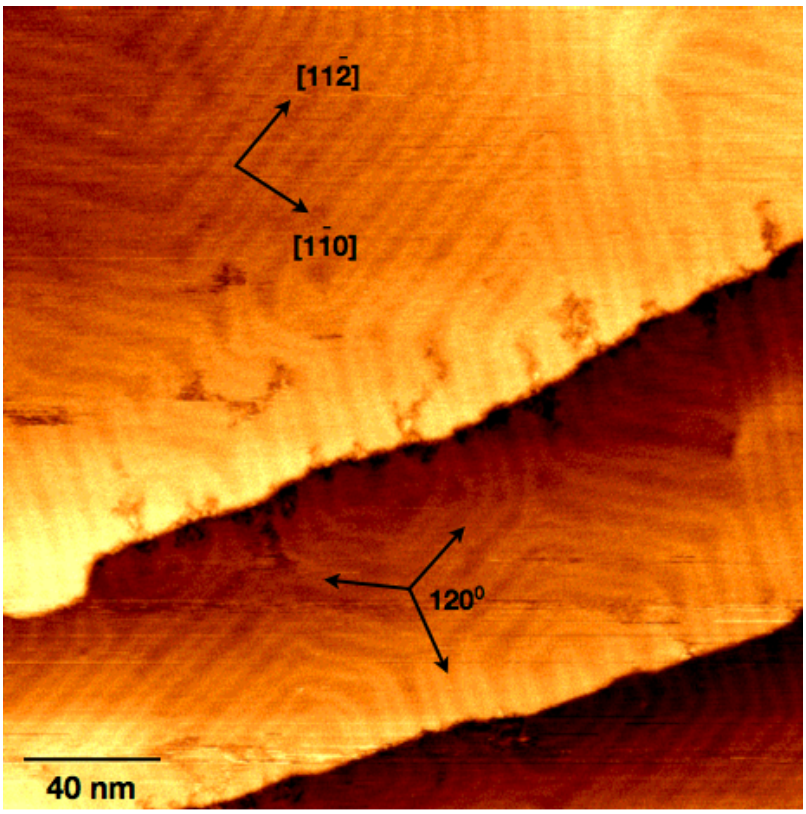

Figure 5.2. A medium-scale STM image of Au (111) surface showing edges of two monoatomic steps with the clearly defined corrugation lines of the reconstruction pattern. 120° periodicity and typical U-shaped connections terminating a line pair are visible on this image. The reconstruction crosses over the terrace edges without interrupting. The dark pit-like patches near the step edges are the high current induced defects, created by the repeated imaging of the area. The measured monoatomic step height is 2.38 Å. Image was taken at -1.25 V bias voltage and 0.1 nA current in constant current mode and at ambient temperature.

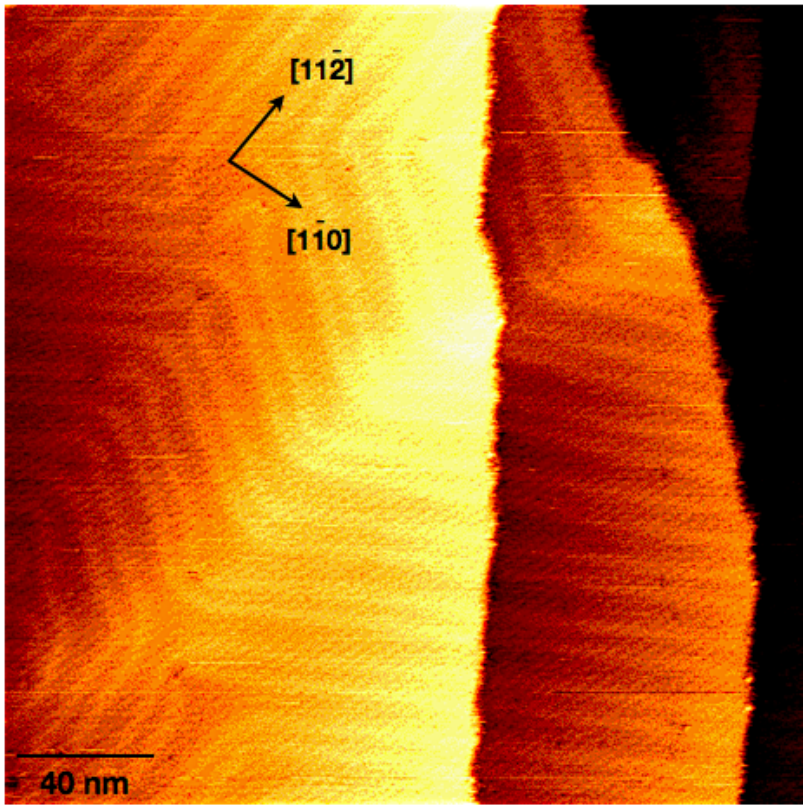

Figure 5.3. A typical medium-scale STM image of Au (111) surface showing step edges with the clearly defined corrugation lines of the reconstruction pattern without the U-shaped connections terminating a line pair. Both rotational domains and the parallel domains of the corrugation lines are present in this area. This image also shows the reconstruction crossing over the terrace edges without interrupting. Image was taken at -1.25 V bias voltage and 0.1 nA current in constant current mode and at ambient temperature.

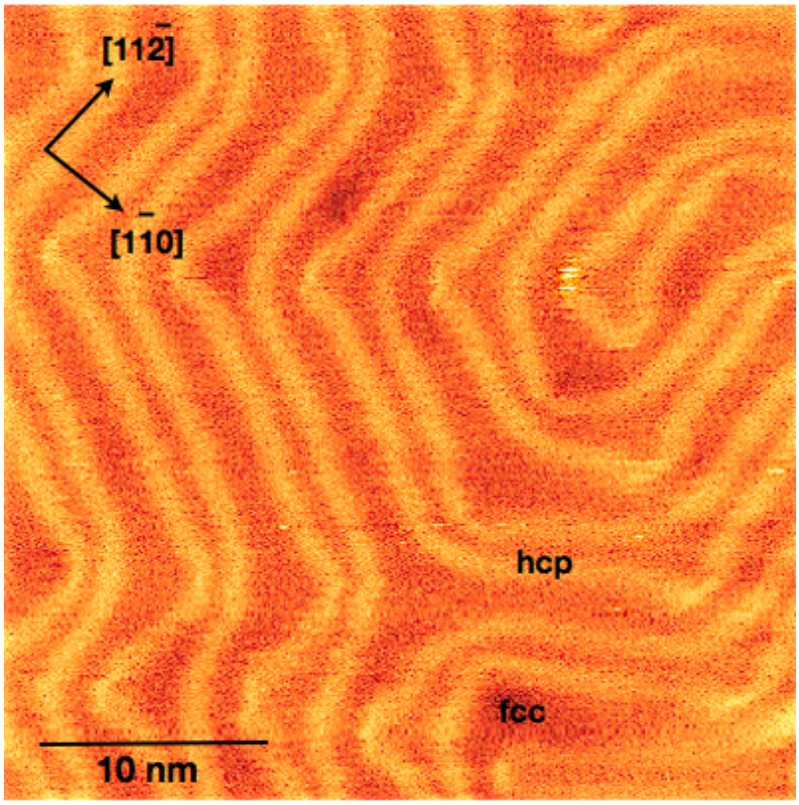

Figure 5.4. A small-scale STM image of Au (111) surface showing the rotational domains of the corrugation lines on top of the terrace. The hcp and the fcc stacking regions regions are indicated. Image was taken at -1.25 V bias voltage and 0.1 nA current in constant current mode and at ambient temperature.

The corrugation lines of the Au (111) reconstruction visible in STM images as bright "ridges" are the boundaries between the unfaulted fcc and faulted hcp stacking regions of the top layer of atoms. The fcc stacking is suggested for the wider regions as it agrees with the fcc bulk structure of Au (111) and is energetically more favourable[86]. The hcp stacking is suggested for the narrower regions as indicated the Figure 4.4. The regular arrangements of stacking fault regions form a (22 x $\sqrt{3}$) surface unit cell with the corrugation lines aligned to <112> direction[87].

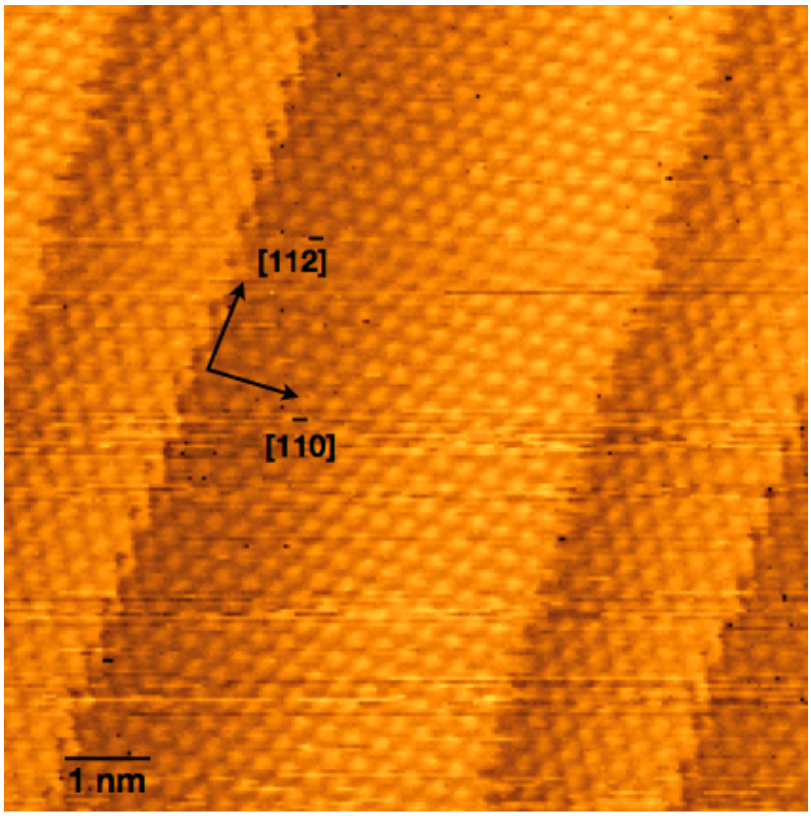

Figure 4.5. An atomic resolution STM image showing two corrugation lines of the reconstructed Au (111) surface. The measured height of the reconstruction is 0.2±0.05 Å. The measured distance between the neighbouring reconstructions in the [1,-1,0] direction is 6.3±0.3 nm in uniform regions as shown by the one shown here. The measured distance between the individual lines within a reconstruction is 4.4±0.2 nm. These measurements are in very good correlation with the observations made by Barth et al.[86] The image was taken at 1.7 V bias voltage and 0.9 nA current at constant height mode and at -190 °C.

To summarise, a well-prepared Au (111) surface exhibits wide flat terraces with a characteristic reconstruction pattern of 0.2 Å total vertical corrugation and has three different rotational domains oriented at 120° to each other, which reflects the threefold symmetry of the fcc (111) bulk substrate. The surface is considered to be inert in general with possible increased local reactivity of the surface on the transition regions i.e. corrugation lines of the reconstruction[88], particularly at the kink sites[86].

5.3. Pyrite (100) surface preparation

Interactions between living organisms and pyrite surfaces were important in the history of the evolution of living organisms as demonstrated by many sulphur and iron-metabolising microbes, especially sulphate reducers, evidence of which is found between 3.4 and 2.7 billion years ago[89,90]. The discovery of life forms with pyrite-orientated chemical metabolism has sparked interest in pyrite surfaces in the field of molecular biology, especially in problems related to the self-assembly of complex organic polymers[57,91]. In this part of the chapter a short description is given of pyrite as a mineral and of general properties of its surfaces as well as the surface preparation techniques I used.

5.3.1. Pyrite as a mineral

Pyrite is the most common of all sulphide minerals in the Earth's crust and is found in a wide variety of geological formations ranging from sedimentary deposits to hydrothermal veins and as a constituent of magmatic and metamorphic rocks [www.mindata.org]. Pyrite crystals are pale brass yellow colour with metallic lustre. The hardness of pyrite is 6.5 on Mohs scale and the density 4.9 g/cm^3. The crystals are brittle with poor or indistinct cleavage on (100) crystallographic planes and show irregular conchoidal fracture. Natural (100) surfaces often display striation[92]. Chemical Formula: FeS_2 (chalcogenide). Molecular weight = 119.98 gm. Impurities in pyrite include Ni, Co, As, Cu, Zn, Ag, Au, Tl, Se and V[93].

Pyrite starts to decompose at 310 ºC as pyrrohotite ($Fe_{0.83\text{-}1}S$) forms on the surface creating

a metastable pyrrhotite-pyrite solvus[94]. If heated further in neutral or reducing gases under atmospheric pressure it decomposes to sulphur and iron(II) sulphate ($FeSO_4$) between 550 ºC and 700 ºC. In air it oxidises between 445 ºC and 660 ºC forming sulphur dioxide (SO_2) and hematite (Fe_2O_3) and fully decomposes to sulphur (S_2) and pyrrhotite at 742 ºC[95]. If compositions at the pyrrhotite solvus are heated to just above the decomposition temperature they form smythite ($Fe_{13}S_{16}$) and metastable monoclinic Fe_3S_4. Water vapour has an insignificant effect on these reactions[89]. The melting point of pyrrhotite is 1,177–1,188 ºC.

Pyrite is typically cubic, but can also be octahedral or, more rarely, pyritohedral. It belongs to the isometric crystal system with space group Pa3. The Fe atoms form a sublattice with face-centered cubic symmetry and the S atoms form a reduced symmetry sublattice with diatomic sulphur groups. The bonds of the sulphur molecules are orientated along the four different <111> directions[96]. Thus each Fe atom is coordinated to six neighbouring S_2 dimers, with one S at each of the vertices of a distorted octahedron, while each S atom is coordinated to three Fe atoms and one S atom in a tetrahedral configuration as shown in Figure 3.1[97]. Three coordination octahedra meet at each end of the S dumbbell with no edge sharing present[89]. The cubic lattice constant for the FeS_2 lattice was given by Finklea et al.[98] as a=5.417 Å; the unit cell volume calculated from the unit cell is V=158.96 Å³ [99], the Fe-S distance in pyrite is 2.26 Å [99], the S-S distance is 2.14 Å[89].

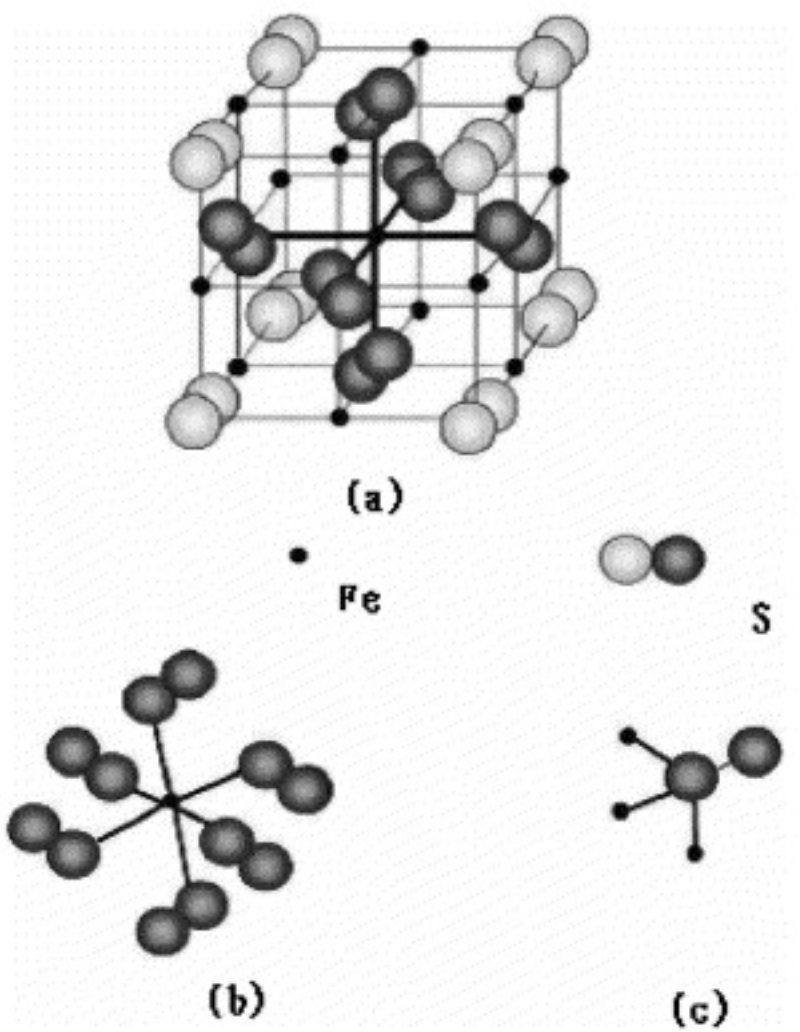

Figure 5.6. Crystal structure of pyrite, FeS_2. (a) Unit cell; (b) the local environment of Fe atom; (c) the local environment of S pair[100].

Observed LEED patterns of the fresh pyrite (100) surface shown in Figure 5.7 demonstrates the reciprocal face centred cubic cell and less intense spots with half the periodicity attributed to the 2x2 superstructure of disulphate groups[101].

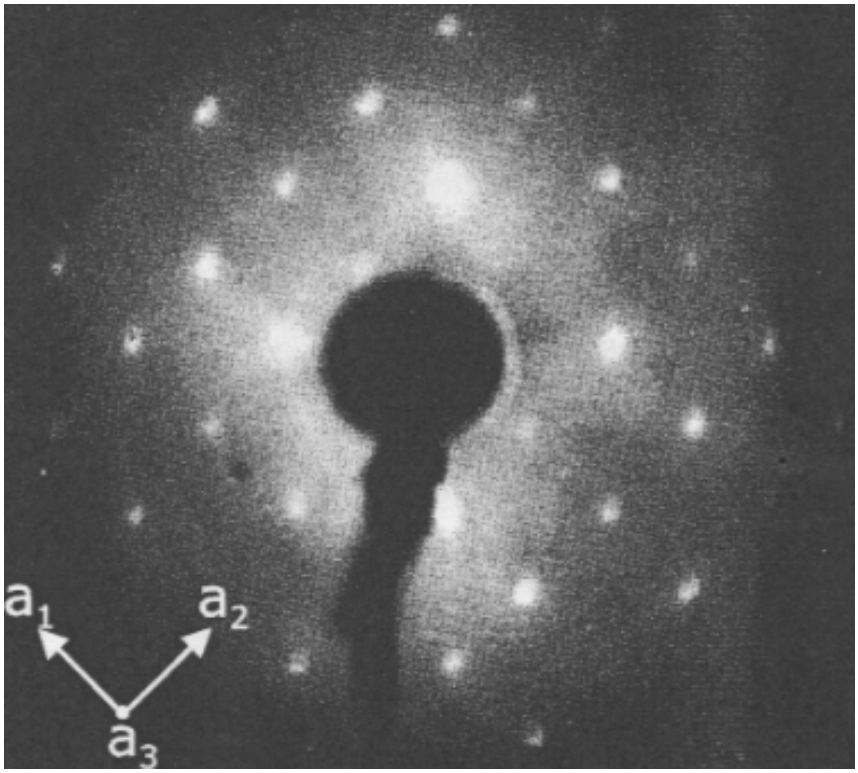

Figure 5.7. LEED image of pyrite (100) surface cleaved in vacuum. The crystal orientation is indicated by the axis[101].

The bulk structure of pyrite has been extensively studied both experimentally using photoemission, STM[102] and ultraviolet photoelectron spectroscopy and theoretically using various modelling methods such as *ab initio* pseudo-potential method[103], ligand field theory[101,104], MO (molecular orbitals)[83,105] and DFT (density functional theory)[106,107]. There have also been a few studies of the effects on pyrite's properties of deviations in stoichiometry from the ideal 1:2 ratio. Birkholz et al.[108] has demonstrated by detailed X-ray diffraction experiments that synthetic pyrite shows sulphur deficiency. Ellmer and Hopfner[109] have confirmed that deviations from the ideal stoichiometry exist in natural crystals but do not exceed 1 at%, which, however, is a sufficient variation to have an impact on electrical properties.

The electrical properties of bulk pyrite have been described both theoretically (band

structure calculations) and experimentally and are those of an n-type semiconductor[83] with a band gap of 0.9-0.95 eV[70]. The conductivity type of pyrite can be adjusted by doping with P, As, Sb (p-type) or with Ni, Co, Au, Cl, Br (n-type)[89].

Natural pyrite can sometimes demonstrate either n-type and p-type conductivity. It has been recently suggested that pyrite formed at lower temperatures exhibits p-type conductivity (iron deficient) and pyrite formed at high temperatures exhibits n-type conductivity (sulphur deficient)[89]. Synthetic pyrite crystals are dominantly n-type semiconductors and Scheik et al.[110] have reported difficulties in synthesising p-type pyrite crystals.

The electronic states at the top of the valence band region comprise a narrow band of non-bonding iron 3*d* t_{2g} orbital states, which lies a little above the main bonding band composed of mixed sulphur 3*p* and iron 3*d* orbital states (σ, π and π^* S_2^{2-} 3*p* states and e_g Fe 3*d* states). The high degree of mixing between cation and anion states in pyrite shows strong covalent bonds. The bottom of the conduction band is composed of mixed sulphur 3*p* and iron 3*d* orbital states (σ^* S 3*p* and e_g^* Fe 3*d* states)[89]. However, it was also suggested that the bottom of the conduction band may contain only S 3*p* states, resulting from a larger splitting of S 3*p* states from strong S-S σ interaction[111]. In this study Eyert et al. have also suggested that t_{2g} states at the top of the valence band are not completely non-bonding and there is a weak π-bonding between iron 3*d* t_{2g} and sulphur 3*p* orbitals. X-ray, Mössbauer and magnetic susceptibility measurements indicate Fe 3*d* electrons to be in a low-spin state with no hyperfine magnetic field. The phenomenon of an electric field gradient occurring in pyrite could be explained by a shift of Fe sites from cubic symmetry[99].

The conductivity of pyrite at room temperature is reported to be about 1 $\Omega^{-1}cm^{-1}$ [105]. The

measured electrical resistivity of pyrite is 1.74 Ωcm[112]. The thermoelectric Seebeck coefficient measured for pyrite is -500 μV/K and correlates with a conduction process via electrons excited from the localised t_{2g} levels in the e_g band.

5.3.2. Pyrite surfaces

Naturally occurring cleaved or grown (100) surfaces of pyrite are well described in the literature. It is suggested that cleaving does not usually break the strong S-S bonds of the sulphur diatomic molecules[105] and the (100) surface that is formed by cleaving Fe-S sites is usually observed. If only Fe-S bonds are broken then there should be a 1:1 ratio of dangling bonds of iron and sulphur atoms at the (100) surface. If all participating electrons are counted, it shows that all anion dangling bonds on the (100) surface are completely filled[113]. Thus the (100) surface of pyrite is charge-neutral and is believed to be "autocompensated" which means it is very stable, has low surface energy and will not reconstruct[114].

A ball and stick model of pyrite (100) surface is shown in Figure 5.8.

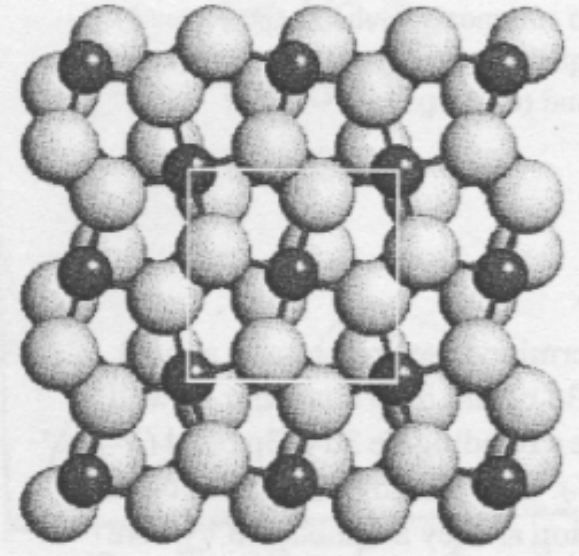

Figure 5.8. Ball and stick model of pyrite (100) surface showing the unit cell. Dark spheres represent iron atoms and light spheres represent sulphur atoms[115].

The (100) surfaces appear to be composed of flat terraces (usually no larger than 20-30 nm) and curved step edges with a step height at 2.8 Å (approx. half a unit cell) and high kink density[101]. Cleaved (100) surfaces of pyrite were imaged by STM[96,116,117] and a typical image is shown in Figure 5.9.

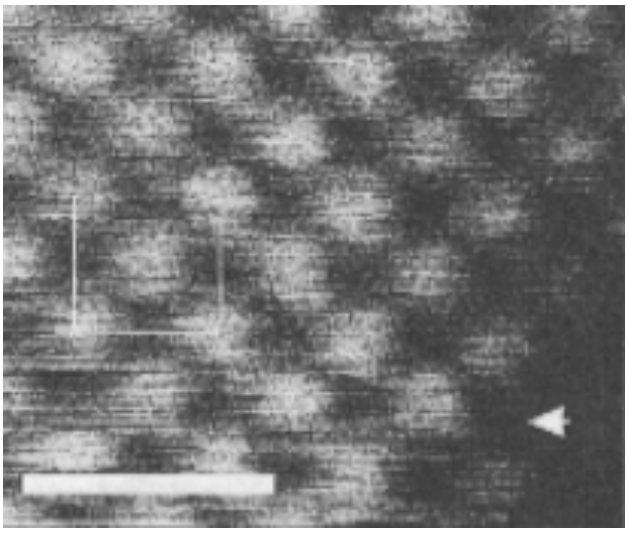

Figure 5.9. Atomic resolution STM image of a pyrite (100) surface taken by Rosso et al.[101] under UHV conditions at -0.2 V sample bias and 2.0 nA tunneling current. The solid white arrow points to a corner site at the step edge; the scale bar represents 10 Å; the centre cubic solid cell is outlined[101].

States that appear on the image in Figure 5.9 at low negative sample bias as a row of distinct bright spots were considered to be localised Fe 3*d* states with one dangling bond. The S groups were considered to be located at the low tunneling current sites, which is in general agreement with previous MO and UPS studies[101].

It is suggested by Rosso et al. that the (100) surface undergoes very little relaxation and can be approximated by a simple termination of the bulk structure along a plane of cleaved Fe-S bonds[101]. Recent DFT calculations show that most of the relaxation occurs along the surface normal direction[118]. The uppermost S layer moves outward relative to a simple bulk trancation by 17 %, the uppermost Fe layer moves inward by 32 %, and the uppermost S-Fe bond shortens by ~0.1 Å. The uppermost S-S bond is believed to be left unchanged[119].

Bronold et al.[107] have suggested that the highest occupied and lowest unoccupied surface states on the (100) surface of pyrite are localised on the five-fold coordinated Fe atoms. The highest occupied surface state is attributed to Fe 3*d* orbitals. The lowest unoccupied surface state is attributed to a mixture of Fe 3*d* and S 3*p* orbitals. A slab calculation performed by Rosso et al.[116] predicted that the loss of coordination on the surface results primarily in the displacement of Fe 3*d* surface states into the bulk band gap. The energy for a relaxed (100) surface in vacuum was given as 1.06 J/m^2 by Huang et al.[120] and confirmed by Cai and Philpott[119].

The atomic structure, with respect to the Fe lattice and local density of occupied states is unchanged at the step edges on (100) surfaces of pyrite[116]. X-ray photoelectron spectra (XPS) showed the presence of monosulphides at the step edge (presumably resulting from

broken S-S bonds) which, according to Eggleston and Hochella, does not lead to occupied states higher in energy than 3*d* dangling bond states at Fe sites[96].

Sulphur vacancies and a presence of Fe^{3+} have been discovered on clean (100) surfaces of pyrite. Nesbitt et al.[121] have suggested that the presence of Fe^{3+} together with broken S-S bonds on a surface may indicate an oxidation process along the lines of $Fe^{2+} + S^{-} \rightarrow Fe^{3+} + S^{2-}$ on a cleaved plane. Sulphur deficient surfaces can also be created on (100) surface in ultra high vacuum by sputtering or annealing procedures[122]. It has been predicted theoretically that if significant quantities of S vacancies are present on (100) surface, part of the surface may become paramagnetic[120].

Most of the work on pyrite reactivity has been done on the (100) surface with respect to gaseous species (O_2, H_2O and CH_3OH)[89]. However, due to the conchoidal nature of pyrite cleavage along (100) planes, most analytical spectroscopic methods do not access the true (100) surfaces and necessarily include other structures present on the fracture[89].

Investigation of the interactions of the pyrite (100) surface and H_2O and between the pyrite (100) surface and CH_3OH by temperature programmed desorption (TPD) and photoemission of adsorbed xenon (PAX) were undertaken by Guevremont et al.[123]. Both species were shown to adsorb at 90 K and thermally desorb between 170-400 K. The sites at which the sorption starts are believed by the same authors to be defect sites or sulphur deficiencies[124]; when these sites are saturated, the process is suggested to move onto a less reactive stoichiometric surface[125].

Interactions with H_2O vapour demonstrated a small amount of oxidation on (100) surfaces[126]

and iron oxide, sulphur oxide, thiosulfate and various polysulphide species were suggested as possible reaction products[127].

Cleaved (100) surfaces were shown to react with pure O_2 forming iron (III) oxide and intermediate sulphur oxidation products including elemental sulphur[101]. Growth (100) surfaces did not exhibit any significant reactivity with pure O_2 for pressures up to 1 bar, showing dissociative chemisorption of O_2 on Fe sites[126]. However, both cleaved and growth (100) surfaces of pyrite show substantial reaction with a H_2O/O_2 mixture. The products of oxidation were similar to the products of the reactions with H_2O but the degree of oxidation of the surface was much greater[126].

The other pyrite surfaces that are formed by growth or cleavage of pyrite crystals are the (110), (111) and (210) crystallographic planes. The observed cleaved surfaces are the conchoidal deviations of (100) and (110) surfaces with some monosulphide species derived from broken S-S bonds[115]. The most commonly observed naturally grown surfaces are pyrite (100) surfaces on cubic crystals and (111) surfaces on octahedral crystals[116]. The properties of (100), (111) and (210) pyrite surfaces given below are the results of *ab initio* calculations, density functional theory and molecular modelling and have not been obtained experimentally.

The charge-neutral (110) surface is generated by cleavage on (110) of Fe-S bonds and terminated by 4-coordinated Fe atoms. The (110) surface shows little relaxation, which is only shown by reducing lengths of Fe-S bonds opposite missing S ligands, similar to the (100) surface[89].

The uppermost Fe atoms in (110) are polarised. Surface states on (110) surface are attributed to Fe 3*d* orbitals and are predicted to span the bulk gap[120]. The energy of the (110) relaxed surface in vacuum was given as 1.68 J/m^2 by same authors.

The (111) surface of pyrite is a stable growth face but it cannot be created by cleavage, as there is no weak plane in the structure in the <111> direction. For STM experiments clean (111) surfaces are produced from naturally grown (111) faces by a series of low-energy sputtering/annealing cycles[127].

The charge-neutral stable (111) surface is formed by a planar cut through S-S bonds. Surface relaxation is greater on the (111) plane than on the (100) plane and the occupied S 3*p* states are displaced above the top of the bulk valence band. Surface states are attributed to sulphur atoms in the (111) surface[89].

The energy of the relaxed (111) surface is almost 1.5 times as large as the energy of the (100) surface and was given as 1.40 J/m^2 in vacuum by Hung et al.[128] and 1.60 J/m^2 in vacuum by Rosso[129]. Chemical reactions, particularly the processes of surface oxidation, have been demonstrated to have a significantly larger effect on pyrite (111) surfaces than on (100) surfaces, forming similar oxidation products[127].

The (210) surface of pyrite is one of the least stable pyrite surfaces. The charge-neutral (210) surface is terminated by rows of 4- and 5-fold coordinated Fe atoms, and 2- and 3-fold coordinated S atoms[89]. The surface states of (210) surface are attributed to Fe 3*d* atoms. The energy of relaxed (210) surface in vacuum was given as 1.50 J/m^2 by Hung et al.[128]

5.3.3. Pyrite samples

Natural pyrite crystals of unknown locality with well-developed natural (100) surfaces were obtained from Prof. D. G. Fraser at the Earth Sciences Department.

Figure 5.10. Natural pyrite crystals, which were cut, polished and used in the STM experiments.

The single crystals were at least 10x10x10 mm or larger, big enough for the samples to be cut out using the natural (100) surfaces for orientation. However, the additional difficulty arose from the fact that the crystal surfaces were not flat but slightly curved, often not parallel to each other and displayed uneven striation as shown in Figure 5.10. This

presented considerable difficulties for choosing the orientation of the sample prior to cutting; I had to resort to additional techniques to confirm the orientation of the polished samples as (100) such as EBSD.

The pyrite single crystals were cut in air using a slow saw into 8x4x0.8 mm pieces parallel to a natural (100) surface and polished on one side. The manual polishing procedure was as follows: a sample was mounted on a ceramic disk and flanked by four pieces of 5 mm thin glass to prevent an uneven polishing. The adhesive used was the UV light cured epoxy (Norland Optical Adhesive 60). The cold resin, which is usually used for such tasks produced inferior results. The sample was then ground on a SiC abrasive disk (mesh 240) and polished on a lapping machine with 15 µm, 6 µm, 3 µm, 1µm, 0.5 µm and 0.1 µm nylon disks until the scratches and other damage from the previous polishing stage could not be seen under the optical microscope. Finally, the samples were polished with a colloidal silica aqueous alkaline solution with particles size around 8 nm ("Mastermet", pH 9.25) on "Microcloth" (Buehler Ltd.) for 30 min or until the surface appeared uniform. The speed used was 100 rpm. Only very light hand pressure was applied to samples during all steps of preparation. This final polishing step, which combined chemical and mechanical abrasion, was performed immediately before the sample was placed under vacuum. One sample from every batch was checked to confirm the crystallographic orientation of the sample surface (EBSD) and the surface roughness (AFM). The polishing with colloidal silica solution was recommended by Libowitzky[130], who found that the mechanical polishing without chemical abrasion caused considerable deformation of the surface layer.

EBSD was used to confirm the crystal orientation before cutting, the results of the EBSD performed on the samples deemed to be suitable for the STM experiments are shown in

Figure 5.11. The crystal cell, indexed pattern and the inverse pole figure map obtained were characteristic of a (100) surface of a cubic single crystal. The calculated angle of the samples used in the experiments was within 1 degree from the ideal (100) surface, which is within the sensitivity of the method.

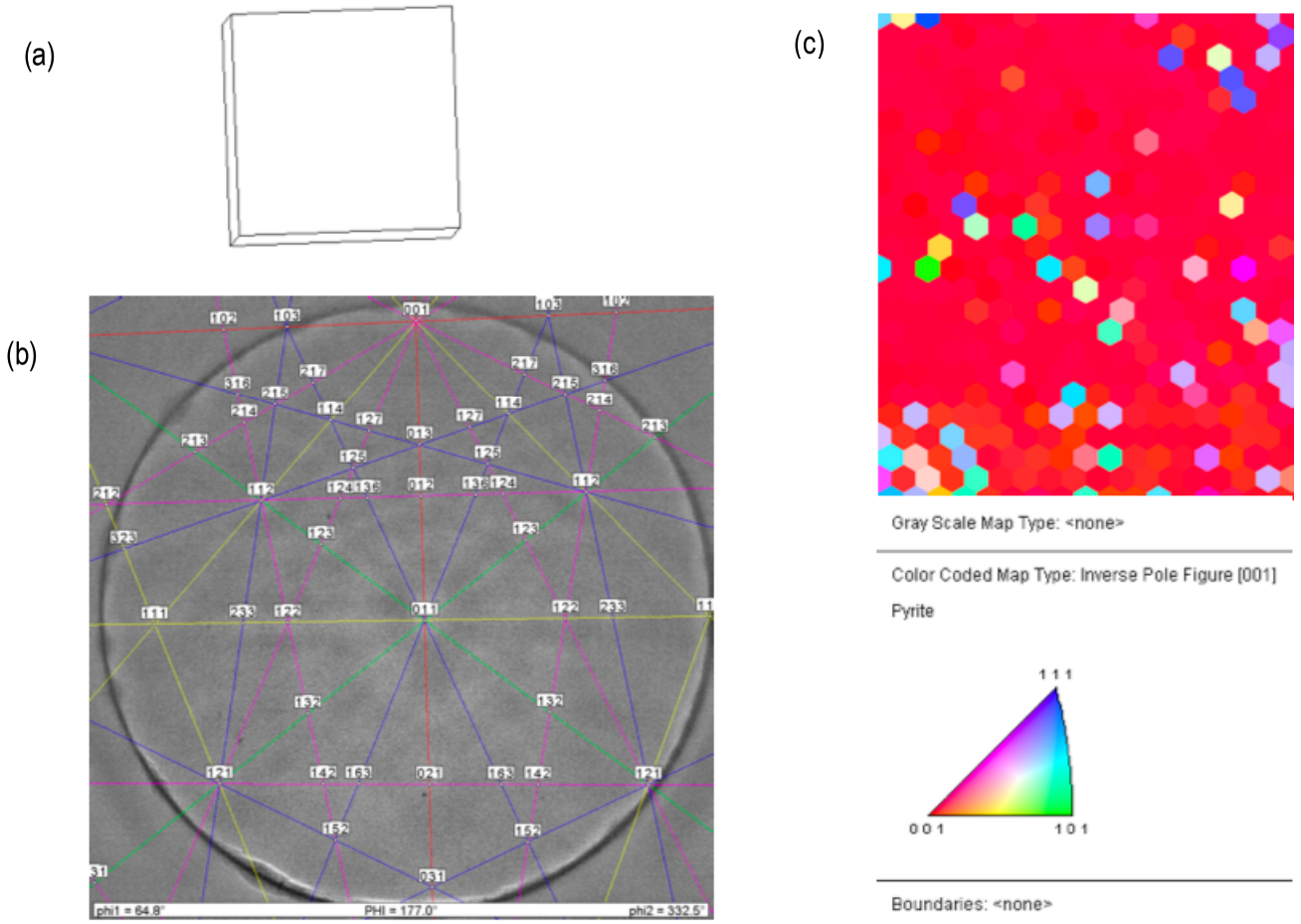

Figure 5.11. The results of the EBSD performed on the polished pyrite samples. (a) 70° crystal cell, showing (100) orientation, (b) 70° indexed pattern, (c) inverse pole figure map with legend, red colour indicates (100) orientation of the majority of the crystal surface, the other colours show grain inclusions which are randomly orientated.

The surface roughness of the polished samples presented another problem, which arose from the sample preparation process. Pyrite is a soft material, with hardness only 6.5 on the Mohs scale, and after checking the sample surface in the AFM I discovered that the final polishing procedure with colloidal silica solution leaves embedded silica particles on the surface, arranged along the polishing lines (see Figure 5.12).

(a)

(b)

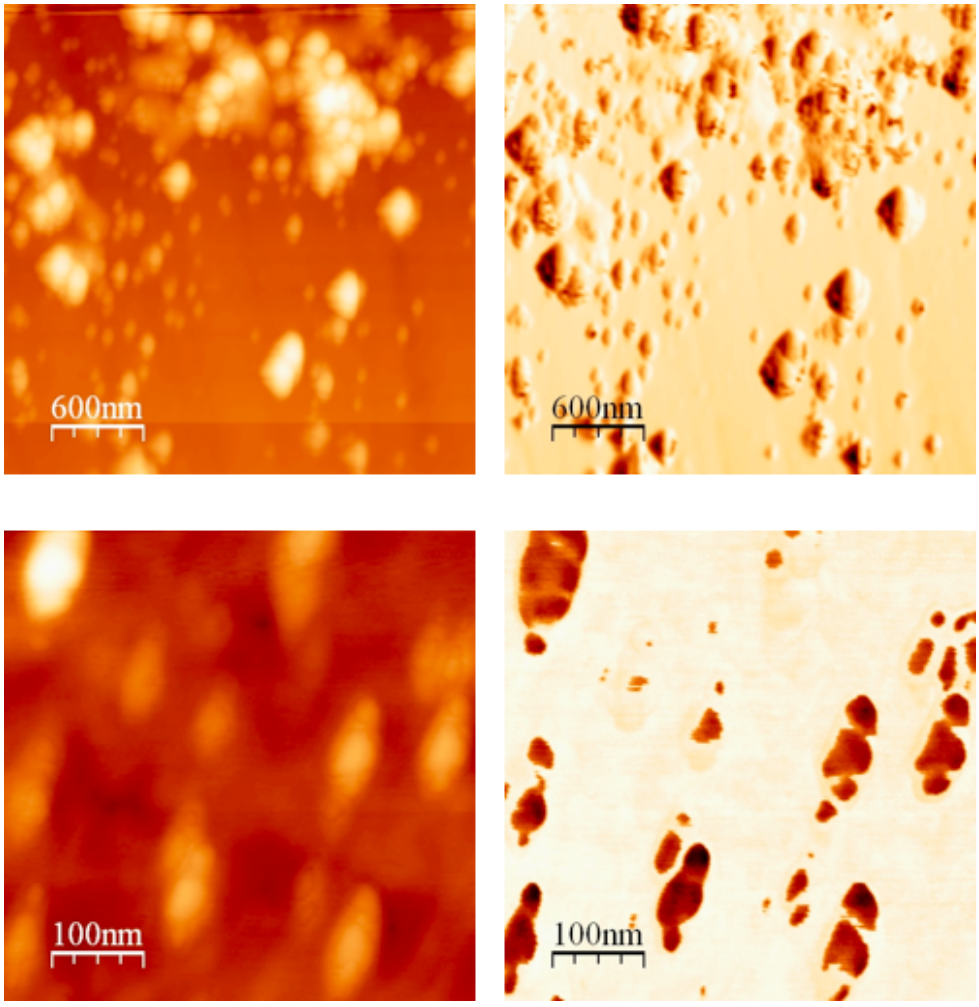

Figure 5.12. The AFM images of a pyrite (100) sample surface after the final polishing procedure: (a) a large-scale topographic image and corresponding phase contrast image, (b) a close-up topographic image and corresponding phase contrast image. The images were taken in tapping mode and in 25 nm dynamic vertical range.

The silica particles and agglomerates embedded in the surface can be clearly seen in both images in Figure 5.12 as tall features arranged along the main polishing direction, and are

very well defined on the phase contrast images as a different phase to the surface material. The height of the silica agglomerates was quite significant and the surface roughness of the samples was estimated at 9.4 nm.

The contamination of the surface by such large inclusions of non-conducting material made the imaging in the STM very difficult so a way had to be found to clean the surface from the silica particles. Very good results were produced by sonicating the sample in 20 % NaOH water solution for 10 minutes, followed by sonicating in distilled water for 3 minutes and in 10 % DTA-Na solution in water for 10 minutes. The final rinsing in distilled water and sonicating the sample twice for 3 min in isopropanol was found beneficial. This may seem an unnecessarily complex cleaning procedure; however, I found that the NaOH solution removes the large conglomerates of colloidal silica and the subsequent sonicating in water stops alkaline etching of the surface. DTA-Na solution, though not strong enough to attack the large conglomerates, dissolves the small silica particles remaining on the surface and the final sonication in isopropanol removes the traces of DTA salt. The resulting surface is reasonably clean and has a roughness of a silicon wafer, the AFM image of the cleaned surface is shown below in Figure 5.13.

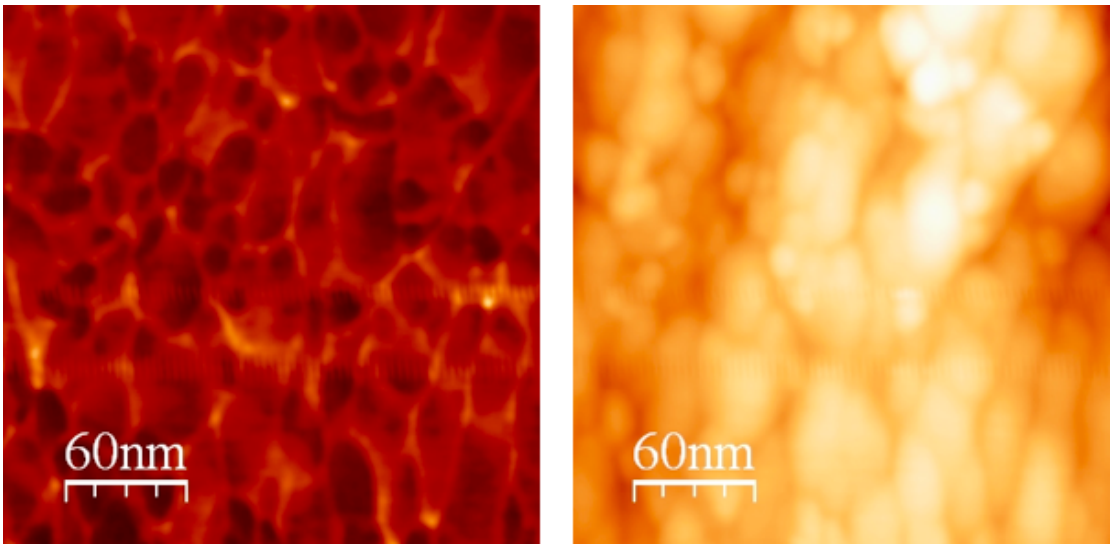

Figure 5.13. An AFM image of a pyrite (100) surface after cleaning: a small-scale topographic image and corresponding phase contrast image. No silica particles can be found on the surface and small terraces can be seen in both images. The roughness of the surface achieved after the cleaning is 0.5 nm.

5.4. Pyrite (100) surface: STM

A pyrite sample with a clean polished (100) surface was degassed *in situ* at 150˚C for 48 hours to remove loosely bonded gas and water molecules. After degassing the imaging showed terrace edges but the surface of the sample appeared dirty in the STM image, probably because it was covered by products of oxidation. The sample was then annealed at 275 ºC for 10 minutes (the highest temperature permitted as pyrrohotite starts to form on the surface of pyrite at 310 ºC[94]). Post-annealing, the sample was slowly cooled to approximately 100 ºC, transferred to the STM main chamber and allowed to cool naturally for 1 hour.

The best imaging conditions were found to be 2.15 nA current and 0.5 V bias voltage for empty states (sulfur groups) and -1.2 V bias voltage for filled states (iron 3*d* states). Annealing improved the sample surface enough to enable natural terraces to be seen under positive bias voltage (see Figure 5.14); the atomic resolution of pyrite (100) surface was also achieved (see Figure 5.15).

The typical step pattern with rectangular form elongated in one axes and perpendicular to [110] direction is shown in Figure (5.14). The measured monoatomic terrace step height is 5.45±0.2 Å, which is in close agreement with the pyrite unit cell 5.17 Å given in literature[98]. The lateral width of the terraces in [110] direction varies between 5 nm and 40 nm depending on the part of the sample imaged. This may be simply a result of the natural crystals having macro distortions (striations). As the natural (100) faces of the crystal I used to cut were curved rather then straight, the variation of the angle between the cut surface and the "ideal" (100) surface may vary slightly across the sample.

The terraces of the (100) surface appear atomically flat with some local defects present. The surface of the sample appears clean, with no contamination or adsorbed material on the step edges or on the surface of the terraces and there is no image noise.

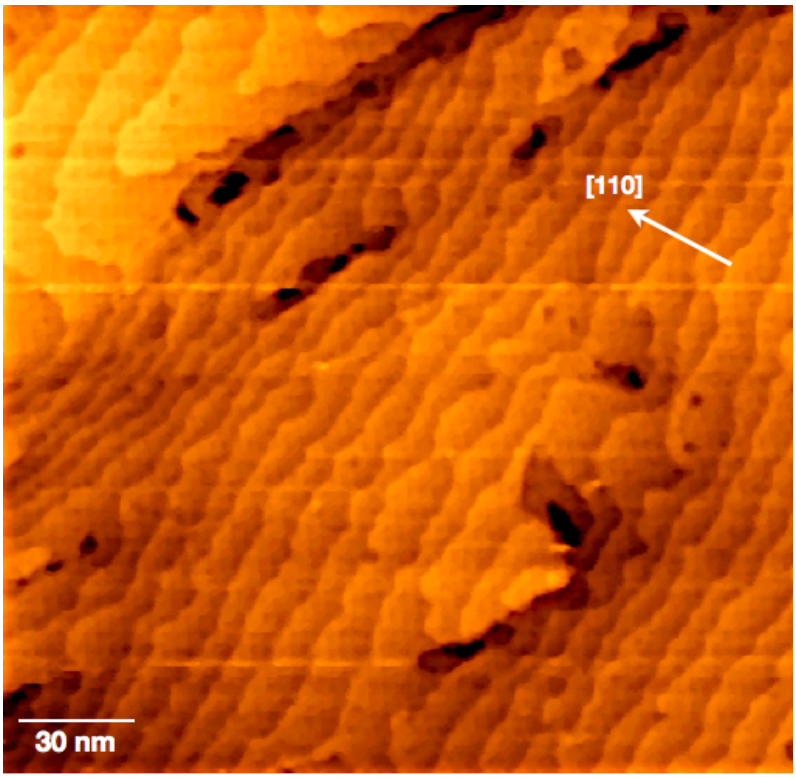

Figure 5.14. An STM image of the pyrite (100) surface after annealing. This image shows the natural terraces on the pyrite surface and was taken at ambient temperature at 2.16 V bias voltage and 0.5 nA current. Median noise reduction averaging was applied to the image to reduce lateral lines associated with electrical interference.

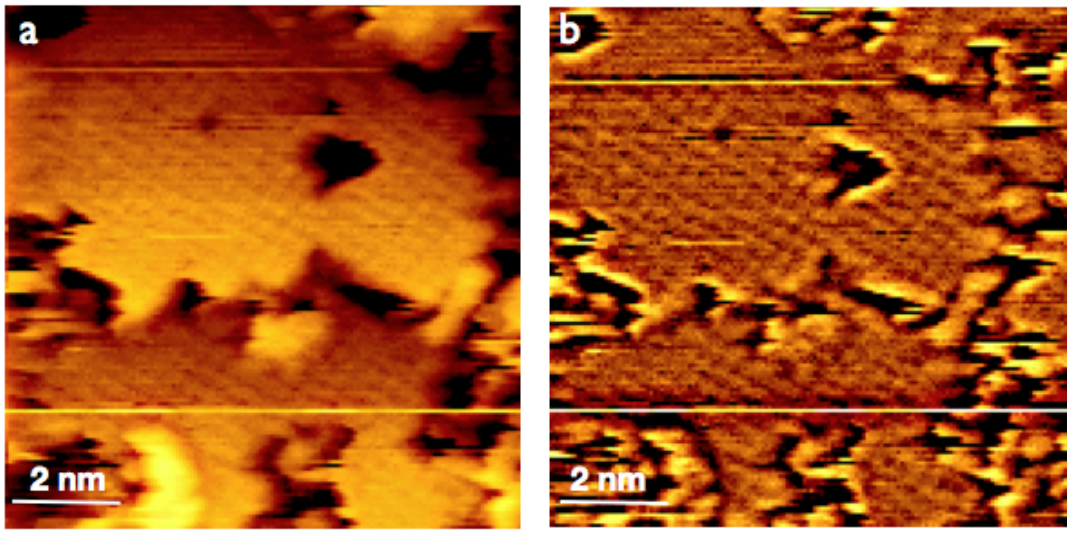

Figure 5.15. An atomic resolution STM image of the pyrite (100) surface. The image (a) is unprocessed, the image (b) had a lowpass filter applied in an attempt to make the atoms appear more prominent. The centered square unit cell and the atomic scale periodicity 3.5±0.1 Å can be seen in both images as expected for Fe substructure. The imaging conditions were 1.1 nA current and 0.5 V and -1.2 V bias voltage at the ambient temperature.

I had some difficulty in obtaining atomic resolution on pyrite which I suggest results primarily from the rapid formation of an oxide layer on the top of the sample surface after the final stage of polishing and before the sample is transferred to the vacuum chamber though the utmost care was taken to reduce the time the sample is exposed to air. On the parts of the sample where the thin oxide layer had formed it was impossible to obtain atomic resolution, though the terraces and the step edges were perfectly visible in the STM.

It is generally well known that the mineral phases in redox state react with the oxygen in the air and it was shown by Schaufuss et al.[131] that the exposure of a freshly cleaved pyrite surface to the oxygen in the air for 1 minute is sufficient for 30-40 % of the surface to oxidise. I have calculated the thermodynamically most probable state of the surface of pyrite using the HCh specialised software. This program allows the user to calculate the equilibrium of the chemical system at the given pressure and temperature by the minimization of the free Gibbs energy of the system[132]. This method only gives the probable state of the system as it calculates the absolute chemical equilibrium and does not account for the metastable states (i.e. the states when their phase transition into the equilibrium states is limited by kinetics) and the configuration of the phases in 3-dimensional space. However, the limitations of this method can be accounted for by understanding the characteristics of the system modeled and can be useful when the actual experimental investigation of the system is too cumbersome or time-consuming.

Pyrite is one of the most common minerals on Earth and thus can be considered a thermodynamically stable phase under the ambient conditions. At the first modeling stage, I calculated the behaviour of the system consisting of 1 mmole of pyrite (FeS_2) and 1 mole of

a gaseous phase imitating the macrocomponents of the atmosphere under the standard conditions (pressure – 1 bar, temperature 25 ºC). All stable mineral phases consisting of elements Fe, S and O listed in the standardised thermodynamic data base Unitherm[133] were allowed in the calculations. The gaseous phase consisted of 80 % N_2 and 20 % O_2, the volatile S_2 and SO_2 initially not present in the gaseous phase were included in the list of possible components. The calculations showed that the equilibrium state of such a system is comprised of 0.5 mmole of hematite (Fe_2O_3) and the gaseous phase with additional 0.2 % SO_2. This is obviously not the case, as pyrite is stable under atmospheric conditions. Therefore, I assume that bare surfaces of pyrite do not exist in nature. The reaction of the type $2FeS_2 + 3.5O_2 \Rightarrow Fe_2O_3 + 2SO_2\uparrow$ occurs on the exposed mineral surface and the resulting thin layer of hematite isolates the bulk of the mineral and prevents further oxidation.

The second modeling stage was concerned with calculating whether the thin layer of the oxide on the surface of pyrite could be removed by the low-temperature annealing in vacuum (10^{-10} bar). I used the same possible mineral phases to describe the chemical system as at the first modeling stage with the following amendment: the atmospheric O_2 was excluded from the system and the initial mineral composition was modeled to include 1 mole of pyrite and 1 mole of hematite. The results have shown that the mineral phases are stable at low temperatures and without the free oxygen allowed, but go through the phase transformation with the change of the temperature as shown in Figure 5.16.

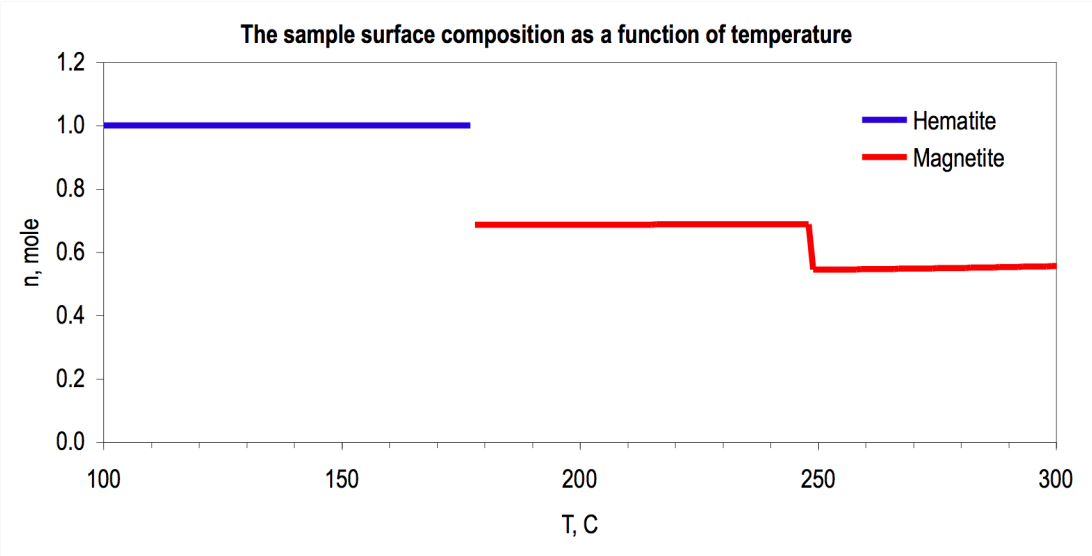

Figure 5.16. The modeled composition of the thin layer of oxidised material on the exposed surface of pyrite (quantity in moles) as a function of temperature. The temperature of phase transition between the hematite and magnetite is 178 ºC.

Figure 5.16 shows the changes to the composition of the oxide layer on the pyrite surface. At temperature close to 178 ºC a loss of a small amount of O_2 occurs, as hematite (Fe_2O_3) transforms to magnetite (Fe_3O_4). I have observed experimentally the change of the state of the sample surface visible by eye at the temperature interval 175-185 ºC, which was accompanied by a small fluctuation of the base pressure in the vacuum chamber (about $5x10^{-8}$ Pa). The polished surface of the sample has become dull, although there were no changes in the STM images or in the surface roughness and the formation of a different phase on the surface could plausibly explain my observations. Figure 5.17 shows the changes in the composition of the bulk of the pyrite as the temperature elevates. When the temperature reaches 249 ºC the pyrite is replaced by pyrrhotite ($Fe_{0.877}S$), this phase transition is accompanied by the loss of part of the sulphur and its release in a gaseous state.

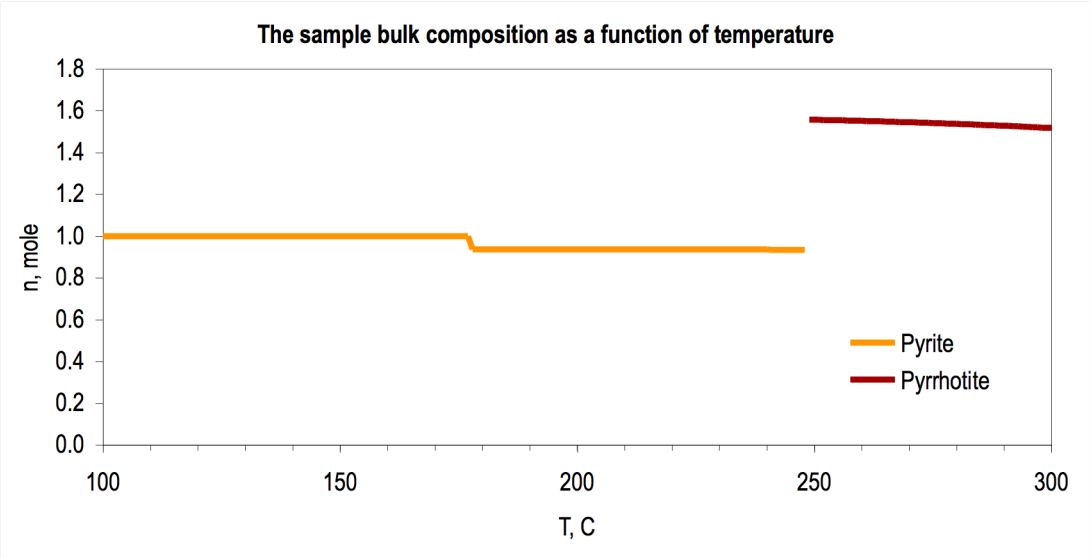

Figure 5.17. The composition of the bulk of the sample (quantity in moles) as a function of temperature. The temperature of the pyrite-pyrrhotite phase transition is 249 ºC.

Thus, the thermodynamic modeling has shown that at extremely low pressure, similar to the base pressure in the STM chambers, the increase of temperature results in two phase transitions: firstly, a phase transition of the surface oxide layer, with the release of O_2 at 178 ºC, and secondly, a phase transition of the bulk of pyrite, with the release of S_2 at 249 ºC. The result of the modeling allows me to conclude that if the oxide layer has formed on the surface of pyrite, it is impossible to restore the surface by annealing at the temperatures that are lower than the temperature of the phase transition of the bulk of pyrite, which results in complete deterioration of the sample. I tried to use Ar+ sputtering-annealing cycles at lower temperatures and found that this method did not remove the oxide layer. The sputtering is not recommended for the pyrite samples as it has resulted in the permanent roughening of the surface which was not recovered by the subsequent annealing below the phase transition temperature.

To summarise, a well-prepared pyrite (100) surface exhibits narrow atomically flat elongated terraces with 5.17 Å height and the atomic arrangement of Fe substructure (filled states)

which reflects the symmetry of the fcc (100) bulk substrate. The surface is considered to be chemically active in general, particularly on Fe^{+2} sites[134], with possible increased local reactivity of the surface on the step edges. The surface should be prepared in the oxygen free atmosphere or cleaved in vacuum to avoid the formation of the oxide layer. If the oxide layer has formed, it is impossible to remove it without compromising the integrity of the surface. When I describe the results of the experiments on the pyrite surfaces in Chapter 8 I assume that the majority of the surface area has been oxidized.

Chapter 6

Uracil self-assembly on Au (111)

This chapter concerns the self-assembly of uracil on the Au (111) surface. The ability of RNA bases to self-assemble into larger structures is an important research area relevant to the origins of life. If nucleobases are regarded as fundamental building blocks for macromolecules like RNA, the self-assembly of RNA bases on surfaces may assist our understanding of the problem of the origins of life and offer an insight into the processes of the biochemical evolution before the complex organisms were created.

The surface may play a significant role in the process of the self-assembly. For example, it can act as a catalyser, inducing chemical reactions[6] or facilitate otherwise unfavourable chemical reactions by limiting the rotational and translational degrees of freedom of adsorbed molecules[135]. It has been demonstrated that adsorption on highly reactive surfaces can lead to the formation of peptide bonds between amino acids[3,54] and cause chiral selectivity[136-24]. But to judge accurately the impact of surface-molecular interactions I must first consider the self-assembly of nucleobases on a catalytically inert surface which allows diffusion and the formation of lateral bonds. Thus I should be able to observe molecular networks, which are determined by the spatial arrangements of the molecules and by intermolecular bonds under conditions such as that the surface has a weak or no effect on the ordering.

Here I report the results of a large experimental study of the self-assembly of uracil on the

Au (111) surface. Not much experimental work has been done to date on the 2-dimensional self-assembly of uracil, though the 3-dimensional self-assembly of these molecules has been studied extensively[137,138]. A few studies of the adsorption of adenine, cytosine, guanine and thymine on Au (111) surface, both experimental and theoretical, are available[29,139]. Adsorption of uracil at high coverages on the Au (111) and the Ag (111) surfaces in vacuum and co-adsorption of adenine and uracil have been studied previously in liquid on the MoS_2 surface using STM and aperiodical bimolecular structures were observed in-situ and reported[140-143]. However, to my knowledge there are no recent comprehensive studies of the formation of low coverage structures and chiral porous networks of uracil on the Au (111) surface in UHV. Unfortunately, it has not yet been possible to resolve small nucleobases at the atomic level experimentally due to small corrugations of the local density of states at the Fermi level[31], so the molecules appear as round objects in the STM image. It should be noted that uracil molecules can assume two planar configurations when absorbed on a flat surface, and can form chiral networks stabilized by hydrogen bonds[29,144,44]. These chiral networks have an added interest as all known life forms use only one chiral form of amino acids in their DNA-coded enzymes and proteins[74].

The results of this study demonstrate a number of lateral molecular assemblies that can be achieved on a chemically inert surface with minimal molecule-surface interaction. Two of the molecular phases described here were observed for the first time, and one of these phases could be comprised of alternating chiral domains. In this chapter I will discuss the influence of the surface symmetry of the catalitically inert surface, the degree of coverage and the geometry and strength of the hydrogen bonds on the self-assembled uracil networks and the chiral selectivity of the Au (111) surface.

6.1. Experimental methods

For clarity, I briefly repeat here the methods used and the conditions in which the experiments with uracil molecules on the Au (111) surface were carried out. More details on the experimental methods can be found in Chapter 2 and more detailed information about the sample preparation and the surfaces used is given in Chapter 4. All experiments were performed *in situ* at ambient temperature using ultra high vacuum scanning tunneling microscope JEOL JSTM4500S under base pressure of 1.5 x 10^{-8} Pa. I used Au (111) films grown on mica (Agilent) as a substrate. The substrates were mounted on top of polished $SrTiO_3$ to allow the use of direct DC resistive heating; the resistance of the mounted samples was typically 4-6 Ω. All Au (111) surfaces were prepared by argon sputtering and subsequent annealing to 600 ºC for 1.5 hours and featured large terraces with the characteristic 22 x √3 surface reconstruction. Electrochemically etched tungsten tips were used to obtain images in constant current mode with bias voltage applied to the sample.

Uracil molecules (Aldrich, 99 % purity) were sublimed at 90 ºC onto the substrate held at ambient temperature with the deposition rate of 0.2 ML per minute. I used Image SXM and WSxM software for processing and analyzing of all images[145].

6.2. Uracil on Au (111)

Uracil forms a variety of networks on the Au (111) surface at ambient temperature shown in Figure 6.1.

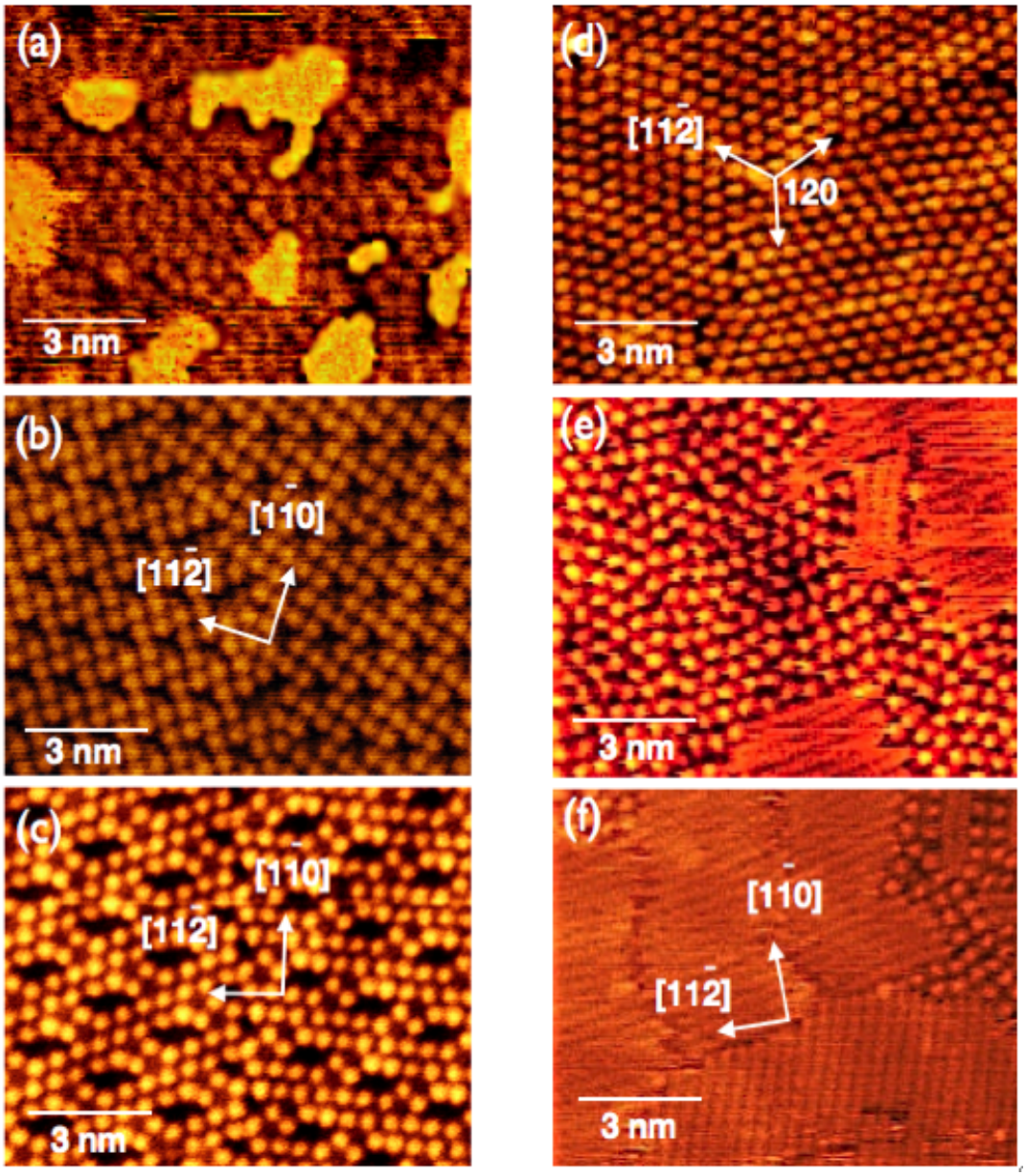

Figure 6.1. STM images of different molecular networks of uracil on Au (111) surface in order of coverage: (a) double chains and basic ordering elements, 0.25-0.4 ML coverage; (b) tip-induced square structure, 0.4-0.75 ML; (c) porous structure, 0.4-0.75 ML coverage; (d) close-packed (hexagonal) packing, 0.75-1 ML; (e) elements of condensed structure, where uracil molecules are tilted rather than laying parallel to the surface as in (a)-(d), above 1ML; (f) condensed structure, above 1 ML. The crystallographic directions of the underlying Au (111) reconstructed surface are indicated by the arrows. The imaging conditions are the same for all images: -1.6 V bias voltage and 0.1 nA and the images were taken at ambient temperatures.

Image (a) in figure 6.1 shows the basic semi-stable elements formed by diffusing uracil molecules, which are usually linked together into unstable double chains or dilines of 5-6

molecular pairs joining in ring-like structures[139] by more stable five-membered ring arrangements. I suggest that these are the basic elements formed by unconstrained uracil molecules when the strong double lateral bonds are dominant and determine the molecular arrangement on the surface. Under closer inspection some variations in the five-member rings can be seen: single five-membered rings, joined five-membered rings and double five-member rings, all of these can be found in the image (a). These structures are very mobile on the surface and change as an area is being scanned; the basic elements, however, stay the same. Possible molecular models for these elements are suggested in Figure 6.3. Image (b) shows a square structure, which I consider to be tip-induced. This structure is rare and only can be seen locally after the area with double chains present at higher coverages (about 0.4 ML) has been imaged for some time; the domains grow larger with the amount of scans until all the molecules in the area have been utilised. The image (c) shows a porous network with five-membered joined rings, and elements of a close-packed arrangement incorporated into the unit cell. This structure is predominant at 0.4-0.75 ML coverages, and coexists with the double chains and the square structure at lower coverages, and with the close-packed arrangement at higher coverages. Possible molecular models for the square and the porous structures are also shown in Figure 6.3. The faint corrugation lines of the surface reconstruction that show through the molecular arrangements can be seen on most images allow us to identify the influence of the underlying surface symmetry on the self-assembly of uracil.

At near monolayer coverage uracil forms a highly ordered close-packed network with a hexagonal packing arrangement as shown in image (d) in Figure 6.1. This structure has been reported before on both Au (111) and Ag (111) surfaces[140,141]. In this structure each uracil molecule is bonded to three of its neighbours, with no five-membered elements

present, and the molecules lie flat on the surface. I have also observed a condensed phase shown in the images (e) and (f) at different stages of development, which occurs only at coverages higher than 1 monolayer (ML). The condensed phase has also been reported previously and the packing model was proposed by Cavallini et al. for uracil adsorption on the silver (111) surface[140]. However, in this model, uracil molecules appear to lie flat on the surface with each uracil molecule bonded to two neighbours within the same row and only the molecules of one orientation have been used. I propose that this structure should comprise uracil molecules of both configurations. Also from the STM images I can see that the width of the rows is 0.51 nm ± 0.004 which is narrower than the width of uracil molecules lying flat (0.65 nm ± 0.008) as in the molecular arrangement below or at 1 ML coverage. I therefore assume that the uracil molecules in the condensed phase are tilted in respect to the surface in order to accommodate more molecules per surface area.

To interpret the molecular arrangements I have observed at the atomic level I used the geometry of hydrogen bonds and maximised the number of stable O...HN or N...HN bonds. I propose possible molecular models based on the following conditions. It has been suggested that DNA bases are rigid molecules and should adsorb flat on the surface, and also at some distance above it, if the surface-molecular interactions are weak as in the case of their adsorption on Au (111)[146]. I assume this applies for uracil, which is very similar to thymine in its structure and the distribution of its bonding sites[29]. I also assume that two planar configurations of uracil molecules are possible at all times and are obtained by flipping the molecule in the molecular plane on the surface. Uracil molecules interact with each other forming strong, near-linear N-HN hydrogen bonds with an average length of 2.82 Å and an angle of 176°, and O-HN hydrogen bonds with an average length of 2.74 Å and angle of 175°[29,27,28]. No data are available for the intermolecular interaction energy for

uracil-uracil pairs at the time of writing. However, Kelly et al. mention that for uracil, the calculated stability of the uracil homopairs is very similar to that of the complementary heteropair (adenine-uracil)[29], and in this case it should vary from -0.99 eV to -0.78 eV, depending on the binding site position.

According to Kelly et al., each uracil molecule has six active bonding sites[29], shown in Figure 6.2, and any molecule could bind to these sites by forming hydrogen bonds. Sites 1-4 contain one acceptor and one donor and sites 5 and 6 contain two adjacent hydrogen atoms. For uracil-uracil networks, only the four sites that contain one acceptor and one donor are valid; sites with two adjacent donors require a molecule with a different structure (with two adjacent acceptors) to create a bond. Therefore, I only considered sites 1-4 to interpret the network configurations; in addition, as site 1 forms a weaker bond than the other three sites[29] the preference was given to sites 2-4 where two strongest bonds can be created. Following the approach suggested by Kelly et al. for heteropairing of DNA bases[29], I have first considered all possible dimers with one donor and one acceptor bonds present, 15 in total, and then used these dimers to build the basic semi-stable elements that have been identified in the STM images at low coverages (see Figure 6.1 for the STM images and 6.3 for the molecular models suggested). Both left and right configurations of uracil are accounted for in our models.

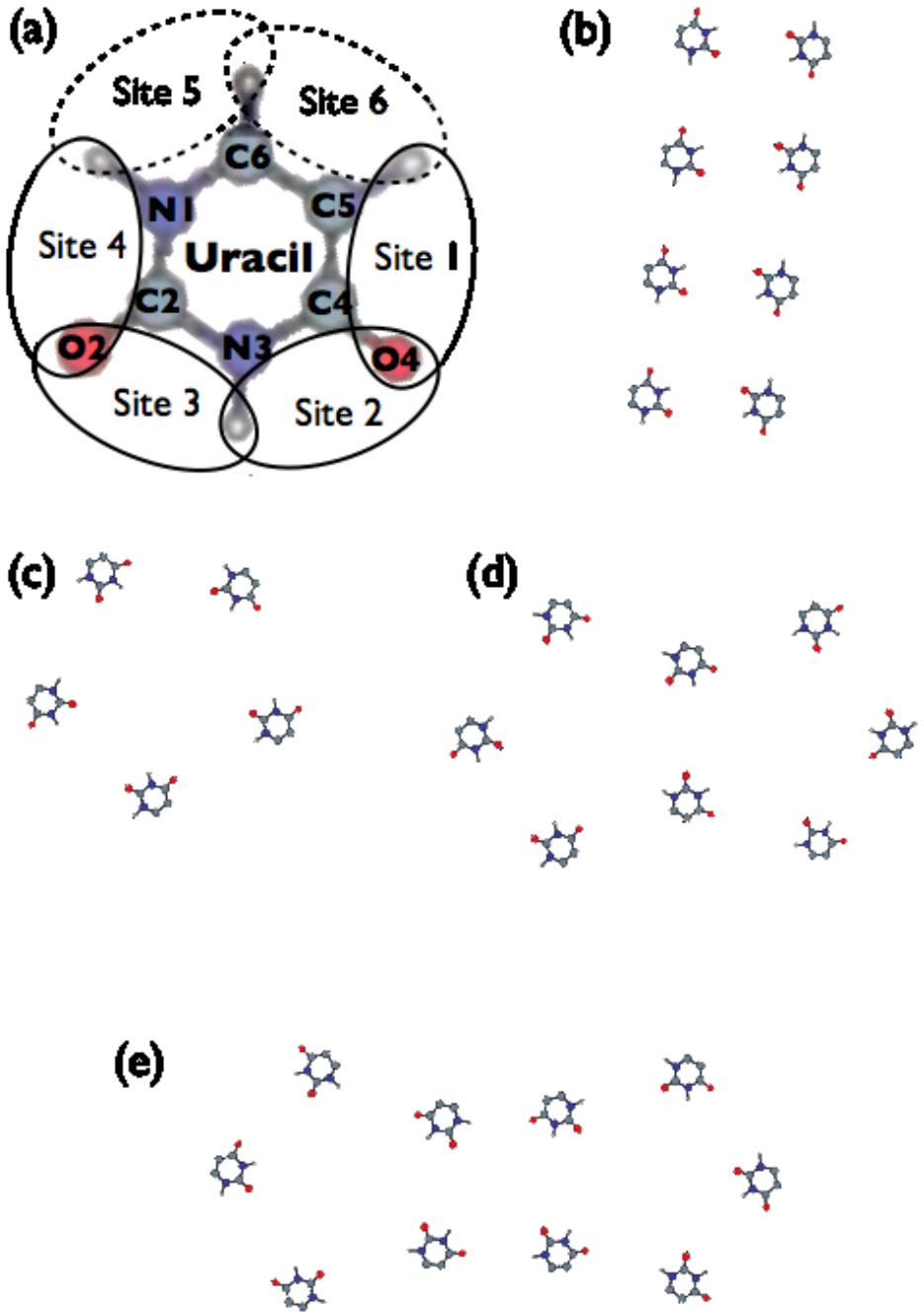

Figure 6.2. The basic elements of the self-assembly of uracil at the low coverages. (a) the chemical structure and the bonding sites of the uracil molecule. The solid lines indicate the sites with one donor and one acceptor, the dashed lines indicate the two hydrogen sites. (b) double chains or dilines, (c) five-membered ring, (d) five-membered joint ring, (e) five-membered double ring. Note that the two hydrogen sites are not shown in the models.

I have used the basic elements described above to propose the possible molecular

arrangements for the two structures I have observed at coverages below 1 ML (Figure 6.3).

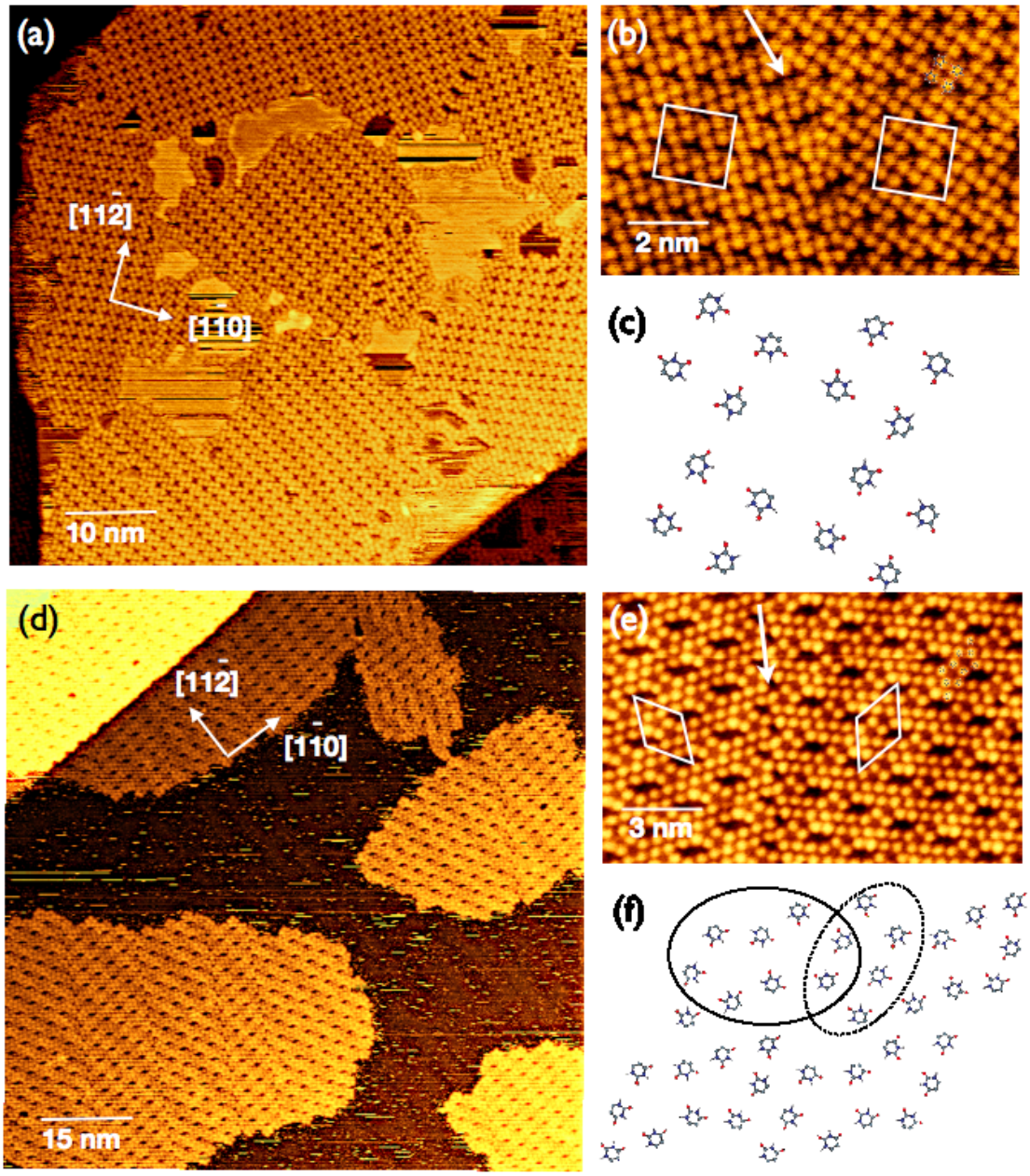

Figure 6.3. STM images of 2D uracil islands which occur at coverages below 0.75 ML. (a) Square molecular network; the unit cells are arranged along three main crystallographic directions of the underlaying Au (111) surface; the surface reconstruction can be seen underneath the molecular arrangement. (b) Close-up image of the square network; the arrow indicates the growth boundary between two islands. (c) The possible racemic model of the square molecular arrangement at the atomic level with 1 donor and 1 acceptor bonds stabilizing the unit cells. (d) Porous molecular network, the unit cells are also arranged along the main crystallographic directions of the Au (111) surface; the faint corrugation lines of the surface reconstruction shows clearly through the molecular

Fig. 6.3 (contd). arrangement. Note the different chiral domains within the islands with clear boundaries. (e) Close-up image of the porous network, the arrow indicates the growth boundary between two neighbouring domains. (f) The possible racemic model of the porous arrangement at the atomic level with some 1 donor and 1 acceptor bonds still present, the solid line shows the five-fold elements, the dashed line shows the elements of the close-packed (hexagonal) arrangement.

6.3. Discussion

As with adenine, I expected that the effect of the surface on the hydrogen bonding between two uracil molecules would be negligible; however, in the case of a larger molecular arrangement the cumulative effect of the underlying surface will start to register and may influence the energetically preferred configuration of bonds between the molecules and the periodicity of the molecular structures[31]. I suggest that the self-assembly of uracil molecules strongly depends on the coverage, and the molecular arrangements are determined by the geometry of the hydrogen bonds at the low coverages when the spatial arrangements necessary for accommodating the five-fold configurations are possible. With increasing amounts of molecules on the surface, it becomes impossible to maintain the five-fold arrangements and hexagonal packing, determined by the surface symmetry, becomes more and more dominant. Eventually, at high coverages the five-fold elements disappear completely and I can only see the close-packed (hexagonal) packing arrangement.

It is interesting to note that the porous molecular network I described above is chiral. I can clearly identify alternating chiral domains of random width within 2-dimensional islands over the size of 50 nm^2; the unit cells in the neighbouring domains are the mirror image of each other. Smaller islands consist of only one domain. The mechanism for the formation of these domains is not clear and to give a definite answer to the appearance of these

domains I need to refer to theoretical calculations. However, simply from looking at the STM images I can suggest that the boundary between the different domains is a growth boundary, and the domains could have started as single domain islands which have grown together to form a larger structure. Alternatively, the propensity of the uracil molecules to flip could cause them to grow a mirror image domain. Possibly, as the domains get larger and the forces within the mono-chiral domain experience some relaxation, the attachment of the opposite chiral form of uracil to the domain boundary could become slightly more energetically preferable. In this case, the formation of alternating chiral domains within a large island could be considered the inherent property in the sheet of either domain.

In conclusion, the results of this study demonstrate a number of lateral molecular assemblies of uracil that can be achieved with minimal molecular-surface interaction. I have proposed possible 2-dimensional arrangements of uracil molecules based on their planar orientation and the geometry of hydrogen bonds. The interaction of uracil with the Au (111) surface is fairly weak as the molecules do not lift the surface reconstruction. However, the self-assembly of uracil appears to be weakly influenced by the Au (111) surface as the unit cells are arranged along the main crystallographic directions of the Au (111). The results of this study also demonstrate that intramolecular bonding rather than bonding to the surface dominates chiral selectivity on the Au (111) surface and the resulting molecular networks strongly depend on coverage. These results will provide a reference point for future studies of the role of surface symmetry and bonding mechanisms in the self-assembly of nucleobases. This study can also provide a useful reference for the future experiments with more chemically active surfaces.

Chapter 7

Uracil and adenine self-assembly on Au (111)

As I have mentioned in the previous chapters, the RNA precursor can be regarded as the first and the simplest living system on Earth. RNA plays the major role in modern living systems, particularly fulfilling transport and catalytic functions in cells, and the sequences of bases, codons, in the RNA molecule carry the genetic information and assist its replication. In the RNA helix the bases are arranged on a sugar-phosphate carcass but it has been suggested that it is likely that the initial ordering was formed on a flat surface[3]. Thus, the surface adsorption and self-assembly of these molecules, the fundamental building blocks of the genetic code, could provide the understanding of the relevant prebiotic process that led to the formation of the RNA precursor, and could be related to the origin of life. Both adenine and uracil are present in the RNA structure as a complementary pair, and adenine-uracil combination is unique to this molecule (in DNA uracil is replaced with thymine). The deciphering of the RNA code showed that adenine-uracil pair is involved in all three stop codons[147]. In this chapter I describe a study of the self-assembly of adenine-uracil mixture on the Au (111) surface.

In the study of the adsorption of uracil on the Au (111) surface I demonstrated that even a relatively inert surface does play a role in the process of the self-assembly as the surface symmetry determines the orientation of 2-dimensional molecular networks (as 2-dimensional network here I describe lateral molecular arrangements on the surface, where the wetting process dominates as opposed to 3-dimensional nanocrystals, which are formed

by clumping). It is possible, that the subtle effect of the molecular-surface interaction leads to less stable bonds to form these networks by limiting the rotational and translational degrees of freedom of adsorbed molecules[135]. In the study described in this chapter I continued the investigation of the behaviour of RNA bases on an inert surface and have used adenine, the RNA base complementary to uracil, and adenine-uracil mixture. I use the same Au (111) surface as a substrate as before.

Not much experimental work has been done to date on the 2-dimensional self-assembly of complementary RNA nucleobases. A few studies of the separate adsorption of adenine and uracil on the Au (111) surface, both experimental and theoretical, are available[29,31,144,139,141]. Co-adsorption of adenine and uracil, had been studied previously in liquid on the MoS_2 surface using STM and aperiodical bimolecular structures were observed in-situ and reported[142,143,45]. The STM images of the 2-dimensional structures of adenine molecule on MoS_2 showed the enantiomorphic chiral structures (see Figure 3.18 in Chapter 3). The STM images of the self-assembly of uracil on MoS_2 showed a herring bone pattern, which possibly originated from the initial hydrogen bonded dimer formation as predicted by theoretical calculations of the planar arranged uracil molecules on MoS_2 lattice (see Figure 3.18 in Chapter 3). However, to my knowledge the adenine-uracil co-adsorption experiments in UHV on the Au (111) surface have not been reported so far.

It has been suggested that adenine like other DNA bases is a rigid molecule and should adsorb flat on the surface, and at some distance above it, if the surface-molecular interactions are weak as in the case of its physisorption on the Au (111)[146]. I assume it is the same with uracil, which is very similar to thymine in its structure and the distribution of the bonding sites[29]. All RNA bases have two planar configurations, and when absorbed on a

flat surface can form chiral networks stabilised by hydrogen bonds[29,31,144,44]. These chiral networks have an added interest as all known life forms use only one chiral form of amino acids in their DNA-coded enzymes and proteins[74]. Unfortunately, is has not yet been possible to resolve small nucleobases at the atomic level experimentally due to small corrugation of the local density of states at typical STM imaging biases[31], and the molecules appear round in the STM image. In this thesis I assume that two planar configurations are possible at all times, and are obtained by flipping of the molecule in the molecular plane on the surface.

7.1. Experimental Methods

All experiments were performed *in situ* at ambient temperature using ultra high vacuum scanning tunneling microscope JEOL JSTM4500S under base pressure of 1.5 x 10^{-8} Pa. I used Au (111) films grown on mica (Agilent) as a substrate. The substrates were mounted on top of polished $SrTiO_3$ to allow us to use direct DC resistive heating; the resistance of the mounted samples was typically 4-6 Ω. All Au (111) surfaces were prepared by argon sputtering and subsequent annealing to 600 ºC for 1.5 hours and featured large terraces with the characteristic 22 x √3 surface reconstruction. Electrochemically etched tungsten tips were used to obtain images in constant current mode with bias voltage applied to the sample. More details on the experimental methods can be found in Chapter 2 and more details about the sample preparation and the surfaces used in Chapter 5.

The uracil molecules used for this study were the same as in the previous one (Aldrich, 99 % purity) and were sublimed at 90 ºC onto the substrate held at ambient temperature with the deposition rate of 0.2 ML per minute; adenine molecules (Aldrich, 99 % purity) were

sublimed at 115 ºC with a similar deposition rate. I have performed solo deposition of both adenine on the Au (111) surface, followed by co-deposition by sublimation of uracil followed by adenine for the first series of experiments and adenine followed by uracil in the second series with no difference in the resulting structures. Post-deposition annealing typically for 12 hours was performed on some of the samples; shorter annealing produced less ordered structures. I used Image SXM and WSxM software for processing and analysing of all images [145].

7.2. Adenine on Au (111)

The self-assembly on adenine molecules on the Au (111) surface has been recently studied both theoretically and experimentally (STM) by Kelly et al[31],[27]. Though I have familiarized myself with these works and have used the suggested approach to the interpretation of the STM images and the proposed DFT calculated molecular models of the self-assembled adenine networks, I decided it necessary to repeat the experiments with adenine on the Au (111) surface. Firstly, to ensure the repeatability of the experiments both at ambient temperature and after annealing, and secondly, to compare my own STM images of the self-assembly of adenine later with the STM images of the self-assembly of the uracil-adenine pair. The STM images of the adenine self-assembly I show in this Chapter were performed by me and are in excellent agreement with the STM images published by Kelly et al. I have used these authors' theoretical models for the adenine networks only (appropriately attributed throughout the text) to demonstrate the distribution of the hydrogen bonds within the networks and to indicate the chirality of the adsorbed molecules.

Adenine molecules are very mobile and diffuse freely on the Au (111) surface, making it

impossible to image individual molecules or individual dimers at ambient temperature though the organization of adenine molecules into dimers is possible in theory[29]. Adenine forms a more stable basic structural element, a distorted “hexagon” comprised of six molecules, and though I have not observed the individual ones in the STM, all the structures I have imaged are formed by these hexagonal elements. At ambient temperatures the hexagons arrange in single chains at low coverages and, as the coverage increases, start to form highly ordered 2-dimensional networks as shown in Figure 7.1. At high coverages (close to 0.75 ML and above), adenine, similarly to uracil, forms a condensed phase (Fig. 7.1 c).

The faint corrugation lines of the surface reconstruction are showing through the molecular arrangement on images (b) and (c) in Figure 7.1. To interpret the structures at the atomic level I use the geometry of hydrogen bonds and maximised the number of stable N...HN bonds. I have also used the equilibrium geometries of the adenine dimers, which were suggested to be the most stable ones by Kelly and Kantorovich, who performed the detailed *ab initio* DFT calculations and identified the active binding sites[29] of the adenine molecule. The adenine molecule, its binding sites and six most stable dimers are shown in Figure 7.2.

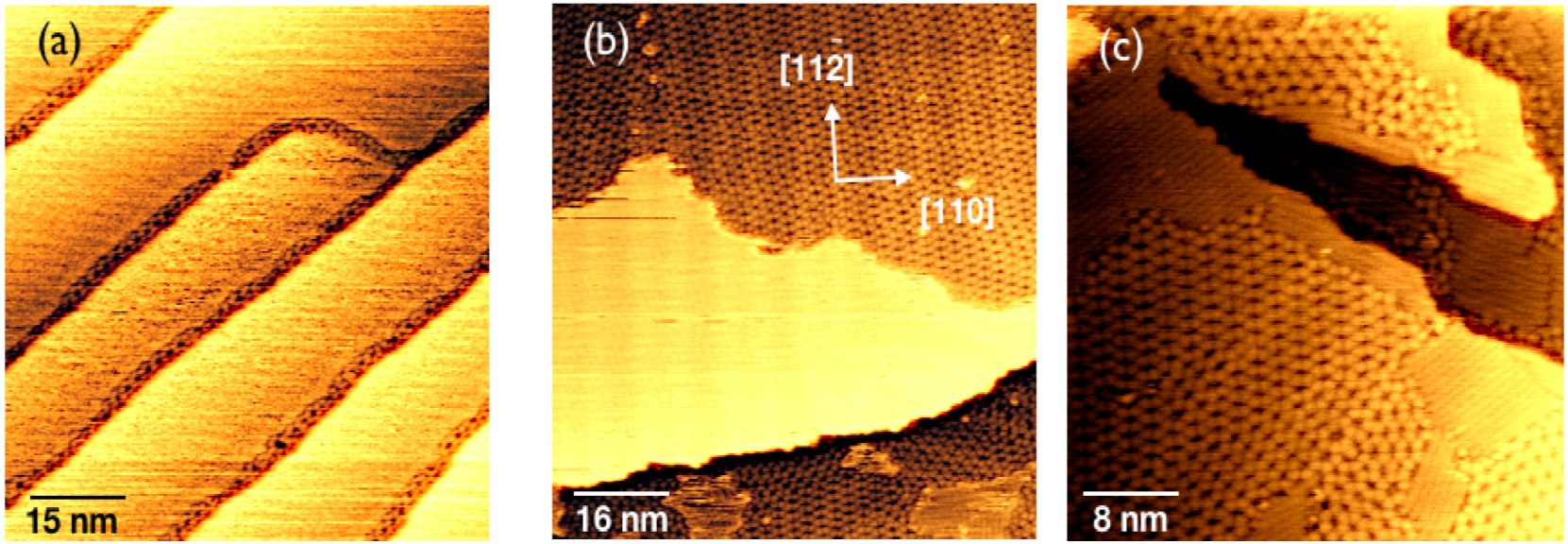

Figure 7.1. STM images of adenine self-assembly on the Au (111) surface at ambient temperature in order of coverage: (a) single chains, originating at the edge of the terraces, less then 0.1 ML coverage; (b) typical hexagon structure, 0.25-0.75 ML coverage; (c) coexisting hexagons and condensed structure, 0.75-1 ML; I suggest that in condensed structure adenine molecules are tilted rather than laying parallel to the surface, similar to the uracil condensed structure as shown in Fig. 6.1 image (f). The crystallographic directions of the underlying Au (111) reconstructed surface are indicated by the arrows on image (b). The imaging conditions are the same for all images in this chapter: -1.6 V bias voltage and 0.1 nA current, the images were taken at ambient temperatures.

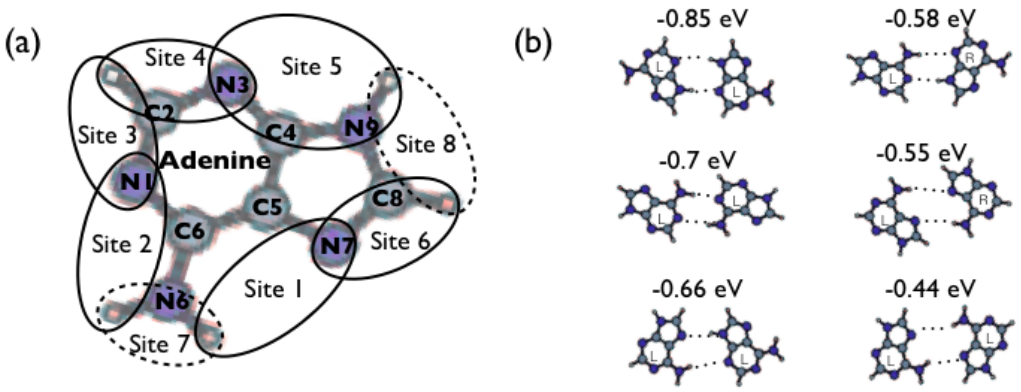

Figure 7.2. The planar adenine molecule in its left-handed configuration and its most stable dimers[148]. (a) The adenine molecule structure with the C and N atom positions and N…HN bonding sites indicated. (b) The six most stable adenine dimers, both chiral and non-chiral monomers, are shown, and their corresponding energies are indicated. The right configuration of adenine used in the dimers is obtained by flipping the adenine of left configuration in the molecular plane.

I assume that two planar configurations of adenine molecules are possible at all times and are obtained by flipping the molecule in the molecular plane on the surface. Adenine molecules interact with each other forming strong near linear N-HN hydrogen bonds with the average length of 2.82 Å and the angle of 176°[29,27,28]. Each adenine molecule has eight possible bonding as sites shown in Figure 6.2, and any molecule could bind to these sites by forming hydrogen bonds. Sites 1-6 as shown contain one acceptor and one donor and sites 7 and 8 contain two adjacent hydrogen atoms. For adenine-adenine networks only the six sites, which contain one acceptor and one donor are valid; sites with two adjacent donors require a molecule with a different structure (with two adjacent acceptors) to create a bond. In total 21 stable dimers are possible, however, Kelly et al.[29] have calculated the energies of hydrogen bonds for all possible adenine-adenine pairs and only the six ones were found to form the networks I have observed in the STM experiments. The energy of hydrogen bonds for six adenine pairs on the Au (111) surface from left top to right bottom as

they are drawn in Figure 6.2 b are -0.85 eV, -0.7 eV, -0.66 eV, -0.58 eV, -0.55 eV, and -0.44 eV and the binding sites 1, 2 and 5 in both left and right configurations of the adenine molecule were found to create the strongest hydrogen bonds.

Kelly et al. have suggested that adenine molecules lie flat on the surface at a distance of 3.5 Å above it, which is in good agreement with other observations for weakly bound π^* systems lying flat on fcc (111) metal surfaces[31,35]. The same authors state that calculated charge-difference density of the molecule on the surface reveals a small charge redistribution between the molecule and the surface for the amino groups, which are not participating in the hydrogen bonding, where the pyramidal formation was observed with H atoms pointing downwards and the N atom pointing upwards, indicating the sp^3 hybridization state[31]. While this may be true for the adenine dimers, it is not necessarily so for the large islands of 2-dimensional networks as the accumulated strain due to the surface epitaxy may have a stronger effect on the molecular ordering within the network. The STM experiments reported in this thesis and cited papers have shown that the interaction of adenine networks with the surface is very small as the molecules do not lift the surface reconstructions, however, the networks are aligned along the main crystallographic directions of the Au (111).

The highly ordered adenine network shown in Figure 7.1 (b) and 7.1 (c) is prevalent at ambient temperatures. It is possible to create another 2-dimensional molecular network, comprised of the similar structural elements, which are aligned differently in relation to each other in comparison with the regular network by annealing the sample at 100 ºC for 12 hours. Both structures and their interpretations are shown in Figure 7.3.

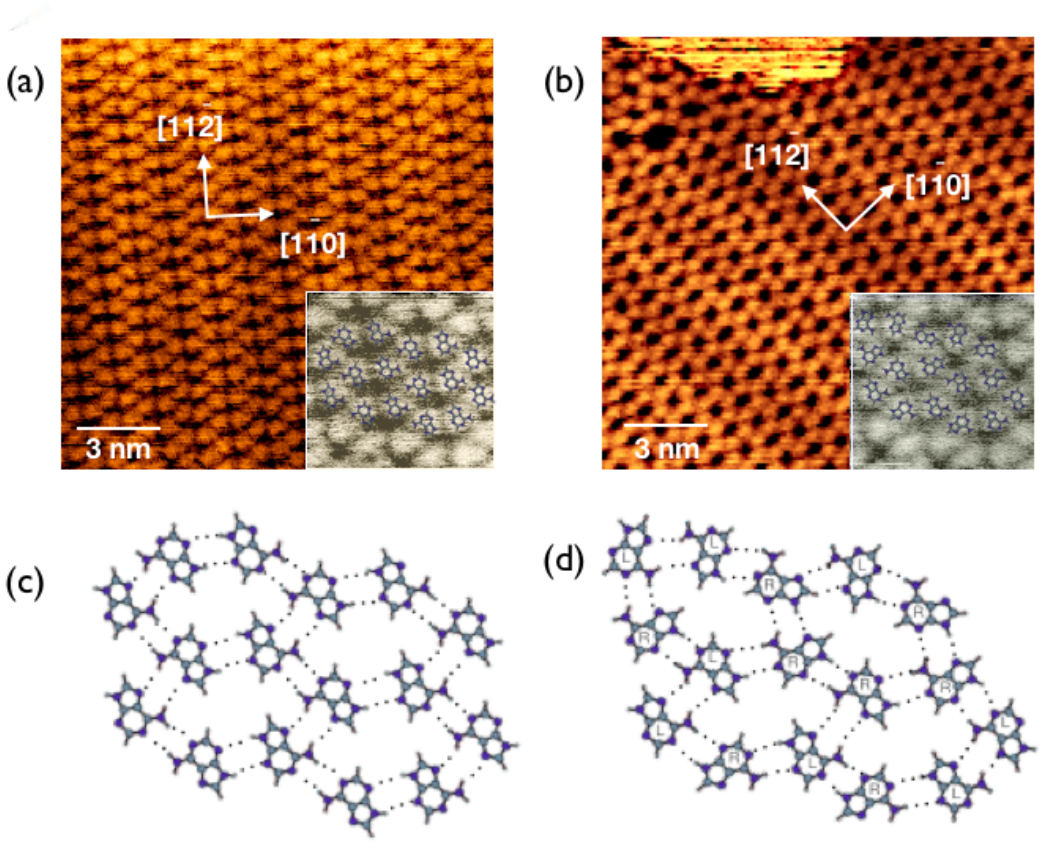

Figure 7.3. STM images of adenine self-assembly on Au (111) surface with high resolution inserts. (a) the regular monochiral network, prevalent at ambient temperature. (b) The polychiral network, prevalent after annealing at 100 ºC, which consists of an equal number of adenine molecules with left and right configurations. This network can also occasionally be found at ambient temperature at the elbow sites of the surface reconstruction of the Au (111). (c) A molecular arrangement for the structure (a) suggested by Kelly et al. who performed the detailed DFT calculations for the self-assembly of adenine networks on Au (111). (d) A molecular arrangement for the structure (b) suggested by the same authors[31].

The molecular arrangements shown here were suggested by Kelly et al.[31]. These authors have reported both adenine structures, as observed in the STM in ultra high vacuum, and performed the detailed DFT calculations to identify both phases. Interestingly, the gas phase stabilities were very similar for both structures: -0.88 eV for structure (a) and -0.91 eV for structure (b). The STM images I took repeating the experiments published by Kelly et al. are in excellent agreement with this study.

7.3. Self-Assembly of Uracil and Adenine Pairs on Au (111)

Adenine and uracil molecules interact with each other forming strong near linear N-HN hydrogen bonds with the average length of 2.82 Å and the angle of 176° and O-HN hydrogen bonds with the average length of 2.74 Å and angle of 175° [29,27,28]. The most stable adenine-uracil pairs out of 21 possible combinations are shown in Figure 7.4.

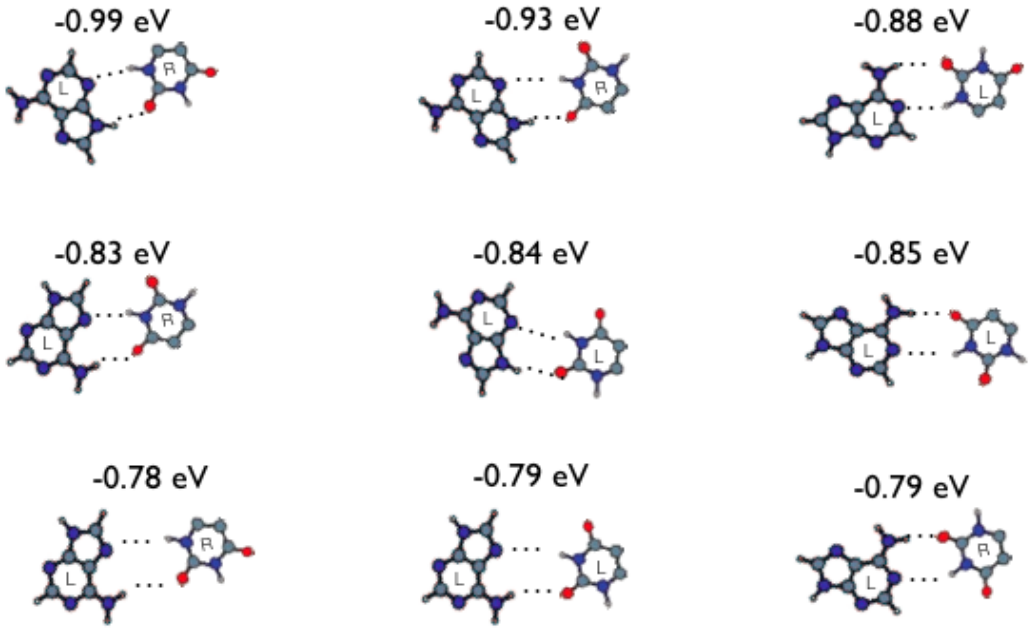

Figure 7.4. Nine most stable adenine-uracil pairs in order of stability showing the N…HN and O…HN bonds and the interaction energies (the image adapted from Kelly and Kantorovich[29]).

Bonding sites 1-6 in adenine molecule and bonding sites 1-4 in uracil molecule, which all contain one acceptor and one donor sites, are capable of forming double hydrogen bonds which are the most stable. I have incorporated these bonds into the molecular models for the networks I observed whenever possible. However, only possible molecular

arrangements are proposed in this thesis when interpreting the molecule arrangements within the adenine-uracil networks, theoretical DFT calculation may be necessary to confirm the interpretation.

Intermolecular interaction energy for adenine-uracil pair varies from -0.99 eV to -0.78 eV, depending on the binding site position; interestingly both Watson-Crick and Hoogsteen configurations[149], found in RNA base pairing, are not the most stable in the gas phase at -0.85 eV[29]. Similar energy values of -0.90 eV and –0.88 eV were reported for adenine-adenine pair[31] and for uracil-uracil pair no data is available at the time of writing, though the same authors mention that for both uracil and adenine the calculated stability of the homopairs is very similar to the one of their complementary heteropairs[29], which makes co-existence of these structures on the inert surface probable, and it is indeed what I have observed in some of the STM images.

Adenine and uracil do not form bi-molecular networks on the Au (111) at ambient temperature, a little extra energy is needed for overcome the energy barrier and allow the molecules to move and flip on the surface, which is provided by low temperature annealing in further experiments. As shown in Figure 7.5 at ambient temperature the molecules form two separate phases, which are clearly distinguishable in the STM image as different domains with clearly defined borders.

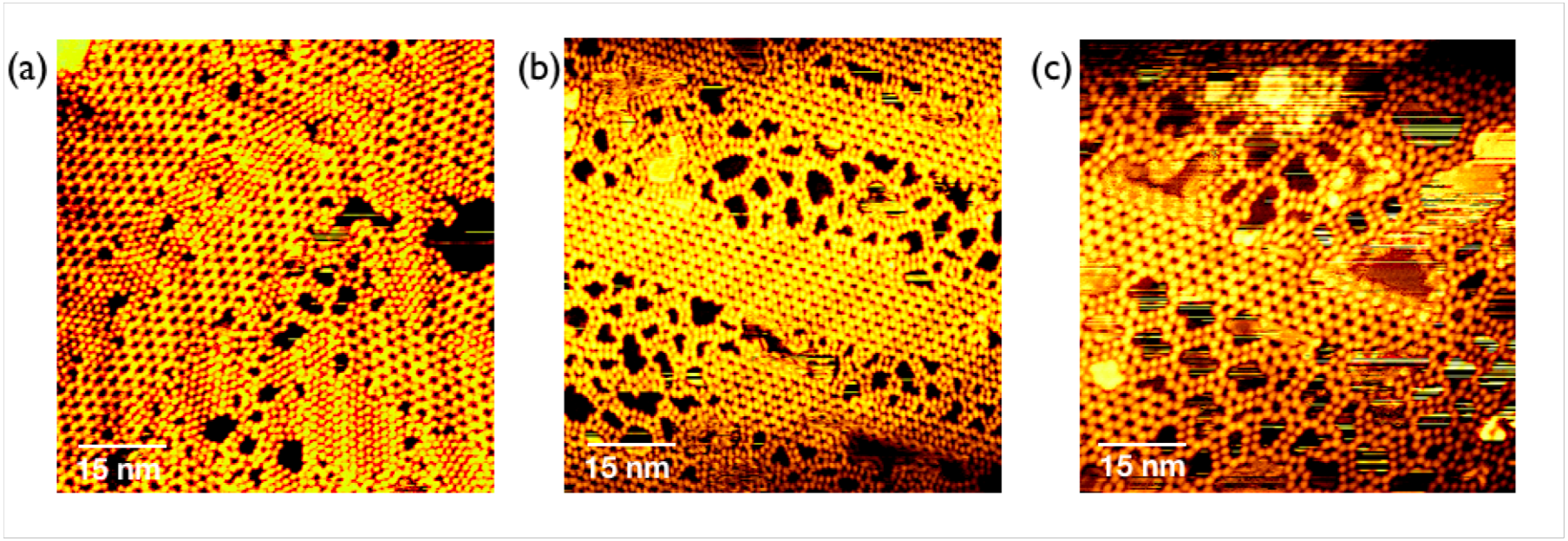

Figure 7.5. STM images of adenine and uracil domains forming coverages near 1 ML on the Au (111) surface. (a) An STM image taken after the initial co-deposition of adenine and uracil molecules. The molecules form two clearly distinguishable phases on the surface; the corrugation lines of the reconstruction are visible underneath the molecular arrangements on the STM image. (b) Transition stage, with some loss of uracil from the surface. (c) Mixed adenine and uracil phase with some elements of an ordered structure.

A series of post-deposition annealing experiments for 12 hours in 5-10 ºC increments were performed on this sample. After annealing at 80 ºC adenine islands started to break up and a mixed adenine-uracil phase with some elements of an ordered structure was formed as shown in Figure 7.5 (c). Further annealing between 85 ºC and 100 ºC allowed me to create the regular bimolecular adenine and uracil structure shown in Figure 7.6 (b). By varying the amount of uracil molecules deposited on the surface while keeping the amount of adenine molecules constant, three different regular bimolecular networks of adenine and uracil with a large unit cell were created by annealing the samples at 100 ºC (see Fig. 6.6 and Fig. 7.7). The main difference between the networks is in the number and the position of uracil molecules incorporated in the unit cell. When the annealing temperature reached 110 ºC all regular bimolecular structures deteriorated and uracil sublimed from the surface leaving islands of pure adenine as shown previously. All these molecular phases are very different from pure uracil and pure adenine phases observed in the previous experiments. In some of the images (say, image (b) in Fig. 7.7) it is possible to visually distinguish between adenine (larger molecules of triangular shape) and uracil (smaller molecules of round shape).

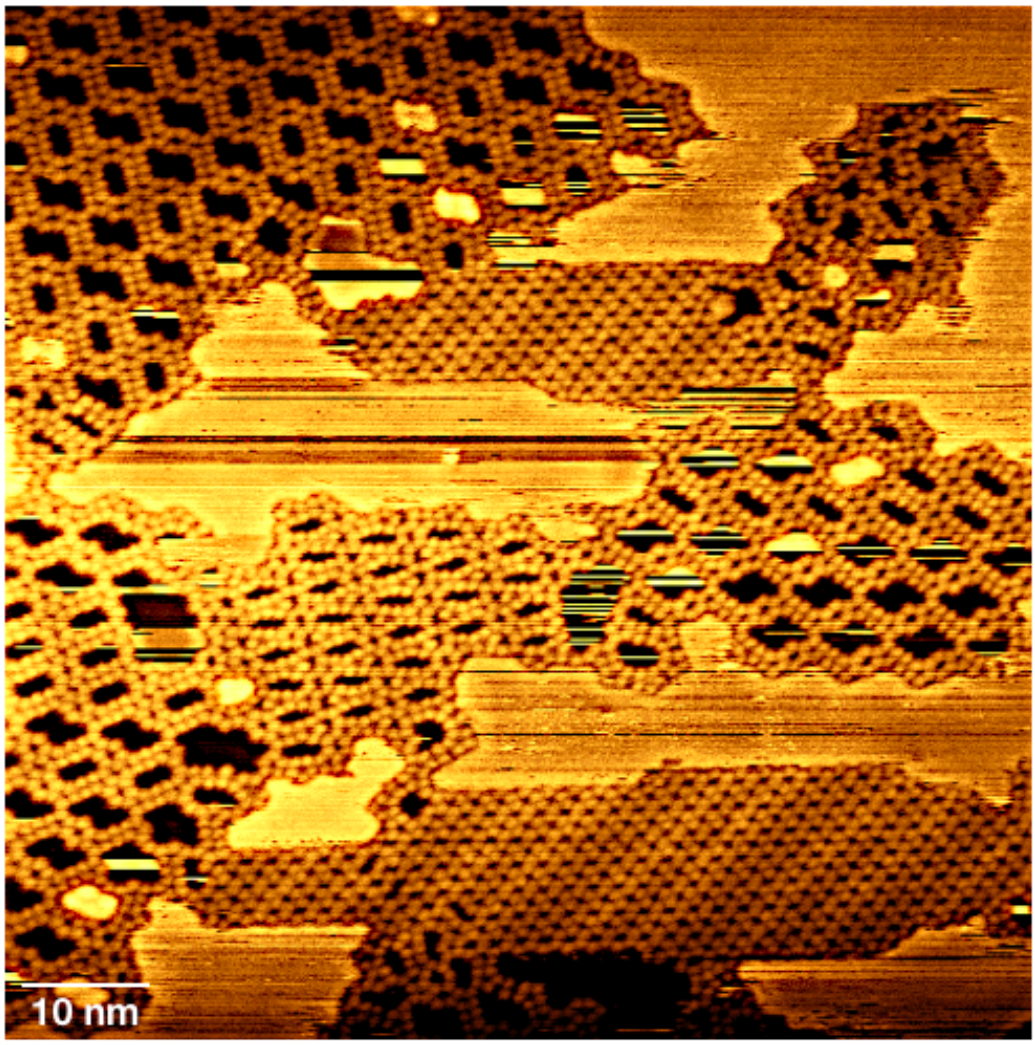

Figure 7.6. A typical STM image showing coexistence of all three networks and the presence of pure adenine islands of polychiral adenine structure. All bimolecular networks align along the main crystallographic directions of the underlying Au (111) surface. The faint corrugation lines of the surface reconstruction can be seen showing through pure adenine islands.

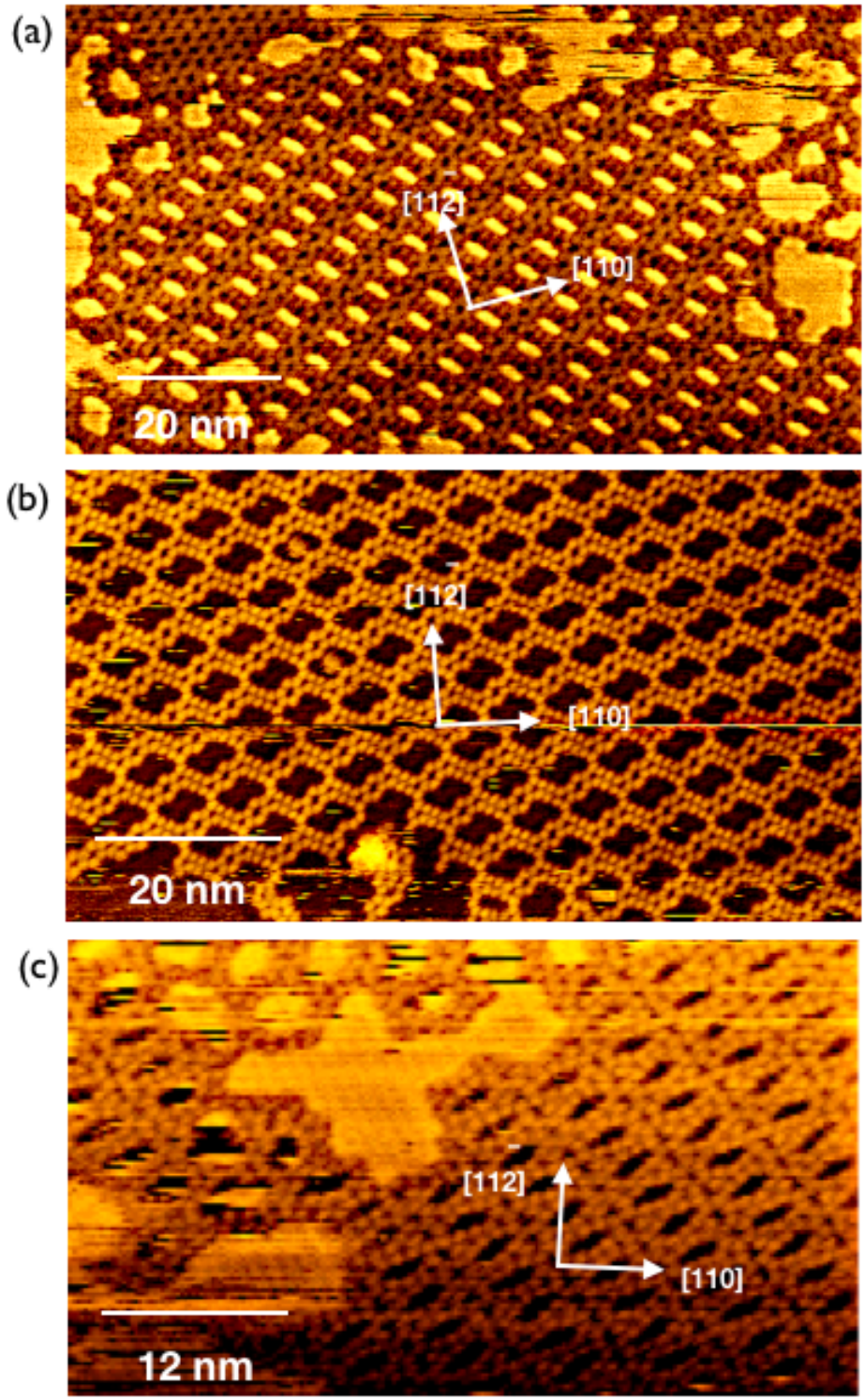

Figure 7.7. STM images of adenine and uracil bimolecular networks on the Au (111) surface. (a) An STM image of a large island of porous bimolecular network I call “O” structure in this thesis as suggested by the shape of the pores. (b) An STM image of a large island of a porous bimolecular network I call “S” structure. “O” and “S” often are present in the same island as can be seen in Figure 7.6. (c) An STM image of an island of a porous bimolecular network I call an “X” structure as suggested by the configuration of the uracil molecules between the lines of adenine hexagons.

Some of the pores of the “S” structure in Figure 7.6 appear dark or “empty” and some appear “filled” in the STM image. My interpretation is that an Au adatom is occasionally trapped in the pore of the network and cannot escape. However, at room temperature the diffusion is much faster than the STM scanning rate so the adatom appears as continuously bright within the pore making it look as if it is “filled”.

Close-up STM images of the adenine-uracil regular porous bimolecular “O” and “S” structures are shown in Figure 7.8. These two networks comprised 80 % of the molecular arrangements on the sample. The bimolecular “X” structure is relatively rare and comprises 10 % of the molecular arrangement on the surface. The other 10 % I identified as the polychiral adenine network as shown previously. I propose possible molecular structures for “O” and “S” bi-molecular networks which involves both planar configurations of uracil and adenine as shown in Figure 7.8 (d) and (e). Both networks are formed by typical distorted hexagon units of adenine joined together by uracil double chains and aligned along <1,1,-2> directions.

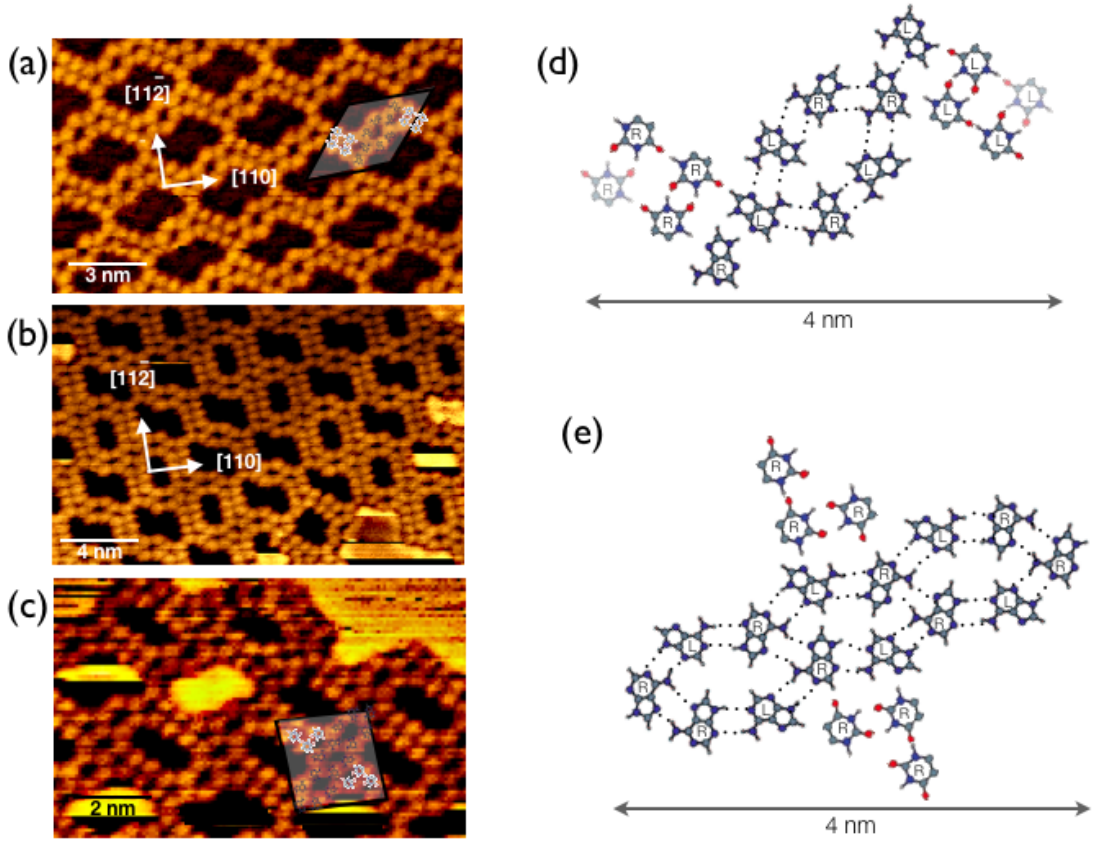

Figure 7.8. Close-up STM images of bimolecular adenine-uracil "O" and "S" structures on the Au (111); the adenine molecules are indicated in blue and the uracil molecules are indicated with white within the structural motifs outlined in black in (a) and (c). (a) An STM image of "S" structure with molecular resolution. In this image it is possible to distinguish visually between adenine and uracil – adenine molecules appear larger and slightly triangular in shape, uracil molecules are smaller and more round. It is, however, a very rare state of the tip with allows imaging with such precision at ambient temperatures. (b) An STM image of alternating "S" and "O" structures within the same island with molecular resolution. (c) An STM image of "O" structure with molecular resolution. (d) Possible molecular structure for the "S" network corresponding to a unit cell indicated on the STM image (a). (e) Possible molecular structure of the "O" network corresponding to a motif element indicated on the STM image (c).

It can be seen from the STM images that the "O" network can be formed from the "S" network by moving the adenine hexagon element by half periodicity to create a more compact structure. Most of the islands I have observed include elements of both networks as seen in Figure 7.8 (b); occasionally I have seen large islands of either structure "O" or

structure “S” as shown in Figure 7.6.

The third bimolecular adenine-uracil structure “X” is comprised of the same adenine hexagon elements and uracil double chains but both structural elements are distorted (see Figure 7.9). This structure is rare and though I have observed the individual islands, they comprise only 10 % of all molecular arrangements on the surface. The island size distribution is very similar for “O” and “S” molecular networks and varies between 600 nm^2 and 1066 nm^2 but the “X” structure forms smaller islands with maximum size of 170 nm^2.

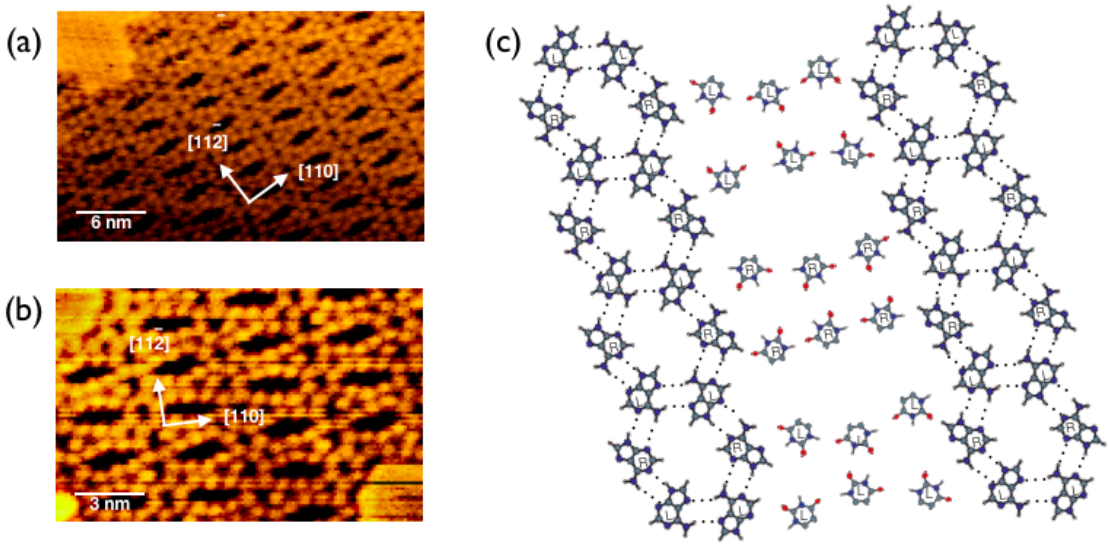

Figure 7.9. The bimolecular adenine-uracil “X” structure on the Au (111) surface. (a) The STM image of an island of the “X” structure, the crystallographic directions of the substrate are indicated by the arrows. (b) A molecular resolution STM image of the “X” structure. (c) An ‘ideal’ molecular model of the “X” structure showing the main basic elements of adenine and uracil without the distortion to the adenine hexagons.

The distortion of uracil double chains is shown in the model but the corresponding distortion of the adenine dimers is not. I have drawn the model in an "ideal" configuration to make the periodicity and the repeating elements of the structure easier to observe. On the STM image it can be seen that only every third adenine hexagon has retained its "original" shape, the other ones have one molecule "pulled" to one side, I assume, by the strong double bonds. This structure can be regarded as a variant of the "O" network but with double bonds between adenine and uracil molecules present at some junctions, which cause the distortion of adenine hexagons. Interestingly, this arrangement allows the incorporating of Hoogsteen configuration of the hydrogen double bonds[149], found in RNA base pairing, into the model. A large-scale molecular model of the "X" structure is shown in Figure 7.10.

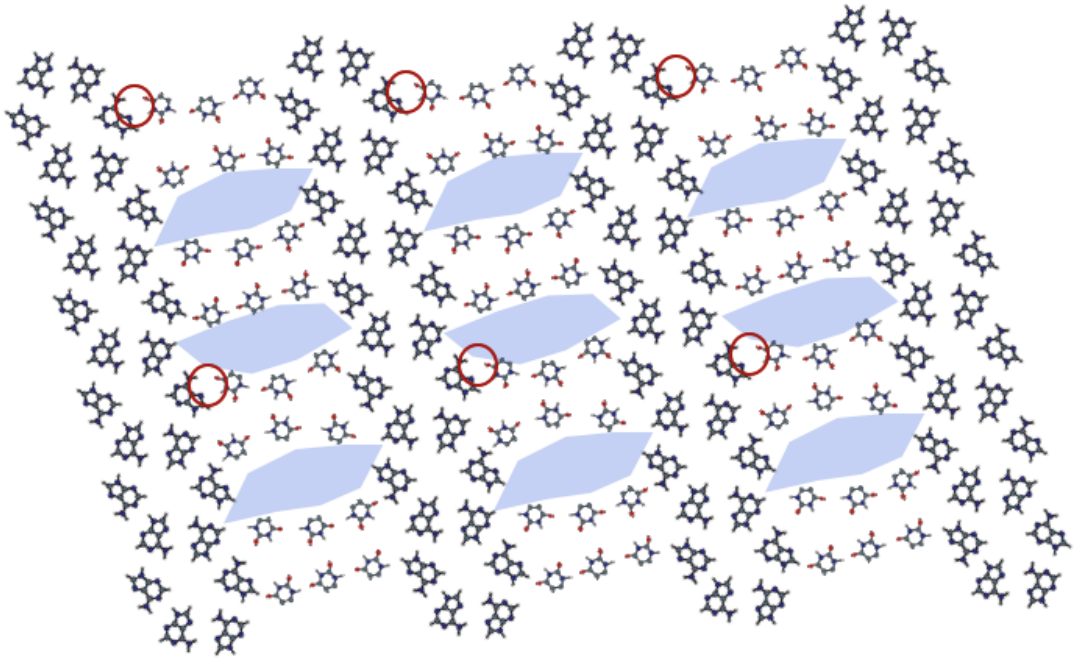

Figure 7.10. A large-scale molecular model of adenine-uracil "X" structure showing the periodicity of the structure. The pores are indicated by the light blue polygons and the red circles show the Hoogsteen configuration of hydrogen bonds between adenine and uracil molecules.

7.5. Discussion

Similar to the uracil self-assembly on the Au (111) surface, the effect of the molecule-surface interaction can be observed for both adenine and adenine-uracil mixture as the networks align along the main crystallographic directions of the substrate. I suggest that the self-assembly of uracil and adenine networks depends on coverage and on the local ratio between adeine and uracil molecules on the surface. As in the case with pure uracil and pure adenine, the resulting molecular arrangements are determined by the geometry and the strength of hydrogen bonds.

When the molecules are deposited on the surface at ambient temperature, they aggregate naturally into the strongest base units, appropriate for the coverage achieved. I note that low temperature annealing of the sample is necessary for obtaining a mixed adenine-uracil phase. The reason for it could be that as the temperature increases some loss of both uracil and adenine occurs and as a result a larger space is available for molecules left on the surface, which facilitates the formation of a mixed phase. At the elevated temperatures molecules can also flip, detach from the edges of the islands easier, diffuse across the surface and attach again or desorb and re-adsorb, with the surface symmetry having some effect on the new growing structures.

Six molecular phases were described in this chapter, three of which are mixed adenine-uracil phases and were observed in the STM for the first time to coexist on the Au (111) surface. There are no previous STM studies to date that report a mixed phase of adenine

and uracil on any surface. I have proposed the possible 2-dimensional arrangements of adenine and uracil networks based on the molecular resolution STM images, the planar orientation of the molecules and the geometry of hydrogen bonds. One of the phases shown may incorporate the Hoogsteen configuration of hydrogen bonds, as found in the RNA helix, in the regular porous structure. The interaction of both adenine and uracil with the Au (111) surface is fairly weak as the molecules do not lift the surface reconstruction. However, the self-assembly of uracil and adenine appears to be weakly influenced by the Au (111) surface as the unit cells are arranged along the main crystallographic directions. However, without theoretical calculations I can only speculate what is the role of the Au (111) surface in the formation of bi-molecular networks. A large and comprehensive study of adenine adsorption on the Au (111) surface by Kelly et al.[31] has demonstrated that the effect of the surface on the hydrogen bonding between two adenine molecules is negligible, however, it is possible that in the case of a larger molecular arrangement the cumulative effect of the underlying surface may influence the energetically preferred configuration of bonds between the molecules and the periodicity of the molecular structures. I believe this could be also true for the formation of bimolecular adenine-uracil networks on Au (111) surface.

The results of the study of the self-assembly of adenine and uracil described in this chapter form the basis for the further the experiments with the same molecules using a pyrite (100) surface as a substrate. I will use the results discussed above as a reference point for study of the possible role of the surface of pyrite in the self-assembly of nucleobases, described in the next chapter.

Chapter 8

Uracil and adenine self-assembly on pyrite (100)

In this chapter I describe the study of the self-assembly of adenine, uracil and adenine-uracil mixture on the pyrite (100) surface. As mentioned before, the ability of RNA bases to self-assemble into larger structures could be relevant to the origins of life, and the surface of pyrite has been suggested as a one of the possible catalysts, which could assist the formation of large macromolecules from the nucleic bases, and provide a template for this process[5]. This is the first STM study of the self-assembly of the RNA bases on the surface of pyrite as far as I know; and I have chosen to start with the (100) surface as it is the most stable naturally-occurring surface in pyrite crystals. The adsorption of adenine on the (100) surface of pyrite has been studied before by photoemission and soft X-ray photoadsorption spectroscopy[40]. The results suggested that the adenine molecule could be binding to the surface of pyrite in two ways: firstly, physisorbed in condensed multilayers, which are not oriented on the surface and secondly, chemisorbed, with molecules bonded with the molecular plane edge-on to the substrate surface. The angle of the tilt of the molecule with respect to the surface was not possible to determine. Interestingly, the second orientation was observed on both clean and oxidised surfaces and the valence band of adenine in this state showed some changes that were attributed by the authors to the chemisorption process.[40] However, from the results published by Plekan at al.[40] it is difficult to say with certainty whether the (100) surface of pyrite does indeed impose a highly ordered molecular adsorption or not, though some ionic bonding to the surface definitely takes place. The STM experiments made it possible to observe the adsorption of adenine molecules on the (100)

surface of pyrite directly.

In the study of the adsorption of uracil and adenine on the Au (111) surface described in the previous chapters, I have seen that even a catalytically inert surface does play a role in the process of the self-assembly as the surface symmetry determines the orientation of 2-dimensional molecular networks. It is possible that the effect of the strong molecular-surface interaction as in the case of chemisorption, leads to an arrangement that fully reflects the surface symmetry, particularly the Fe (positively charged) sites. In the study described in this chapter, I have conducted an investigation of the behaviour of RNA bases on a potentially catalytically active surface and have used adenine, uracil, and adenine-uracil mixture for deposition. I used the pyrite samples with home-made polished (100) surface as a substrate, as described in Chapter 5.

8.1. Experimental methods

All experiments were performed *in situ* at ambient temperature using the ultra high vacuum scanning tunneling microscope JEOL JSTM4500S under a base pressure of 1.5 x 10^{-8} Pa. I used pyrite samples cut out of the monocrystals with strirated {100} faces and polished parallel to a natural (100) plane. The substrates were mounted directly in the sample holder, which allows me to use direct DC resistive heating; the resistance of the mounted samples was typically 8-12 Ω. All pyrite (100) surfaces were prepared by low temperature annealing at 300 °C for 1.5 hours or until the pressure in the chamber returned to the base level and featured small elongated terraces with a width of 5-40 nm in the <110> direction. Electrochemically etched tungsten tips were used to obtain images in constant current mode with bias voltage applied to the sample. More details on the experimental methods

can be found in Chapter 2 and more details about the sample preparation and the surfaces used in Chapter 5.

The adenine and uracil molecules used for this study were the same as in the previous ones (Aldrich, 99 % purity) and were sublimed at 90 °C onto the substrate held at ambient temperature with the deposition rate of 0.2 ML per minute; adenine molecules (Aldrich, 99 % purity) were sublimed at 115 °C with a similar deposition rate. I performed a solo deposition of both adenine and uracil on the pyrite (100) surface, followed by a co-deposition by sublimation of uracil followed by adenine in the first series of experiments and adenine followed by uracil in the second series with no difference in the resulting structures. Post-deposition annealing (at the same temperature ranges as for the experiments on the Au (111) surface), typically for 12 hours was performed on some of the samples; the annealing had no effect on the structures observed. I used Image SXM and WSxM software for processing and analysing of all images [145].

8.2. Adenine on pyrite (100)

At coverages below 0.30 ML adenine molecules adsorb preferentially at the edges of the terraces, where the uncompensated S-S bonds could be found, as shown in Figure 8.1 (a). Adenine molecules appear oval in the STM image rather than round, as I have seen them previously, when adsorbed on the Au (111) surface, and it is possible that as suggested by Plekan et al.[40], adenine adsorbs with the molecular plane edge-on to the surface substrate.

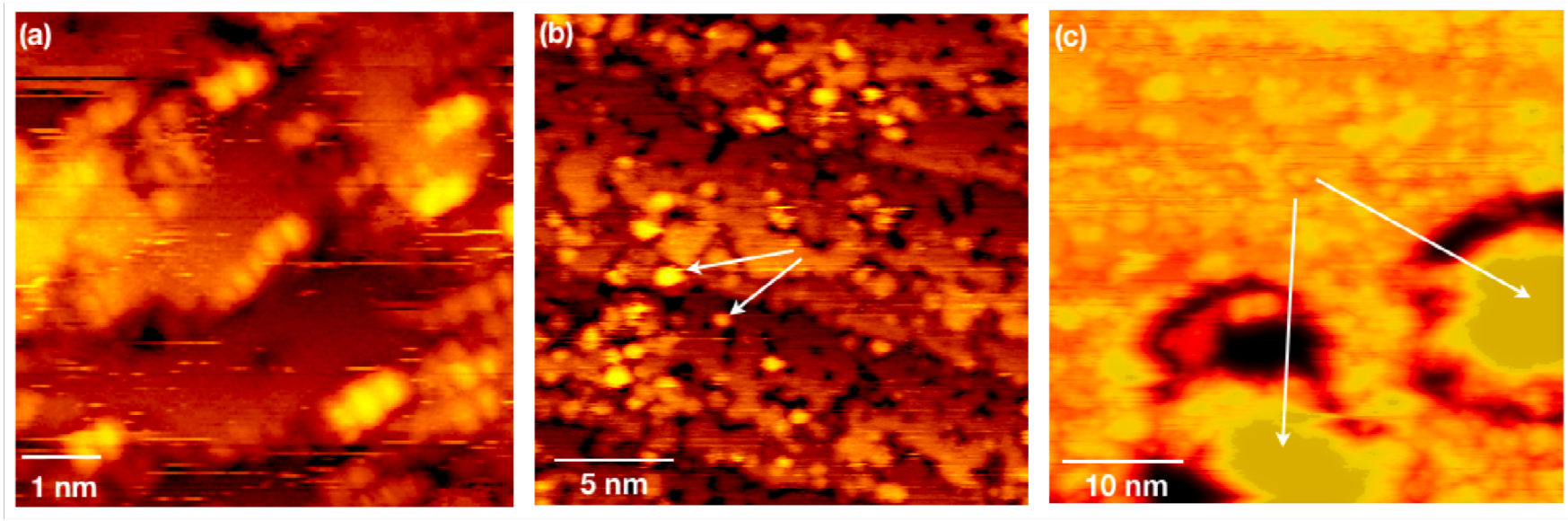

Figure 8.1. STM images of the self-assembly of adenine on the pyrite (100) surface in order of deposition time. (a) A close-up image on adenine with molecular resolution at low coverage (<0.3 ML, deposition time: 2 minutes) showing short chains of single molecules. The molecules appear oval in the image, so could be tilted with respect to the surface. Unfortunately there is some evidence of the "double tip" effect in this image. (b) A medium-scale STM image of adenine on the pyrite (100) surface (deposition time: 5 minutes). Individual molecules can no longer be resolved as small 3-dimensional aggregates or crystals (indicated by arrows) have formed on the surface in places, where the first molecules had absorbed. (c) A medium-scale STM image showing two adenine crystals indicated by arrows (deposition time: 10 min). The edges of the terraces and the bare surface of pyrite are clearly visible in all three images. The images were taken at 1.6 V bias voltage and 0.1 nA current at the constant current mode and at ambient temperature.

The time of the deposition was doubled for the next experiment in an attempt to create longer chains and extend the coverage beyond the terrace edges. When the surface was imaged post-deposition, the individual molecules could no longer be observed and small aggregates or crystals have formed near the edges of terraces or local defects, presumably on the sites where the initial nucleation has started – see Figure 8.1 (b). The edges of the terraces and the bare surface of pyrite are still visible in the STM image so one can see that no 2-dimensional structures were formed on the terraces.

The time of the deposition was doubled again for the last experiment and as can be seen in Figure 8.1 (c), the small crystals have grown into larger ones (about 15 nm across). The adenine crystals I have observed are over 4 nm in height with a uniformly flat top face and are increasingly difficult to image in the STM. The terrace edges and the bare surface of pyrite can still be resolved in the STM image, so I propose that all adenine molecules deposited on the surface formed 3-dimensional crystals. The dark shadow surrounding the crystals is a common tip effect that arises from the tip compensating for the sharp change in height over the scanned area. Low temperature annealing up to 110 ºC did not produce any effect on the 3-dimensional adenine structures. When the temperature has reached 115 ºC adenine started to sublime from the surface.

8.3. Uracil on pyrite (100)

It was not possible to resolve uracil adsorption on the pyrite (100) surface at the molecular level. Even at low coverages, uracil formed amorphous aggregates on the surface, located at the local defect sites as can be seen in Figure 8.2 (a).

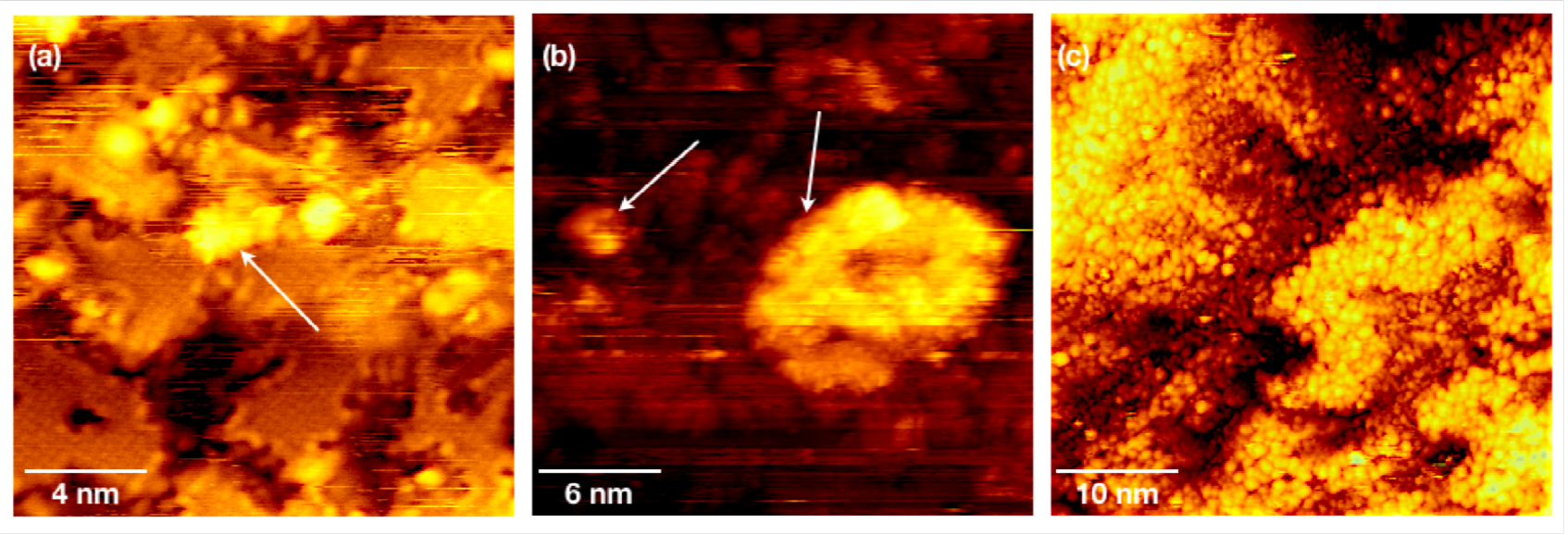

Figure 8.2. STM images of the self-assembly of uracil on the pyrite (100) surface in order of the deposition time. (a) At low coverages uracil forms small amorphous aggregates indicated by the arrow (deposition time: 2 minutes). The terraces are shown with atomic resolution in this image. (b) An STM image showing two 3-dimensional islands of amorphous aggregates clumped together (indicated by arrows). The height of the small island is 1.4 nm, the height of the large one is 2 nm. The bare surface of pyrite is still visible in the image. Deposition time: 5 minutes. (c) An STM image showing a surface area completely covered by the thin layer of the amorphous uracil; the step edges can just about be seen underneath. Uracil does not appear to form crystallize. Deposition time: 10 min. All three images were taken at 1.7 V bias voltage, 0.1 nA current in constant current mode and at the ambient temperature.

Unlike adenine, uracil does not seem to react with the uncompensated S-S bonds so does not decorate the edges of the terraces. The increased deposition time leads to formation of large amorphous islands, composed of small uracil aggregates, clumped together as shown in Figure 8.2 (b), which eventually, with enough molecules deposited, cover the entire surface as shown in Figure 8.2 (c). Low temperature annealing up to 90 ºC does not have any effect on the observed structures, and at 100 ºC uracil sublimed from the surface.

8.4. Co-deposition of uracil and adenine on pyrite (100)

I have performed a co-deposition experiment by subliming adenine on the surface first, followed by uracil for the first series of experiments, and *vice versa* for the second series of experiments with no difference in resulting structures. It is possible to see two different types of aggregates in a molecular resolution STM image: the typical amorphous aggregates formed by uracil and positioned randomly on the surface of the terraces; and the short condensed chains of adenine molecules adsorbed sideways on the edges of the terraces (see Figure 8.3). It can be seen clearly in the image that when all the dangling S-S bonds have been compensated, the adenine molecules do preferentially form 3-dimensional structures (i.e. adsorb on the top of the first chain, forming a second layer), rather than form a 2-dimensional lateral network that stretches across the terraces.

The low temperature annealing up to 100 ºC did not produce any difference in the structures observed. I did not observe any changes within the structures that would allow a speculation for any adenine-uracil interaction taking place on the pyrite (100) surface.

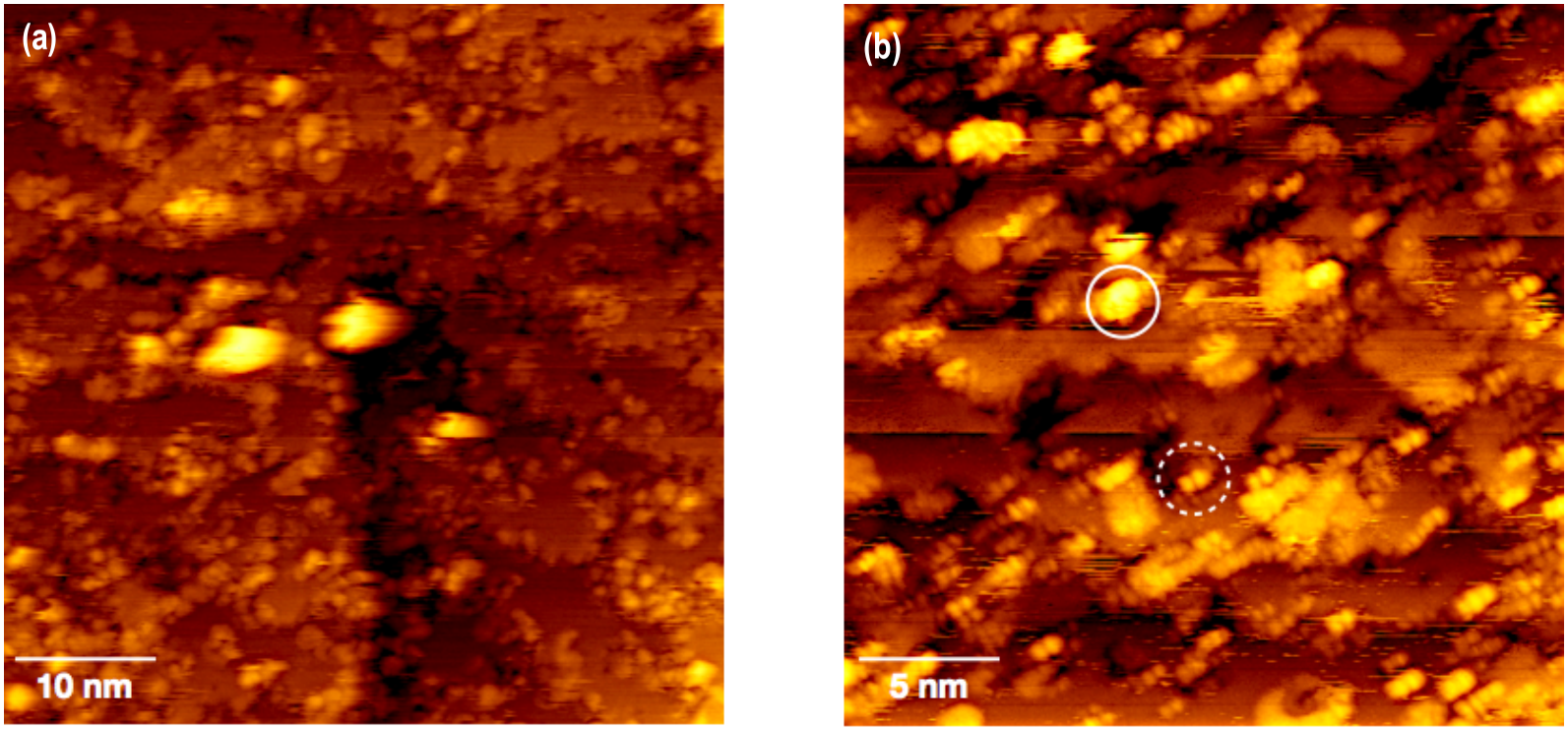

Figure 8.3. STM image of adenine and uracil molecule distribution on the pyrite (100) surface. (a) A medium-scale image showing the small 3-dimensional structures on the surface. (b) A molecular resolution image showing two different types of aggregates. The solid circle outlines the typical amorphous aggregates or small crystals formed by uracil as shown before, the dashed circle outlines the molecules of adenine adsorbed sideways on the edges of the terraces, forming very short condensed chains. Unfortunately this image also has some indication of a “double tip” effect. The images were taken at 1.6 V and 0.1 nA, in constant current mode and at the ambient temperature.

8.5. Discussion

Remarkably, my experiments show that neither uracil nor adenine self-assemble into ordered 2-dimensional structures on the pyrite (100) surface. One can observe the effect of the molecule-surface interaction for adenine only at the edges of the terraces, where one expects to find uncompensated broken S-S bonds, and for both adenine and uracil at the local defect sites. The pyrite (100) surface appears to terminate in a non-stoichiometric way, which provides such low surface energy that RNA bases do not interact with the surface, ordering into a 2-dimensional monolayer, and instead form 3-dimensional amorphous aggregates. The surface symmetry has no effect on the distribution of the amorphous material, nor could I observe any regular ordering of the aggregates.

The oxidation of the surface may also play an important role in the process of the self-assembly of adenine and uracil on the surface of pyrite, as well as the low energy surface termination, in fact the formation of the oxide layer should reduce the surface energy of the pyrite (100) even further, thus making the formation of the monolayer even more unlikely from the thermodynamic point of view. The complete oxidation of the surfaces I used is very probable, as the samples were polished and prepared in the normal laboratory conditions, i.e. in contact with air (for more details on the sample preparation and the presence of the products of oxidation on the sample surface see Chapter 5).

From the results of the experiments described in this chapter, I conclude that the formation of uracil and adenine crystals on the oxidised surface of natural pyrite crystals is perfectly possible, though in the case of uracil the chosen thermodynamic conditions of the experiment (pressure at $5x10^{-8}$ Pa and temperature 25 ºC) may not favour spontaneous

crystal formation. The adenine crystals were observed to grow in vacuum through normal growth mechanisms on the nanostructured $SrTiO_3$ (001) surface[150], graphite (0001) surface[38], and Si wafers[151] and the results are compatible with the structures I have imaged. I cannot speculate on the structure of uracil aggregates based on my STM images, as I did not manage to resolve these aggregates at molecular or atomic level. I can suggest, however, that these molecular arrangements are stabilised by the intermolecular hydrogen bonds and are physisorbed on the surface.

The comparatively low surface energy of the pyrite (100) surface[152] (0.54-1.42 J m^{-2}) prohibits the "wetting" of the surface and no 2-dimensional structures were formed by either uracil or adenine, and the oxidisation of the surface brings the surface energy even lower. My expectations, suggested by theoretical calculation, were that a catalytically active surface would provide sufficient surface energy for the formation of ionic or van der Waals bonds with the RNA bases, and the ordered 2-dimensional molecular networks would be observed in the STM images. Though I have observed the self-assembly of RNA bases on the surface of pyrite into 3-dimensional structures, it only tells us that the sum of the energies of the intermolecular bonds and the energies of the surface-molecular interaction is greater than the surface energy of the oxidised pyrite (100) surface, which results in clumping rather then wetting. It is very difficult to draw a meaningful conclusion directly related to the role of pyrite in the origin of life from the results described here. I would argue that the chances for the polymerisation of the organic molecules are higher for the substrate that imposes an ordered 2-dimensional structures to form, rather than the substrate that only allows non-specific amorphous accumulation or crystal growth but it would be too rash to disqualify the surfaces of pyrite as candidates on the solely basis of this thesis.

Firstly, the surfaces I used for my experiments were most certainly oxidised. It is possible that as the early Earth atmosphere contained essentially no free oxygen[153], the surfaces of pyrite could exist in the unoxidised state, which could have a boosting effect on the surface energy of pyrite, and so could bring it within comparable magnitude with the energies of the surface-molecular interactions and the intermolecular hydrogen bonds, thus creating a possibility for the formation of ordered monolayers. To test this assumption the unoxidised surface of pyrite should be obtained. The crystals could be notched parallel to the (100) face and cleaved in vacuum, and though pyrite has a poor cleavage, a few successful STM images of the small areas of the cleaved (100) surfaces of pyrite have been reported[96]. Another way to create an unoxidised surface could be to polish the sample in the N_2 or, even better, in the CO_2 environment, which would simulate the protoatmosphere, and cover the surface with oil to isolate it from the O_2 in the atmosphere until it is transferred in the vacuum chamber.

Secondly, other low indexed naturally-occurring surfaces of pyrite could be used for a similar study. Recent calculations have shown that the (110) and (111) surfaces of pyrite are considerably more reactive than (100), which is reflected in higher surface energies in the order of 2.36 J m^{-2} for the (110) surface and 3.81-3.92 J m^{-2} for the (111) surface depending whether it is S or Fe terminated[152]. However, these surfaces will also react with the atmospheric O_2, so the careful planning of the experiments to obtain “fresh”, unoxidised surfaces would be paramount.

Taking into account the considerable technical difficulties that would stem from the sample preparation process, further experiments with pyrite surfaces should be subject of another dedicated study. Having said that, the variety and the complexity of the highly ordered bi-

molecular adenine-uracil networks I have shown in the previous chapter are very encouraging and could inspire further work in the direction of this thesis. The question of the ability of the RNA bases to self-assembly into an RNA precursor remains open, but their ability to create regular bimolecular networks which possibly include the Hoogsteen configuration of the hydrogen double bonds, found in RNA base pairing, demonstrate that the possibility of the existence of the self-assembled RNA precursor is not that remote.

Chapter 9

Conclusion

This thesis describes series of experiments on the self-assembly of two complementary RNA bases, adenine and uracil, on metal and mineral surfaces. The particular interest in this research area is based on the hypothesis that the ability of purine and pyrimidine bases to spontaneously form stable 2-dimensional monolayer structures on inorganic surfaces could be relevant to the self-assembly of the RNA precursor, and thus to the origin of life at the very beginning of the biochemical evolution. The Au (111) and the pyrite (100) surfaces were chosen as the templates for the self-assembly in UHV conditions. The bare surfaces were characterised by the STM prior to the deposition of the molecules by sublimation. The molecular 2-dimensional ordering was observed on the Au (111) surface and 3-dimensional ordering was observed on the pyrite (100) surface. This chapter offers a brief summary of the conclusions, which can be drawn from the experimental results I have obtained.

Relatively inert Au (111) surface was chosen to act as a test template for catalytically active (100) surface of pyrite. I have observed that both adenine and uracil form regular 2-dimensional mono- and bimolecular networks on Au (111) surface in UHV, where the surface-molecular interaction is minimal.

A number of lateral molecular assemblies of uracil were imaged and the possible 2-dimensional arrangements of molecules were proposed, based on their planar orientation and the geometry of hydrogen bonds. The self-assembly of uracil appears to be weakly

influenced by the substrate as the unit cells are arranged along the main crystallographic directions of the Au (111). One of the porous molecular networks I described in this thesis is chiral, with alternating monochiral domains comprising large 2-dimensional islands. The mechanism for the formation of these domains is unclear. I suggest that the boundary between the different domains could be a growth boundary and the domains could have started as single domain islands which have grown together to form a larger structure. The intermolecular bonding, rather than the bonding to the surface dominates the chiral selectivity on Au (111), surface and the self-assembled networks strongly depend on coverage. At low coverages the five-fold molecular configurations are possible, and with the increase of the amount of the molecules on the surface and less space available, the more economical hexagonal packing becomes more and more dominant until it remains the only packing arrangement possible at above 0.75 ML.

Similar to the uracil self-assembly on the Au (111) surface, the networks formed by adenine and adenine-uracil mixture also align along the main crystallographic directions of the substrate and are determined by the geometry and the strength of hydrogen bonds. The low temperature annealing is necessary for creating regular adenine-uracil networks. I suggest that the variety of the of bimolecular uracil and adenine networks I observed is due to the effects of coverage and the local ratio between adeine and uracil molecules on the surface.

Five new molecular phases were described in this thesis, two of which are a pure uracil phases and three are a mixed adenine-uracil phases, all of these were observed in the STM for the first time on the Au (111) surface. I have proposed possible 2-dimensional arrangements of bimolecular networks based on the molecular resolution STM images, the planar orientation of the molecules and the geometry of hydrogen bonds. One of the phases

shown may incorporate Hoogsteen configuration of hydrogen bonds, as found in RNA helix.

The results of the study of the self-assembly of adenine and uracil described in this chapter were to form the basis for further experiments with the same molecules using a pyrite (100) surface as a substrate. However, my experiments have shown that neither uracil nor adenine self-assemble into ordered 2-dimensional structures on the pyrite (100) surface. I observed the formation of short 2-dimensional chains for adenine at the edges of the terraces, where uncompensated S-S bonds are located, and as soon as all the S dangling bonds were used, the formation of 3-dimensional structures started at the same sites. I have observed only the amorphous 3-dimensional aggregates formed by uracil. I therefore assume that the pyrite (100) surface appears to be largely oxidized and to terminate in a non-stoichiometric way, which provides such low surface energy that the wetting of the surface does not occur after the deposition, and both of adenine and uracil preferentially form 3-dimensional structures. The surface symmetry has no effect on the distribution or orientation of these structures and I suggest that the 3-dimensional structures are stabilised by the intermolecular hydrogen bonds and are physisorbed on the surface.

The oxidation of the surface may play an important role in the process of the self-assembly of adenine and uracil on the (100) surface of pyrite by reducing the surface energy even further thus making the formation of the monolayer even more unlikely. The complete oxidisation of the surfaces I used is very probable as the samples were polished and prepared in the normal laboratory conditions i.e. in contact with air. I expected the catalytically active surface of pyrite to form ionic bonds with the RNA bases as theory suggests[5]. However, the results of our experiments have shown that the sum of the energies of the intermolecular bonds and the surface-molecular interaction is greater than

the surface energy of the oxidised pyrite (100) surface, which results in clumping rather then wetting. It is tempting, therefore, to describe my observations as a negative result and remove pyrite from the list of potential candidates for a mineral surface catalyser for an RNA precursor but I would argue that this decision is likely to be premature.

Since the oxidation of the surface lowers the surface energy and the surface I have used were most certainly oxidised, I would suggest to repeat the experiments on the (100), and also more reactive (110) and (111) surfaces of pyrite (which still exist as natural crystal faces) that are either cleaved in vacuum or prepared in the oxygen-free environment. This would bring the experimental conditions closer to the early Earth environment, which was virtually oxygen-free, so the pyrite surfaces could remain in the unoxidised state.

Apart from further experimental work on the pyrite surfaces, it would be most interesting to perform some theoretical calculations to obtain a more accurate answer to the role of Au (111) in the self-assembly of adenine and uracil in terms of identifying the cumulative effect of the underlying surface on the energetically preferred configuration of bonds between the adsorbed molecules and the periodicity of the molecular structures. Also, the mechanism for the formation of uracil chiral domains is not clear and to give a definite answer to the appearance of these domains, I need to refer to theoretical calculations.

I hope that the variety and the complexity of the highly ordered bi-molecular adenine-uracil networks described in this thesis may inspire further interest in the self-assembly of the RNA bases of the surfaces of pyrite and other sulphide minerals, and generally in the “iron-sulphur world” theory. Until the RNA precursor is discovered experimentally and not just merely predicted theoretically, one of the crucial steps in the origin of life as the chemical to

biological evolution will remain unproven.

Even without the interest in the origin of life aspect, which can be viewed with some suspicion by more practical minds, the results described in this thesis could still offer some foundation for further research into the nature of molecular networks stabilised by hydrogen bonds, surface chiral selectivity, surface-induced catalytic effects, and chiral packing mechanisms to anyone who choses to use it in that fashion.

Approximate word count of thesis: 30500

References

1 Kuan, Y.J. et al., Interstellar Glycine. *The Astrophysical Journal* **593**, 848 (2003).

2 Woese, C., The universal ancestor *Proc. Natl. Acad. Sci. USA* **95**, 6854 (1998).

3 Brack, A. ed., *The Molecular origins of life: assembling the pieces of the puzzle*. (Cambridge University Press, Cambridge, 1998).

4 Ferris, J. P., Hill, A. R., Liu, R., and Orgel, L. E., Synthesis of long prebiotic oligomers on mineral surfaces. *Nature* **381**, 59 (1996).

5 Wächtershäuser, G., Pyrite formation, the first energy source for life: A hypothesis. *System Appl. Microiol.* **10**, 207 (1988).

6 Wächtershäuser, G., Before enzymes and templates: Theory of surface metabolism. *Microbiol. Rev.* **52** (Dec), 452 (1988).

7 Binnig, G., Rohrer, H, Gerber, C., and Weibel, E., Tunneling through a controllable vacuum gap. *Appl. Phys. Lett.* **40** (2), 178 (1981).

8 Chen, C. J., *Introduction to Scanning Tunneling Microscopy*. (Oxford University Press, 1993).

9 Tersoff, J. and Hamann, D. R., Theory of scanning tunneling microscope. *Phys. Rev. B* **31** (2), 805 (1984).

10 Newell, D., D.Phil Thesis. University of Oxford, 2008.

11 Butt, H. J., Cappella, B., and Kappl, M., Force measurements with the atomic force microscopy: Technique, interpretation and application. *Surf. Sci. Rep.* **59**, 1 (2005).

12 Giessibl, F. J., Advances in atomic force microscopy. *Rev. Mod. Phys.* **75**, 949 (2003).

13 Randle, V., *Microtexture Determination And Its Applications*. (The Institute of Materials, 1992).

14 Amelinckx, S. and Van Dyck, D., in *Electron Diffraction Techniques*, edited by J. M.

Cowley (Oxford University Press, 1993).

15 Goodfew, P.J. and Humphreys, F. J., *Electron Microscopy and Analysis*. (Taylor & Francis 1988).

16 Gilchrist, T. L., *Heterocyclic Chemistry*, 3rd ed. (1997).

17 Cohn, C. A. et al., Fate of Prebiotic Adenine. *Astrobiology* **1** (4), 477 (2001).

18 Smith, C. A. and Wood, E. J., in *Molecules and Cell Biochemistry* (Champan and Hall, 1991).

19 Brown, D. J., *Heterocyclic Compounds: The Pyrimidines*. (Interscience, New York, 1994).

20 Mamdouh, W et al., Coexistence of homochiral and heterochiral adenine domains at the liquid/solid interface. *J. Chem. Phys. B* **111**, 12048 (2007).

21 Chen, Q. and Richardson, N. V., Enantiometric interactions between nucleic acid bases and amino acids on solid surfaces. *Nature: materials* **2** (May), 324 (2003).

22 Papageorgiou, A.C. et al., Chemical transformations drive complex self-assembly of uracil on close-packed coinage metal surfaces. *ACS Nano* **6** (3), 2477 (2012).

23 Tao, N. J., DeRose, J. A., and Linsay, S. M., Self-assembly of molecular superstructure studies by in situ scanning tunneling microscopy: DNA bases on Au (111). *J. Phys. Chem.* **97**, 910 (1993).

24 Chen, Q., Frankel, D. J., and Richardson, N. V., Self-assembly of adenine on Cu (100) surfaces. *Langmuir* **18**, 3219 (2002).

25 Furukawa, M., Tanaka, H., and Kawai, T., The role of dimer formation in the self-assemblies of DNA base molecules on Cu (111) surfaces: A scanning tunneling microscope study. *J. Chem. Phys.* **115** (7), 3419 (2001).

26 Tanaka, H., Nakagawa, T., and Kawai, T., Two dimensional self-assembly of DNA base molecule on Cu (111) surface. *Surf. Sci.* **364**, L575 (1996).

[27] Kelly, R.E.A. and Kantorovich, L.N., Homopairing possibilities of the DNA base adenine. *J. Phys. Chem. B* **109**, 11933 (2005).

[28] Kelly, R.E.A. and Kantorovich, L.N., Planar nucleic acid base super-structures. *J. Mater. Chem.* **16**, 1894 (2006).

[29] Kelly, R.E.A. and Kantorovich, L.N., Planar heteropairing possibilities of the DNA and RNA bases: an *ab initio* density functional theory study. *J. Phys. Chem. C* **111**, 3883 (2007).

[30] Kelly, R.E.A., Lee, Y.J., and Kantorovich, L.N., Homopairing possibilities of the DNA bases cytosine and guanine: An *ab initio* DFT study. *J. Phys. Chem. B* **109** (46), 22045 (2005).

[31] Kelly, R.E.A. et al., An Investigation into the interactions between self-assembled adenine molecules and an Au (111) surface. *Small* **4** (9), 1494 (2008).

[32] Perdigão, L. M. A. et al., Experimental and theoretical implications of adenine monolayers on Ag-terminated Si (111). *Phys. Rev. B* **73**, 195423 (2006).

[33] Wandlowski, T., Lampner, D., and Lindsay, S.M., Structure and stability of cytosine adlayers on Au (111): an in-situ STM study. *J. Electroan. Chem.* **404**, 215 (1995).

[34] Kelly, R.E.A. et al., Understanding the disorder of the DNA base cytosine on the Au (111) surface. *J. Chem. Phys.* **129**, 184707 (2008).

[35] Otero, R. et al., Elementary structural motifs in a random network of cytosine adsorbed on a gold (111) surface. *Science* **319**, 312 (2008).

[36] Xu, W. et al., Prochiral guanine adsorption on Au (111): An entropy-stabilized intermixed guanine-quartet chiral structure. *Small* **5** (17), 1952 (2009).

[37] Otero, R. et al., Specificity of Watson-Crick base pairing on a solid surface studied at the atomic scale. *Angew. Chem.* **120**, 9810 (2008).

[38] Reiter, M. M., Jamitzky, F., Trixler, K., and Heckel, W. M., STM structure determination

of adenine bilayers by Moire interpretation. *Phys. Stat. Sol. (a)* **187** (1), 171 (2001).

[39] Freund, J. E., Edelwirth, M., Krobel, P., and Heckl, W. M., Structure determination of two-dimensional adenine crystals on graphite. *Phys. Rev. B* **55** (8), 5394 (1996).

[40] Plekan, O. et al., The adsorption of adenine on mineral surfaces: iron pyrite and silicon dioxide. *Surf. Sci.* (601), 1973 (2007).

[41] Fraser, D. G., Deak, D. S., Liu, S., and Castell, M. R., Structure of vapour deposited adenine on a nanostructured perovskite surface studied by STM. *Farad. Discus.* **133**, 303 (2006).

[42] Edelwirth, J., Freund, S.J., Sowerby, S.J., and Heckl, W.M., Molecular mechanics study of hydrogen bonded self-assembled adenine monolayers on graphite. *Surf. Sci.* **417**, 201 (1998).

[43] Xu, S. et al., Coadsorption of guanine and cytosine on graphite: ordered structure based on GC pairing. *ASC: Nano Lettr.* **6** (7), 1434 (2006).

[44] Sowerby, S.J., Heckl, W.M., and Peterson, G.B., Chiral symmetry breaking during the self-assembly of monolayers from achiral purine molecules. *J. Molec. Evol.* **43**, 419 (1996).

[45] Sowerby, S.J. and Heckl, W.M., The role of self-assembled monolayers of the purine and pyrimidine bases in the emergence of life. *Orig. Life Evol. Biosph.* **28**, 283 (1998).

[46] Lazcano, A. and Bada, J.L., The 1953 Stanley L. Miller experiment: Fifty years of prebiotic organic chemistry. *Orig. Life Evol. Biosph.* **33** (3), 235 (2003).

[47] Oró, J, Synthesis of adenine from ammonium cyanide. *Biochem. Biophys. Res. Commun.* **2**, 407 (1960).

[48] Dioses, S.E., Synthesis of uracil from glycine: A possible pathway in prebiotic systems. *Orig. Life Evol. Biosph.* **16**, 287 (1986).

[49] Kasting, J.F. *Earth's early atmosphere* **259**, 920 (1993).

[50] Cronin, J.R. and al, et eds., *Meteorites and the early Solar system*. (University of Arizona Press, 1988).

[51] Doolittle, W. F., Fun with genealogy. *Proc. Natl. Acad. Sci. USA* **94**, 12751 (1997).

[52] Ferris, J.P., Montmorillonite catalysis of 30-50mer oligonucleotides: Laboratory demonstration of potential steps in the origin of the RNA world. *Orig. Life Evol. Biosph.* **32** (4), 311 (2002).

[53] Schoonen, M., Smirnov, A., and Cohn, C., A perspective on the role of minerals in prebiotic synthesis. *Ambio* **33**, 539 (2004).

[54] Orgel, L. E., The origin of life - a review of facts and speculations. *TIBS* **23** (Dec), 491 (1998).

[55] Simonit, B. R. T., Aqueous organic geochemistry at high temperature/high pressure. *Orig. Life Evol. Biosph.* **22**, 53 (1992).

[56] Shock, E. L., Geochemical constraints on the origin of organic compounds in hydrothermal systems. *Orig. Life Evol. Biosph.* **22**, 43 (1990).

[57] Corliss, G. B., Baross, J. A., and Hoffman, S. E., An hypothesis concerning the relationship between submarine hot springs and the origin of life on Earth. *Oceanol. Acta Suppl.* **4**, 59 (1981).

[58] Schoonen, M. A. A., Mechanisms of sedimentary pyrite formation. *Sulfur Biogeochemistry - Past and Present Geological Society of America Special Paper* **379**, 117 (2004).

[59] Wächtershäuser, G., Groundworks for an evolutionary biochemistry: The iron-sulfur world. *Prog. Biosph. Mol. Biol.* **58**, 85 (1992).

[60] Beinhert, H., Holm, R. H., and Munck, E., Iron-sulfur clusters: nature's modular, multipurpose structures. *Science* **277**, 653 (1997).

[61] Cairns-Smith, A. G., The origin of life and the nature of primitive gene. *J. Theoret. Biol.*

10, 53 (1966).

62 DeDuve, C., *Blueprint for a cell*. (Neil Patterson Publ., Burlington N.C., 1991).

63 Bishop, D. H., Pace, N. R., and Spiegelman, S., The mechanism of replication: a novelty polarity reversal in the in vitro synthesis of Q-beta-RNA and its complement. *Proc. Natl. Acad. Sci. USA* **58** (4), 1790 (1967).

64 Witting, P. et al., DNA-like double helix formed by peptide nucleic acid. *Nature* **352**, 516 (1994).

65 Ekland, E.H. and Bartel, D.P., RNA-catalysed RNA polymerisation using nucleoside triphosphates. *Nature* **382**, 373 (1996).

66 Wächtershäuser, G., Evolution of the first metabolic cycles. *Proc. Nadl. Acad. Sci. USA* **87**, 200 (1990).

67 Blöchl, E., Keller, M., Wächtershäuser, G., and Stetter, K. O., Reactions depending on iron sulfide and linking geochemistry with biochemistry. *Proc. Natl. Acad. Sci. USA* **89**, 8117 (1992); Kaschke, M., Russel, M. J., and Cole, W. J., FeS/FeS_2 - a redox system for the origin of life - hypothesis. *Orig. Life Evol. Biosph.* **24**, 43 (1994).

68 Huber, C. and Wächtershäuser, G., Activated acetic acid by carbon fixation on (Fe,Ni)S under primordial conditions. *Science* **276**, 245 (1997).

69 Bebié, J. and Schoonen, M. A. A., Pyrite and phosphate in anoxia and an origin-of-life hypothesis. *Earth Planet Sci. Lett.* **171**, 1 (1999).

70 Borda, M. J., Elsetinow, A. R., Schoonen, M. A., and Strongin, D. R., A mechanism for the production of hydroxyl radical at surface defect sites on pyrite. *Geochem. Cosmochim. Acta* **67**, 935 (2003).

71 Nordstrom, D. K. and Southam, G., Geomicrobiology of sulfide mineral oxidation. *Rev. Mineral.* **35**, 361 (1997).

72 Cody, G. D. et al., Geochemical roots of autotrophic carbon fixation: Hydrothermal

experiments in the system citric acid, H_2O-(±FeS)-(±NiS). *Geochem. Cosmochim. Acta* **65**, 3557 (2001).

73 Cody, G. D. et al., Assaying the catalytic potential of transitional metal sulfides for abiotic carbon fixation. *Geochem. Cosmochim. Acta* **68**, 2185 (2004).

74 Meierhenrich, U., *Amino acids and the asymmetry of life*. (Springer, 2008).

75 Krueger, K.L. and Kissel, J., Biogenesis by cometary grains - thermodynamic aspects of self-organisation. *Orig. Life Evol. Biosph.* **19**, 87 (1989).

76 Idelson, M. and Blout, E.R., Polypeptides. XVIII. A kinetic study of the polymerisation of amino acid N-carboxyanhydrides initiated by strong bases. *J. Am. Chem. Soc.* **80**, 2387 (1958).

77 Matthews, C.N. and Minard, R.D., Hydrogen cyanide polymers, comets and the origin of life. *Farad. Discuss.* **133**, 393 (2006).

78 Pizzarello, S. and Cronin, J.R., Non-racemic amino acids in the Murray and Murchison meteorites. *Geochem. Cosmochim. Acta* **64**, 329 (2000).

79 Lucas, P.W. et al., UV circular polarization in star formation regions: The origin of homochirality? *Orig. Life Evol. Biosph.* **35**, 29 (2005).

80 MacDermott, A.J. ed., *The weak force and the origin of life*. (A. Deepark Publishing, Hampton, Virginia, 1993).

81 Conte, E., Investigation on the chirality of electrons from ^{90}Sr-^{90}Y beta-decay and their asymmetrical interactions with D- and L-alanines. *Lett. Nuovo Cimento* **44**, 641 (1985).

82 Sakamoto, M. ed., *Absolute asymmetric photochemistry using spontaneous chiral crystallisation.* (Marcel Dekker, New York, 2004).

83 Vaughan, D. J., Becker, U., and Wright, K., Sulfide mineral surfaces: Theory and experiment. *Int. J. Min. Process.* **51**, 1 (1997).

84 Woese, C. R., Bacterial Evolution. *Microbiol. Rev.* **51** (2), 221 (1987).

[85] Bulou, H. and Goyhenex, C., Local strain analysis of the herringbone reconstruction of Au (111) through atomistic stimulations. *Phys. Rev. B* **65** (4), 1 (2002).

[86] Barth, J. V., Brune, H., Ertl, G., and Behm, R. J., Scanning tunneling microscopy observations on the reconstructed Au (111) surface: Atomic structure, long-range superstructure, rotational domains, and surface defects. *Phys. Rev. B* **42** (15) (1990).

[87] Silly, F., Shaw, A. Q., D., Briggs G. A., and R., Castell M., Epitaxial ordering of a perylenetetracarboxylic dimide-melamine supramolecular network driven by the Au (111) - (22 x sqr 3) reconstruction. *Appl. Phys. Lettr.* **92** (2008).

[88] Bulou, H. and Goyhenex, C., Local strain analysis of the herringbone reconstruction of Au (111) through atomistic simulations. *Phys. Rev. B* **65** (4), 045407 (2002).

[89] Vaughan, D. J. ed., *Sulfide Mineralogy and Geochemistry*. (Geochemical Society and Mineralogical Society of America, 2006).

[90] Canfeild, D. E. and Raiswell, R., The evolution of the sulfur cycle. *Am. J. Sci.* **299**, 697 (1999).

[91] Russel, M. J. and Hall, A. J., The emergence of life from iron monosulfide bubbles at submarine hydrothermal redox and pH front. *J. Geol. Soc.* **154**, 377 (1997).

[92] Palache, C., Berman, H., and Frondel, C., *The System of Mineralogy of James Dwight Dana and Edward Salisbury Dana Yale University 1837-1892, Volume I: Elements, Sulfides, Sulfosalts, Oxides.*, 7th ed. (John Wiley and Sons, Inc., New York, 1944).

[93] Pridmore, D. F. and Shuey, R. T., The electrical resistivity of galena, pyrite and chalcopyrite. *Am. Mineral.* **61**, 248 (1976).

[94] Robie, R. A., Hemingway, B. S., and Fisher, J. R, *Thermodynamic properties of minerals and related substances at 298.15 K and 1 bar (105 pascals) pressure and at higher temperatures*. (US. Geol. Surv. Bull., 1979).

[95] Chuang, Y. Y., Hseih, K.-C., and Chang, Y. A., Thermodynamics and phase

relationships of transition metal-sulfur systems: Part V. A re-evaluation of the Fe-S system using an associated solution model for the liquid phase. *Metallurg. Transac. B* **16B**, 277 (1985).

96 Eggleston, C. M. and Hochella, M. F. Jr., Scanning tunneling microscopy of pyrite {100}: surface structure and step reconstruction. *Am. Mineral.* **77**, 221 (1992).

97 Kittel, C., *Introduction to Solid State Physics*. (John Wiley & Sons, New York, Chichester, 1996).

98 Finklea, III S. L., Cathey, L., and Amma, E. L., Investigation of the bonding mechanism in pyrite using the Mössbauer effect and X-ray crystallography. *Acta Crys.* **A32**, 529 (1976).

99 Braga, M., Lie, S. K., Taft, C. A., and Lester, W. A., Electronic structure, hyperfine interactions and magnetic properties for iron octahedral sulfides. *Phys. Rev. B* **38** (15), 10 837 (1988).

100 Qiu, G. et al., Theoretical study of the surface energy and electronic structure of pyrite FeS_2 (100) using a total-energy pseudopotential method, CASTEP. *J. Coll. Interf. Sci.* **270** (1), 127 (2004).

101 Rosso, K. M., Becker, U., and Hochella, Jr. M. F., Atomically resolved electronic structure of pyrite (100) surfaces: An experimental and theoretical investigation with implications for reactivity. *Am. Mineral.* **84**, 1535 (1999).

102 Fan, F. R. and Bard, A. J., Scanning tunneling microscopy and tunneling microscopy of n-type iron pyrite (n-FeS_2) single crystals. *J. Phys. Chem.* **95**, 1969 (1991).

103 Opahle, I., Koepernik, K., and Eschrig, H., Full potential band-structure calculation of iron pyrite. *Phys. Rev. B* **60**, 14035 (1999); Mattila, S., Leiro, J. A., and Laajalehto, K., Surface XPS core-level shifts of FeS_2. *Appl. Surf. Sci.* **97**, 212 (2003).

104 Folkerts, W. et al., Electronic structure of some 3D transition-metal pyrites. *J. Phys.*

C20, 4135 (1987).

105 Spencer, M. J. S., Hung, A., Snook, I. K., and Yarovsky, I., Further studies of iron adhesion: (111) surfaces. *Surf. Sci.* **515**, L464 (2002).

106 Ferrer, I. J., Vevskaia, D. M., delasHeras, C., and Sanchez, C., Electronic structure of bulk and (001) surface layers of pyrite FeS_2. *Solid State Commun.* **74**, 913 (1990); Li, E. K., Johnson, K. H., Eastman, D. E., and Freeouf, J. L., Localized and bandlike valence-electron states. *Phys. Rev. Let.* **32** (9), 470 (1974).

107 Bronold, M., Tomm, Y., and Jaegermann, W., Surface states on cubic *d*-band semiconductor FeS_2. *Surf. Sci.* **L931**, 212 (1994).

108 Birkholtz, M., Fiechter, S., Hartmann, A., and Tributsch, H., Sulfur deficiency in iron pyrite (FeS_{2-x}) and its consequences for band-structure models. *Phys. Rev. B* **43**, 11926 (1991).

109 Ellmer, K. and Hopfner, C., On the stoichiometry of the semiconductor pyrite FeS_2. *Phil. Mag. A* **75**, 1129 (1997).

110 Schieck, R. et al., Electrical properties of natural and synthetic pyrite (FeS_2) crystals. *J. Mater. Res.* **5**, 1567 (1990).

111 Eyert, V., Hock, K. H., Fiechter, S., and Tributsch, H., Electronic structure of FeS_2: The critical role of electron-lattice interaction. *Phys. Rev. B* **57**, 6350 (1998).

112 Bither, T. A. et al., New transition metal dichalcogenides formed at high pressure. *Solid State Comm.* **4**, 533 (1996).

113 Harrison, R. J., Neutron diffraction of magnetic materials. *Rev. Mineral. Geochem.* **63**, 113 (2006); Pashley, M. D., Electron counting model and its application to island structures on molecular-beam epitaxy grown GaAs (001) and ZnSe (001). *Phys. Rev. B* **40**, 10481 (1989).

114 Gibson, A. S. and LaFemina, J. P., in *Physics and Chemistry of Mineral Surfaces*,

edited by P. V. Brady (CRC Press, 1996), pp. 1.

115 Rosso, K. M., Becker, U., and Hochella, Jr M. F., The interaction of pyrite (100) surfaces with O_2 and H_2O: Fundamental oxidation mechanisms. *Am. Mineral.* **84**, 1549 (1999).

116 Rosso, K. M., Becker, U., and Hochella, Jr M. F., Surface defects and self-diffusion on pyrite {100}: an ultra-high vacuum scanning tunneling microscopy and theoretical modeling study. *Am. Mineral.* **85**, 1428 (2000).

117 Eggleston, C. M. and Hochella, M. F., Scanning tunneling microscopy of sulfide surfaces. *Geochim. Cosmochim. Acta* **54**, 1511 (1990).

118 Stirling, A., Bernasconi, M., and Parrinello, M., *Ab-initio* simutation of water interaction with the (100) surface of pyrite. *J. Chem. Phys.* **118**, 8917 (2003).

119 Cai, J. and Philpott, M. R., Electronic structure of bulk and (100) surface layers of pyrite FeS_2. *Comp. Mat. Sci.* **30**, 358 (2004).

120 Hung, A., Muscat, J., and Yarovsky, I., Density functional theory studies of pyrite FeS_2 (100) and (110) surfaces. *Surf. Sci.* **513**, 511 (2002).

121 Nesbitt, H. W. et al., Synchrotron XPS evidence for Fe^{2+}-S and Fe^{3+}-S surface species on pyrite fracture surfaces, and their 3*d* electronic states. *Am. Mineral.* **86**, 318 (2000).

122 Chativerdi, S. et al., XPS and LEED study of a single crystal surface of pyrite. *Am. Mineral.* **81**, 261 (1996).

123 Guevremont, J. M., Strongin, D. R., and Schoonen, M. A. A., Photoemission of adsorbed Xenon, X-ray photoemission spectroscopy, and temperature programmed desorption studies of H_2O and Fe_2S (100). *Langmuir* **14**, 1361 (1998).

124 Guevremont, J. M., Strongin, D. R., and Schoonen, M. A. A., Effects of surface imperfections on the binding of CH_3OH and H_2O on FeS_2 (100): using adsorbed Xe as a probe of mineral surface structure. *Surf. Sci.* **513**, 511 (1997).

125 Guevremont, J. M., Strongin, D. R., and Schoonen, M. A. A., Thermal chemistry of H_2S and H_2O on the (100) plane of pyrite: unique reactivity of defect sites. *Am. Mineral.* **83**, 1246 (1998).

126 Guevremont, J. M. et al., Reactivity of the (100) plane of pyrite in oxidizing gaseous and aqueous environments: effects of surface imperfections. *Environ. Sci. Technol.* **32**, 3743 (1998).

127 Guevremont, J. M. et al., Structure sensitivity of pyrite oxidation: comparison of the (100) and (111) planes. *Am. Mineral.* **83**, 1353 (1998).

128 Hung, A., Muscat, J., Yarovsky, I., and Rosso, S. P., Density functional theory studies of pyrite FeS_2 (111) and (210) surfaces. *Surf. Sci* **520**, 111 (2002).

129 Rosso, K. M., Structure and reactivity of semiconducting mineral surfaces: convergence of molecular modeling and experiment. *Rev. Mineral. Geochem.* **42**, 199 (2001).

130 Libowitsky, E., Anisotropic Pyrite: A Polishing Effect. *Phys Chem Minerals* **21**, 97 (1994).

131 Schaufuss, A. G. et al., Incipient oxidation of fractured pyrite surfaces in air. *Electron Spectrosc. Relat. Phenom.* **96-82**, 69 (1998).

132 Shvarov, Y. V., HCh: new potentialities for the thermodynamic simulation of geochemical systems offered by Windows. *Geochem. Intern.* **46**, 834 (2008).

133 Shvarov, Y. V., HCh: new possibilities for thermodynamic modeling of the geochemical processes in Windows. (in Russian). *Geochemistry* (8), 898 (2008).

134 Eggleston, C. M., Ehrhardt, J. J., and Stumm, W., Surface structural controls on pyrite oxidation kinetics: An XPS-UPS, STM, and modeling study. *Am. Mineral.* **81**, 1036 (1996).

135 Kauffman, S.A., *The origins of order: self-organisation and selection in evolution*.

(Oxford University Press Inc, New York, 1993).

136 Orme, C.A. et al., Formation of chiral morphologies through selective binding of amino acids to calcite surface steps. *Nature* **411** 775 (2001).

137 Sessier, J.L. and Jayawickramarajah, J., Functionalized base-pairs: versatile scaffolds for self-assembly. *Chem. Comm.* **14**, 1892 (2005).

138 Sessier, S., Lawrence, C., and Jayawickramarajah, J., Molecular recognition via base-pairing. *Chem. Soc. Rev.* **36**, 314 (2007).

139 Gardener, J.A., Shvarova, O.Y., Briggs, G.A.D., and Castell, M.R, Intricate hydrogen-bonded networks: binary and ternary combinations of uracil. PTCDI, and melamine. *J. Phys. Chem. C* **114** (13) (2010).

140 Cavallini, M., Aloisi, G., and Bracali, M., An in situ STM investigation of uracil on Ag (111). *J. Electroan. Chem.* **444** (1), 75 (1998).

141 Dretschkow, T., Dakkouri, A.S., and Wandlowski, T., *In-situ* scanning tunneling microscopy study of uracil on Au (111) and Au (100). *Langmuir* **13**, 2843 (1997).

142 Sowerby, S.J., Stockwell, P.A., Hekl, W.M., and Peterson, G.B., Self-programmable, self-assembling two-dimensional matter. *Orig. Life Evol. Biosph.* **30** (1), 81 (2000).

143 Sowerby, S.J., Holm, N.G., and Petersen, G.B., Origins of life: a route to nanotechnology. *Biosystems* **61**, 69 (2001).

144 Tao, N.J., DeRose, J.A., and Linsay, S.M., Self-assembly of molecular superstructures studied by in situ scanning tunneling microscopy: DNA bases on Au (111). *J. Phys. Chem.* **97**, 910 (1992).

145 Barrett, S, Image SXM 185-1C, ver. 1.62 (2008).

146 Piana, S and Bilic, A, The nature of the adsorption of nucleobases on the gold (111) surface. *J. Phys. Chem. B* **110**, 23467 (2006).

147 Griffiths, A.J.F., Miller, J.H., Lewontin, R.C., and Gelbart, W.M. eds., *Chapter 10*

(Molecular Biology of Gene Function): Genetic code: Stop codons. . (W.H. Freeman and Company, 2000).

148 Lukas, M. et al., Adenine monolayers on the Au (111) surface: Structure identification by scanning tunneling microscopy experiment and *ab initio* calculations. *J. Chem. Phys.* **130**, 024705 (2009).

149 Rozenberg, M., Shoham, G., Reva, I., and Fausto, R., Spontaneous self-association of adenine and uracil in polycrystals from low temperature FTIR spectra in the range below 1000 cm-1. *Spectrochem. Acta A: Molecular and Bimolecular Spectroscopy* **62** (1-3), 233 (2004).

150 Deak, D. S., D.Phil Thesis. University of Oxford, 2007.

151 Sarantopoulou, E. et al., Preparation of ultra-thin films of DNA bases with laser light at 157 nm. *Thin Solid Films* **495**, 45 (2006).

152 de Leeuw, N.H., Parker, S.C., Sithole, H.M., and Ngoepe, P.E., Modeling the surface structure and reactivity of pyrite: Introducing a potential model for FeS_2. *J. Phys. Chem. B* **104** (33), 7969 (2000).

153 Kasting, J. F., Pollack, J. B., and Crisp, D, Effects of high CO_2 levels on surface temperature and atmospheric oxidation state of the early Earth. *J. Atmos. Chem.* **1**, 403 (1984).